NEW SOFT CHEMICAL ROUTES TO FERROELECTRIC MATERIALS

by

Keshwaree Babooram

B.Sc. (Hons.), University of Mauritius, Mauritius, 1999

THESIS SUBMITTED IN PARTIAL FULFILLMENT OF
THE REQUIREMENTS FOR THE DEGREE OF

DOCTOR OF PHILOSOPHY

In the
Department of Chemistry

SIMON FRASER UNIVERSITY

Spring 2005

APPROVAL

Name: Keshwaree (Vima) Babooram

Degree: Doctor of Philosophy

Title of Thesis: New Soft Chemical Routes to Ferroelectric Materials

Examining Committee:

Chair: Dr. G.W. Leach (Associate Professor)

Dr. Z-G Ye (Professor)
Senior Supervisor

Dr. S. Holdcroft (Professor)
Committee Member

Dr. V.E. Williams (Assistant Professor)
Committee Member

Dr. B.D. Gates (Assistant Professor)
Internal Examiner

Dr. G. Cao (Associate Professor)
External Examiner
Materials Science and Engineering
University of Washington

Date Approved: April 25, 2005

SIMON FRASER UNIVERSITY

PARTIAL COPYRIGHT LICENCE

ABSTRACT

A new soft chemical route has been developed in the first part of this thesis for synthesis of relaxor ferroelectric, $(1-x)Pb(Mg_{1/3}Nb_{2/3})O_3–xPbTiO_3$ [(1-x)PMN–xPT] (x = 0.10, 0.35) ceramics. This polyethylene glycol-based method shows some very interesting features. It allows the sol-gel reactions to be performed at room temperature, eliminating reflux steps usually required in sol-gel processes. Moreover, it does not require excess amounts of lead starting material to compensate for lead oxide loss during sintering as is usually the case in conventional synthesis. The effect of a triol molecule, 1,1,1-tris(hydroxy)methylethane (THOME), a known complexing agent for binding together metal ions in solutions, has also been studied.

Well-sintered 0.90PMN–0.10PT and 0.65PMN–0.35PT ceramics were prepared in a single heat-treatment step of the precursor powder. The use of THOME gives excellent dielectric and ferroelectric properties in stoichiometric 0.90PMN–0.10PT ceramics sintered at 1050 °C. A room temperature dielectric constant, ε'_{RT} of ~25,000 is observed at 1 kHz in this ceramic which is the highest value obtained so far in ceramics of the same composition. A 5% mol excess of lead in the sol-gel process without THOME improves the formation of the perovskite phase but degrades the dielectric properties. The 0.65PMN–0.35PT ceramics prepared with THOME and stoichiometric amounts of lead, and sintered at 1040 °C show pure perovskite phase and very good dielectric and ferroelectric properties (ε'_{RT} >5,000, ε'_{max} ~27,000, and $P_{r,RT}$ = 21 $\mu C/cm^2$).

In the second part of this work, pure perovskite ferroelectric $SrBi_2Ta_2O_9$ (SBT) ceramics have been synthesized by two new soft chemical techniques: a sol-gel process and a co-precipitation method. The sol-gel derived ceramics show denser and more homogeneous microstructure, and ε'_{max} and $P_{r,RT}$ values (950 and 7.6 $\mu C/cm^2$, respectively) higher than in ceramics prepared under the same conditions by the co-precipitation method. These values are also higher than in ceramics prepared by solid state reactions. The superior dielectric and ferroelectric properties of the sol-gel synthesized SBT ceramics are attributed to a more homogeneous microstructure with a better distribution of grain orientations, which eliminates the preferential grain orientation along the [00$\underline{1}$0]-direction.

DEDICATION

To my late father, Rajman, who passed away on July 15th, 1983.

To my dear mother, Padmadevi, my brothers, Vikash and Viraj, and my husband, Ravin.

To my adorable nephews, Arvin and Nilesh, and to my sweet unborn baby.

ACKNOWLEDGEMENTS

I would like to express my deep and sincere thanks to my senior supervisor, Prof. Z.-G. Ye for giving me the opportunity to work in his lab, and for his invaluable guidance, support and encouragement in the realization of this work.

My thanks also go to my supervisory committee members, Dr. S. Holdcroft and Dr. V. Williams, for their helpful advice and suggestions.

I extend my thanks to Dr. B. Gates for accepting to be my internal examiner, for his interest in the work, and some helpful discussions and advice.

I would also like to thank Dr. G. Cao for accepting to be my external examiner.

I also wish to thank Dr. A. Bokov from our research group, and Dr. M. K. Matam (a former group member) for their help with dielectric measurements; Dr. D. Yang of the department of Physics for his help with X-Ray diffraction measurements; Dr. D. Marshall of the department of Earth Science and Dr. Yang Li of the department of Physics for their assistance in the SEM studies.

I would like to thank all former and present members of our research group for all their help, support, and encouragement, and for being great friends. I especially thank Ms. L. Zhang for teaching me helpful sol-gel techniques in the lab, and W. Zhu and H. Tailor for very helpful discussions.

I also thank members of the Chemistry department at Simon Fraser University for their help and support.

I'm highly indebted to my dear mother, Padmadevi, my brothers, Vikash and Viraj, and my husband, Ravin for their devotion and love, and constant support and encouragement. I'm more than indebted to my brothers for having always supported me and making me reach this stage today. My husband has also been exceptional by being there for me all the time in the past five years.

A special thanks to R. Hossany for her constant support and encouragement, and friendship.

TABLE OF CONTENTS

LIST OF FIGURES

LIST OF TABLES

LIST OF ABBREVIATIONS

E_C	Coercive field
ε'_{RT}	Dielectric constant at room temperature
ε'_{max}	Maximum dielectric constant
FTIR	Fourrier Transform Infrared
MPB	Morphotropic Phase Boundary
(1-x)PMN–xPT	Lead magnesium niobium titanate $[(1-x)Pb(Mg_{1/3}Nb_{2/3})O_3–xPbTiO_3]$
PEG	Polyethylene glycol 200
P_r	Remnant polarization
P_S	Spontaneous polarization
T_C	Curie temperature
T_{max}	Temperature at which maximum dielectric permittivity occurs for a relaxor ferroelectric
THOME	1,1,1-tris(hydroxyl)methylethane
TIAA	titanium di-isopropoxide bis-acetyl acetonate
SBT	Strontium bismuth tantalate $[SrBi_2Ta_2O_9]$
SEM	Scanning Electron Microscopy
XRD	X-ray diffraction

10PEG(S)T	$0.90Pb(Mg_{1/3}Nb_{2/3})O_3$–$0.10PbTiO_3$ prepared using stoichiometric amount of lead acetate and THOME
10PEG(S)	$0.90Pb(Mg_{1/3}Nb_{2/3})O_3$–$0.10PbTiO_3$ prepared using stoichiometric amount of lead acetate
10PEG(5)T	$0.90Pb(Mg_{1/3}Nb_{2/3})O_3$–$0.10PbTiO_3$ prepared using 5 % mol excess of lead acetate and THOME
10PEG(5)	$0.90Pb(Mg_{1/3}Nb_{2/3})O_3$–$0.10PbTiO_3$ prepared using 5 % mol excess of lead acetate

CHAPTER 1:
General Introduction

1.1 Ferroelectric Materials

Crystals are classified into 7 systems according to their geometry and based on their symmetry with respect to a given point these systems are further sub-divided into point groups known as crystal classes [1]. There exist 32 such crystal classes and ferroelectricity is allowed in a class of non-centro symmetric and polar crystals that make 10, namely, **1, 2, m, 2mm, 4, 4mm, 3, 3m, 6,** and **6mm,** out of these 32 crystal classes [1,2]. The low symmetry in these materials permits a spontaneous polarization, P_s, along one or more of the crystal axes. In other words, a ferroelectric material possesses a reversible spontaneous polarization in the absence of an external electric field, the direction of which may be altered by the application of an appropriate field and this is possible in a given temperature range. The direction that is parallel to the spontaneous polarization vector is the polar axis. The polarization displayed in a ferroelectric material is a double-valued function of the applied electric field. Generally the direction in which P_s is oriented is not the same all throughout the ferroelectric material, and this leads to the formation of domains. As such, the direction of P_s is the same within a given domain, but varies from one domain to the other. This forms the basis of the occurrence of the ferroelectric hysteresis loop, which will be discussed later. An important class of ferroelectric materials includes compounds of the general formula ABO_3. The structure of these materials, known as perovskite, is formed in such a way that the oxide ions,

together with the A cations, form a 'face-centred cubic (FCC)' array, with the B cation occupying the octahedral site formed by the face-centered oxide ions, in the middle of the cube, as shown in Figure 1.1.

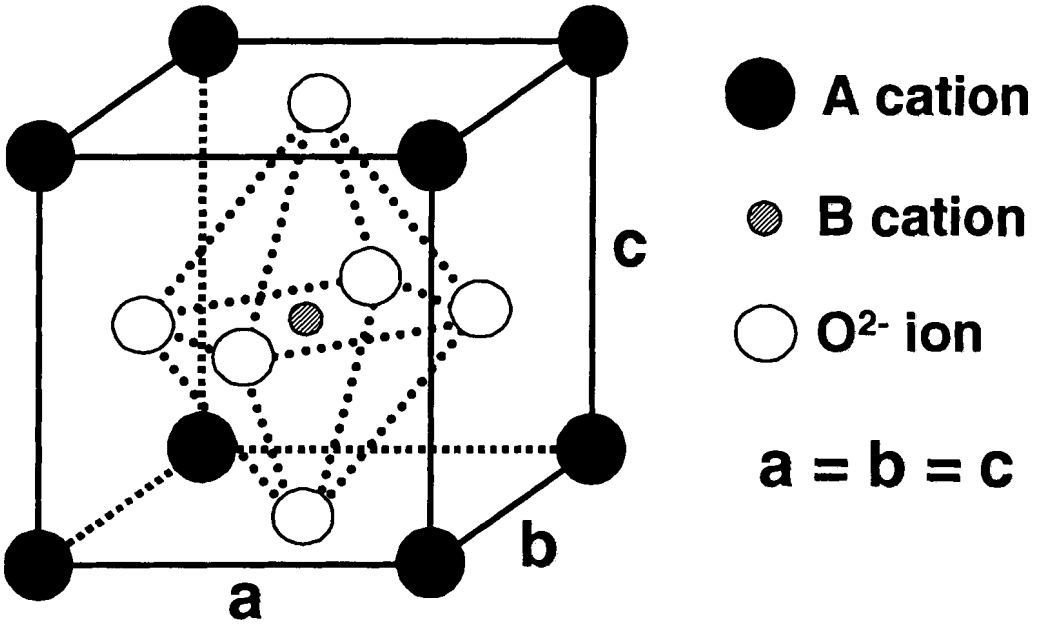

Figure 1.1: The cubic perovskite structure of ABO_3.

In a ferroelectric like lead titanate ($PbTiO_3$), where Pb^{2+} is the 'A' cation and Ti^{4+} is the 'B' cation, the structure below the Curie temperature, T_C = 490°C, is not like that of the ideal perovskite shown in Figure 1.1. In this material, the Ti^{4+} ion, instead of sitting at the center of the octahedron, is slightly displaced off-center by ~ 0.3 Å, towards one of the apical oxide ions. The Pb^{2+} ions are also shifted by about 0.47 Å along the c-direction with respect to the oxygen octahedron. These displacements lead to the formation of dipole moments due to charge separation because the centres of positive and negative charges do not coincide. There are two possible ground orientation states for

polarization, the +P and -P states. In other words, a ferroelectric material remains in thermal equilibrium in either of these states. It is possible to switch between these two stable states by the application of an external electric field. As can be seen from the potential energy diagram in Figure 1.2, the two possible orientations are at the same energy level, and in order to switch between them, an energy barrier has to be overcome for activation.

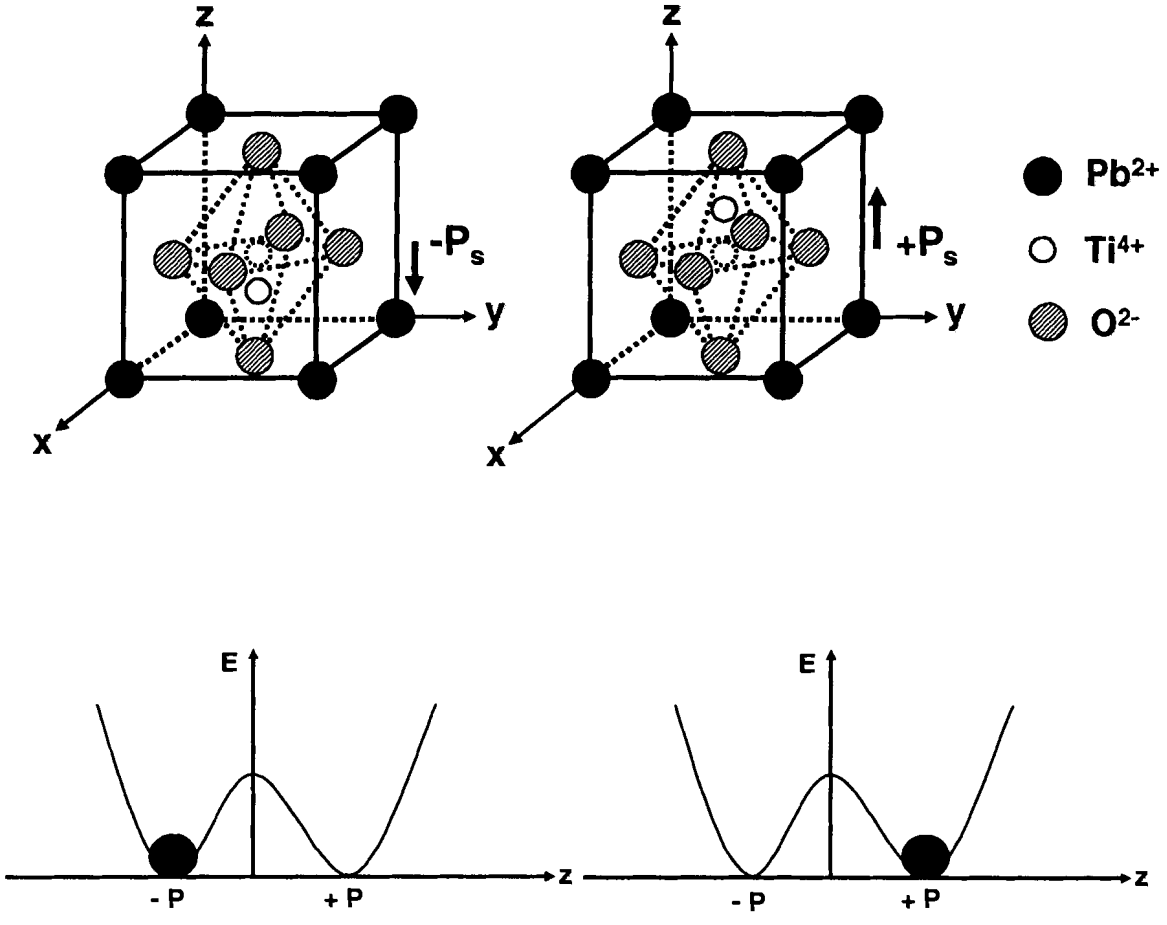

Figure 1.2: The two ground polarization orientation states in ferroelectrics.

$PbTiO_3$ has therefore, a spontaneous polarization, P_S, below its T_C. This displacement occurs in all the octahedra, but the direction of polarization differs, depending on the direction in which Ti^{4+} is displaced, i.e., either along the a, or b, or c axis. This is what causes the formation of small regions called domains, and within each of these domains, the Ti^{4+} in adjacent TiO_6 octahedra are displaced along a common axis, i.e., in the same direction.

When an electric field is applied to the ferroelectric lead titanate, individual dipoles in different domains are forced to align themselves in the direction of the field, until eventually, all Ti^{4+} are displaced in the same direction. At this stage, there is *saturation polarization,* P_{sat}.. Thus, as the magnitude of the applied electric field is increased, polarization increases as the domain walls move, until a point of saturation is reached where all the dipoles are oriented along the same direction. The movement of the domain wall under the application of electric field is illustrated in Figure 1.3.

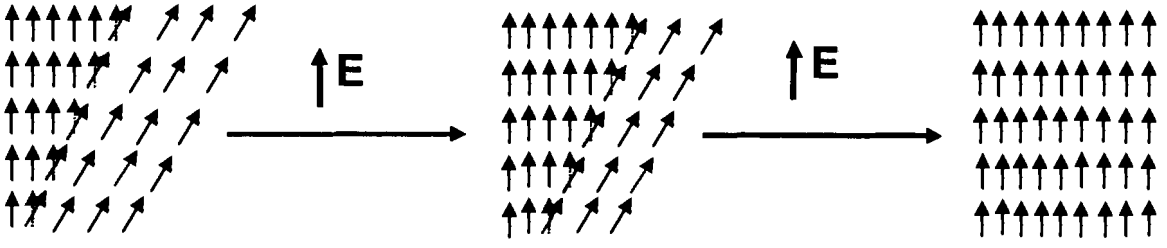

Figure 1.3: Movement of domain wall under the application of an external electric field.

As the magnitude of the applied field is decreased, the amount of polarization also decreases but does not reach zero when the electric field is completely removed. Instead, there is a residual polarization, called the *remnant polarization*, P_r, which is retained by the energy barrier in the material as the voltage, V, is reduced to zero after saturation [1]. To bring the polarization to zero, a *coercive field,* E_c, which is a reverse field, is needed. By continuing to increase the magnitude of the reverse field, all dipoles are caused to switch and re-orient themselves in the opposite direction. Hence, polarization increases again, but in the reverse direction, until an equal but opposite saturation polarization, $-P_{sat.}$, is attained. As the applied voltage is brought back to zero, polarization also decreases, but reaches $-P_r$, which is the value retained after the electric field is switched off. These processes explain the occurrence of hysteresis in ferroelectric materials, as shown in Figure 1.4. In summary, ferroelectrics are those materials (e.g., single crystals, liquid crystals, or polycrystalline ceramics) whose spontaneous electric polarization can be reversed by the application of an external electric field larger than the coercive field, E_C, but smaller than the breakdown field, E_B [3] (If the voltage applied across the dielectric material is too high, electrons are pulled away from their atoms and they flow across the material causing the capacitor to discharge. This causes damage to the material. Each dielectric material can support a given maximum electric field, E_{max}, without breakdown). Ferroelectrics are different from pyroelectric materials although they both belong to the non-centrosymmetric group and possess a spontaneous polarization. The direction of polarization in pyroelectric materials which do not belong to the ferroelectric class cannot be reversed by the application of an external field because it is often restrained by the lack of bi-stable structure. The spontaneous polarization in

both pyroelectrics and ferroelectrics is usually temperature dependent, which is the origin of the pyroelectricity. Therefore, ferroelectrics are necessarily pyroelectrics, but the reverse is not true.

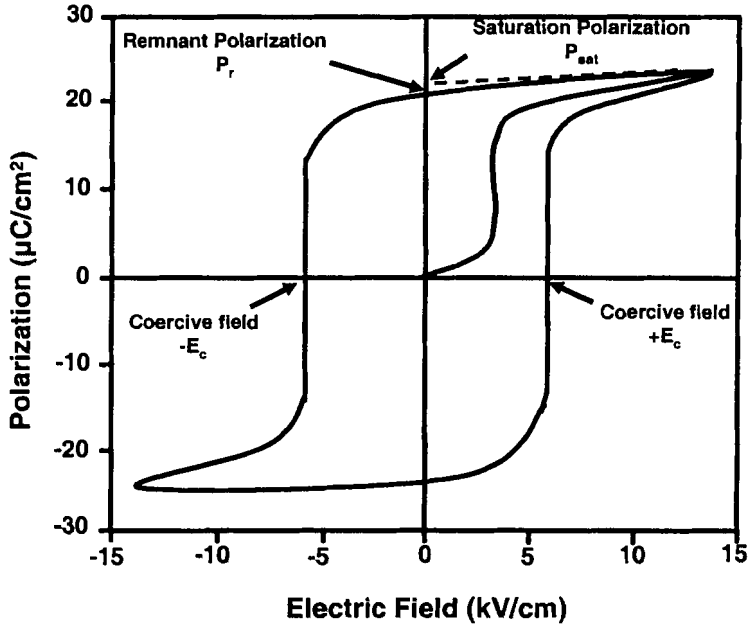

Figure 1.4: Relationship between polarization and applied electric field of a ferroelectric material, giving rise to a P(E) hysteresis loop.

Ferroelectric materials lose their ferroelectric properties above a critical temperature, T_C, called the Curie point, which is the temperature at which the materials undergo a transition from a ferroelectric to a non-ferroelectric (paraelectric) phase. For example, $PbTiO_3$ (PT) has a T_C of 490 °C, meaning that at this temperature, it undergoes a structural change from a ferroelectric phase with tetragonal symmetry to a paraelectric phase with cubic symmetry upon heating [4]. Therefore, the ferroelectricity in the material disappears above T_C.

Based on their dielectric, polarization, and phase transition behavior, ferroelectrics can be classified into three categories: (i) normal ferroelectrics; (ii)

ferroelectrics with a diffuse phase transition; and (iii) relaxor ferroelectrics (or relaxors) [1,5]. Normal ferroelectrics show a sharp anomaly in the dielectric permittivity at the Curie temperature, T_C, which points to a phase transition and hence the vanishing of the spontaneous polarization (upon heating). Ferroelectrics with a diffuse phase transition show a broadening of the dielectric peak which is caused by different kinds of cations being distributed over the 'B' sites of the perovskite structure. On the other hand, relaxors exhibit a broad and frequency-dependent dielectric permittivity peak. With an increase in frequency, the dielectric maximum, ε'_{max}, decreases and the temperature, T_{max}, at which this maximum permittivity is observed, experiences an increase. Figure 1.5 shows the difference in the temperature and frequency dependences of the dielectric constant, ε', between a normal ferroelectric and a relaxor.

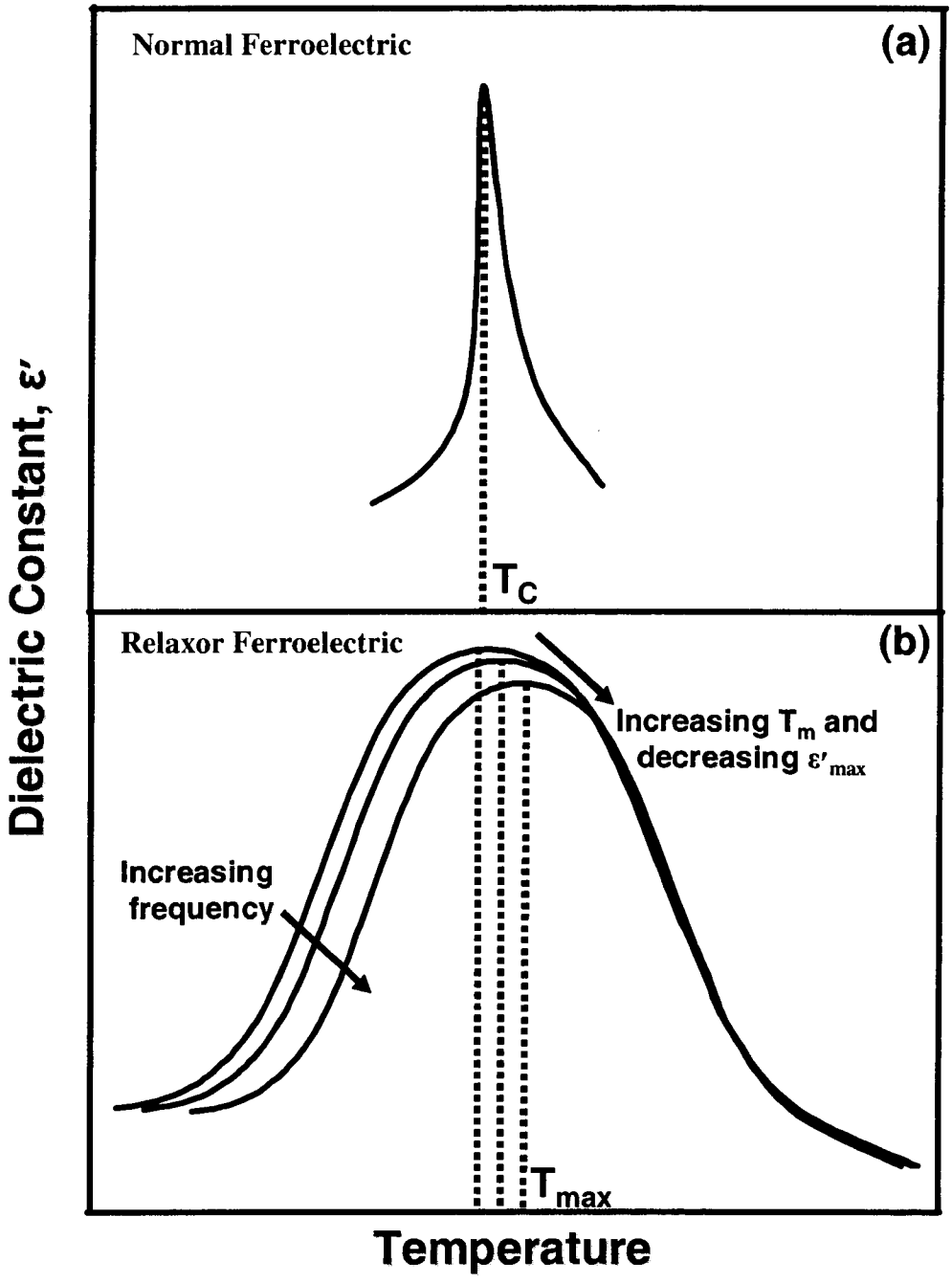

Figure 1.5: (a) Dependence of the dielectric constant, ε′, on temperature, in normal ferroelectric materials; (b) Temperature and frequency dependences of ε' in relaxor ferroelectrics, with the maximum dielectric constant, ε'_{max}, decreasing, and its temperature, T_m, increasing as frequency increases.

The three main physical characteristics possessed by ferroelectrics, namely the switchable spontaneous polarization, the polarization – structure relationship, and the high dielectric permittivities, make them a class of technologically very important materials [6]. First of all, the ability of the ferroelectric materials to switch polarization direction between two stable states forms the basis for binary code-based non-volatile ferroelectric (FE) random-access memories (the two polarization states which are directed in opposite directions represent the '0' and '1' data bits in these memory devices). Ferroelectrics also display piezoelectricity which is a phenomenon that allows these materials to convert mechanical energy into electrical energy and vice versa. This characteristic can be made use of in micro machines such as accelerometers, displacement transducers (sensors and actuators) of different kinds including those required for inkjet printers, VCR head positioning, and medical ultrasonic imaging probes. The other remarkable property of ferroelectric materials is their very high dielectric permittivity values, which have been widely explored in high energy-density miniaturized multilayered capacitors. The high dielectric constant also makes them very important candidates in dynamic random access memory (DRAM) storage capacitors. Ferroelectric materials can also exhibit pyroelectricity which makes them important for use in highly sensitive infrared detectors. In addition to these properties, ferroelectrics show electro-optic activity and non-linear optical effects, making them useful in lasers, computer displays, color filter devices, image storage systems, and optical switches for integrated optical systems [6].

1.2 Relaxor Ferroelectric Materials

Relaxor ferroelectric materials typically exhibit a broad maximum and a significant frequency dispersion of the dielectric permittivity, as depicted in Figure 1.5 (b). Occurring mainly in two families of mixed compounds, such as (i) complex perovskite structure of $A(B'B'')O_3$ composition, and (ii) tungsten-bronze structure of $M_{1-x}Ba_xNb_2O_6$ composition, the relaxor behavior and materials have been extensively studied over the past few decades [7]. Relaxors display a remarkably high value of maximum dielectric permittivity (ε'_{max}) at the temperature T_m, but the dielectric maximum does not relate to any phase transition into macroscopic ferroelectric phase [8]. An increase in the value of T_m is observed with increasing frequency, and the related maximum in the imaginary part of permittivity (ε''_{max}) shows typical behaviour of a relaxational dielectric. The relaxor ferroelectrics also show the characteristic ferroelectric hysteresis loop which in contrast to normal ferroelectrics does not vanish suddenly at the temperature of maximum permittivity, but instead decays more gradually as the temperature is increased. It is now understood that the appearance of a dielectric hysteresis loop in relaxors is in fact due to induced ferroelectricity (induced by the application of an applied external field) [9]. In addition, the relaxors show no optical anisotropy and no splitting of X-ray lines, characteristic of a transition into a lower symmetry (polar) phase, upon cooling. The difference between normal ferroelectrics and relaxors in terms of dielectric permittivity versus temperature and frequency is illustrated in Figure 1.5.

Complex perovskite $Pb(Mg_{1/3}Nb_{2/3})O_3$ [PMN] is a prototypical and thereby the most studied relaxor compound. In PMN the Pb^{2+} ions occupy the A-sites while the B-sites are occupied by two types of ions namely, Mg^{2+} and Nb^{5+}. Therefore, there is a

random distribution of these two types of ions over the available octahedral sites in the perovskite structure (If we recall from section 1.1, the B-sites in $PbTiO_3$ are occupied by only one type of ion, i.e., Ti^{4+}). This random distribution of different types of ions over the same sites gives rise to a compositional disorder and thereby a phase transition region with different local Curie temperatures depending upon the relative concentration of the B-site ions, rather than a phase transition point (as is the case for the normal ferroelectric, $PbTiO_3$). This description, although oversimplified, can explain the broadening of the dielectric permittivity peak and the smearing of phase transition.

Recently, the relaxor behaviour has been shown to be related to the presence of polar nanodomains in the disordered ferroelectrics. It is the slowing down of the dipolar fluctuations (dynamics) within the polar nanodomains at lower temperatures that gives rise to the strong frequency dispersion in the real part of dielectric permittivity [9]. When the temperature is further lowered all the dipolar motion freezes and hence, no more dispersion is observed. Bokov and Ye have recently found a universal relaxation law that describes the dielectric relaxation in PMN and related relaxor materials in which the degree of ferroelectric ordering varies [10,11]. Based on the dielectric spectroscopy results, they have described the universal relaxor polarization using a microscopic model which consists of 'soft' polar nanoregions (PNR) [12]. The unit cells of these PNRs can freely orient themselves in different direction but the direction of the total moment remains the same.

A considerable amount of work was carried out in the past years in order to explain the relaxor ferroelectric behaviour and in the process, various models have been put forward, which include the composition fluctuation model [13], the superparaelectric

model [7], the dipolar glass model [14] and the random field model [15]. Of all these models, the most widely accepted is the one by Smolenskii and Isupov, which explains the formation of polar micro regions by the existence of composition fluctuations in the relaxor ferroelectrics. Many ferroelectric compounds which have a complex oxygen-octahedral composition show diffuse phase transitions [16]. A complex oxygen-octahedral composition means that different types of ions can occupy the same sites in the structure (e.g., in PMN, as described earlier). Smolenskii and co-workers suggested that composition fluctuations which arise because of a random distribution of cations in their sublattices, are the cause of the difference in ferroelectric properties and the diffuseness of phase transitions [13].

Isupov further developed and discussed the concepts and the properties of materials with diffuse ferroelectric phase transitions (DFEPT) [17]. For the purpose of discussion, the prototypical material with diffuse ferroelectric phase transition, PMN, was chosen. In an earlier work on the solid solution of the $(1-x)BaSnO_3$–$xBaTiO_3$ system, which contains more than one type of ions on the octahedral sites in the lattice, the dielectric permitttivity ε' (T) was found to broaden as the concentration of $BaSnO_3$ was increased [18]. This behaviour suggests that the ferroelectric phase transition is made up of a number of local phase transitions resulting from frozen composition fluctuations and varying local Curie temperatures. By analogy, in the complex perovskites with DFEPT, such as PMN, the Mg^{2+} and Nb^{5+} ions are randomly distributed over the B sites. Because of the difference in charges on these cations, each unit cell carries an overall charge and this results in intrinsic electric fields existing in the material. These fields are random and they are frozen because of the frozen composition inhomogeneity. The unit cells in PMN

can also have a permanent dipole moment and because of their random orientation, these dipoles can either cancel each other or they can add up forming a group of unit cells with a larger net dipole moment. There exist different micro-regions because of the difference in the concentration of the Mg^{2+} and Nb^{5+} ions. Therefore, each micro-region has a different local Curie temperature which makes PMN display a broad ε'_{max} rather than a sharp one like in the case of normal ferroelectrics. When the material is cooled down from a temperature higher than the temperature at which ε'_{max} occurs, a polar region (PR) of overcritical size with a ferroelectric dipole moment appears in the paraelectric matrix possessing the highest local Curie temperature. Unlike in the case of normal ferroelectrics, this PR does not grow. However, upon further cooling, the number of PRs increases and these accumulate in the paraelectric matrix. This model was further improved by Isupov by stressing on the fact that deformed paraelectric layers do exist in between the PRs and they play a very important role on the appearance and disappearance of the macro-domain state [19].

Ferroelectric relaxors have displayed considerable importance in electric and microelectronic applications such as multilayered compact capacitors for use in high density random access memory devices because of their remarkably high dielectric permittivity and broad dielectric maxima [7,9,20,21]. The relaxor materials have also been used in precision electrostrictive actuation and positioning [22,23]. Lead-based perovskites having complex compositions with general formula $Pb(B'B'')O_3$, e.g., $Pb(Mg_{1/3}Nb_{2/3})O_3$ (PMN) and related compounds, make up most of these materials, with PMN being, by far, the most studied and documented relaxor compound [24].

1.3 Ferroelectrics – Relaxor Ferroelectrics Solid Solutions

When a normal ferroelectric such as $PbTiO_3$ (PT) is mixed and reacts in varying amounts with a relaxor ferroelectric, e.g., $Pb(Mg_{1/3}Nb_{2/3})O_3$ (PMN), the resulting solid solution $(1-x)Pb(Mg_{1/3}Nb_{2/3})O_3–xPbTiO_3$ [(1-x)PMN–xPT] is formed. This solid solution system combines the properties of both the normal and the relaxor ferroelectric materials. The absence of ferroelectric long-range order because of frustration of local polarization in relaxor ferroelectrics results in no phase transition into a macroscopic ferroelectric phase at the temperature of maximum permittivity in the absence of an electric field [7,8]. PMN exhibits a broad and diffuse dielectric permittivity peak at T_m = -15 °C while PT has a normal and sharp ferroelectric phase transition at the Curie temperature, T_C = 490 °C and a long-range ferroelectric ordering below T_C. The formation of the solid solutions between these two compounds has the effect of lowering the T_C of PT and increasing the Tm of PMN. With increasing PT content in PMN–PT, a long-range ferroelectric ordering develops. This is due to the substitution of Ti^{4+} ions for the complex $(Mg_{1/3}Nb_{2/3})^{4+}$ on the B site of the perovskite structure. Such solid solutions with appropriate amounts of PT present, display very high dielectric and piezoelectric properties, making them excellent candidates for a wide range of applications. Therefore, by adjusting the composition of the PMN–PT system, desired high performance can be achieved. While the compositions with lower PT contents give rise to materials with high dielectric constants and low remnant polarization at room temperature, suitable for dynamic random-access memory (DRAM) devices, those with higher PT contents have low dielectric constants and high remnant polarization [25]. Compositions around the morphotropic phase boundary (MPB) display excellent piezoelectric properties in the form of single crystals. An MPB

separates two phases which are energetically similar but structurally different [26], and in the case of the PMN–PT system, it was initially reported to separate the rhombohedral (pseudo-cubic) and tetragonal phases at $x \approx 0.35$ as shown in Figure 1.6 (a) [27,28]. A great deal of work has been pursued in this field and it was recently discovered that a ferroelectric monoclinic phase exists between the rhombohedral and tetragonal phase [29-31] as illustrated in Figure 1.6 (b). Similar observation was made for the $PbZr_{1-x}Ti_xO_3$ (PZT) solid solution system [32].

Relaxor ferroelectric–ferroelectric solid solutions, especially the lead titanate based $(1-x)Pb(Zn_{1/3}Nb_{2/3})O_3–xPbTiO_3$ [PZN–PT] and $(1-x)Pb(Mg_{1/3}Nb_{2/3})O_3–xPbTiO_3$ [PMN–PT] systems, have been found to have high values of piezoelectric strain (> 1 %) and a large electromechanical coupling factor (k_{33} > 90 %) [33,34]. The MPB compositions in PMN–PT possess large values of piezoelectric coefficient, d_{33} (2500 pC/N), much higher than that of PZT ceramics (widely used in piezoelectric devices for a long time now) [35], hence making them the next generation of piezoelectric materials for a wide range of electromechanical applications, e.g., in ultrasound imaging and diagnosis, in active vibration and noise control, and in undersea communication [35-37].

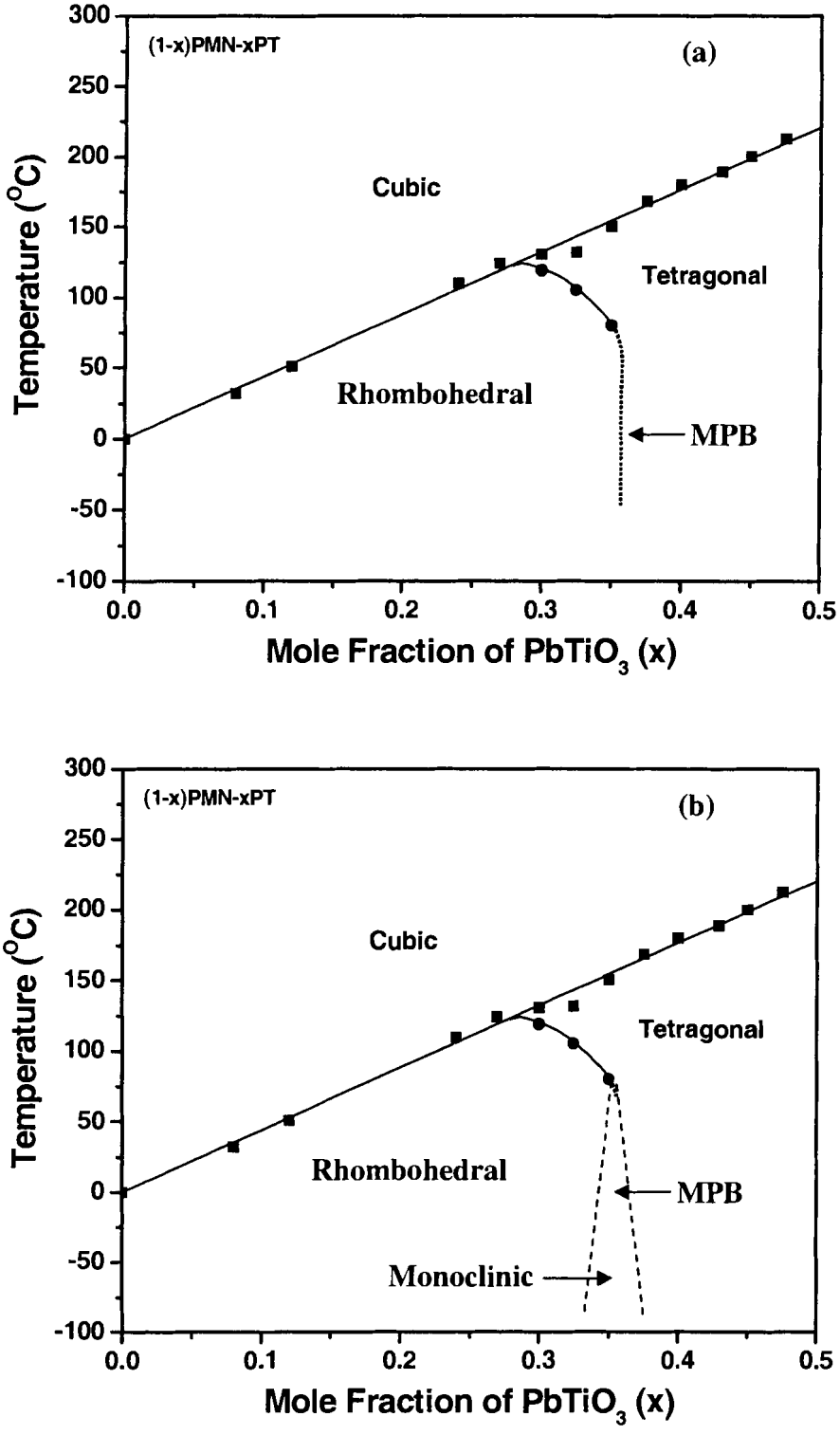

Figure 1.6: Phase diagram of the (1-x)$Pb(Mg_{1/3}Nb_{2/3})O_3$ – x$PbTiO_3$ solid solution system (a) initially reported [36]; (b) recently updated [30,31].

1.4 Perovskites and Layer–Structured Perovskites

Perovskite is a very important type of structure, which is represented by the general formula ABO_3 having a primitive cubic unit cell [2,38,39]. The perovskite structure can also be described as being made up of a framework of corner-sharing BO_6 octahedra and of dodecahedral sites which host the A ions. The A-type ions can be rare earth, alkaline earth, alkali, and large cations such as Pb^{2+} and Bi^{3+}. On the other hand, the B ions occupying the octahedral sites of the structural framework can be 3d, 4d, and 5d transition metal ions. Structural distortions occur in many of the perovskite materials because the A and/or B cations are not exactly of the right size to fit into their respective sites, thus giving rise to a variety of lower-symmetry structures in which the BO_6 octahedra are either twisted or distorted. These structural distortions are valuable because they exhibit very interesting and useful properties, such as ferroelectricity.

The stability of the perovskite structure depends on the tolerance factor, **t**, given by

$$\mathbf{t = (R_A + R_O)/\sqrt{2}\,(R_B + R_O),}$$

where R_A, R_B, and R_O = ionic radii of A, B, and oxygen ions, respectively. The tolerance factor is a measure of the degree to which the structure deviates from that of an ideal cubic perovskite. The values of t in the range of 0.9 – 1.0 is commonly observed for cubic perovskite forms. If $t > 1$, it means that the B ion is too small for the octahedral site of the perovskite structure. Therefore it will prefer a much smaller site of lower coordination number, and this makes the perovskite structure collapse with a structural change. However, a t value just slightly greater than 1 results in structural distortions but still maintains the perovskite structure. The tolerance factor values in the range of 0.85 – 0.90

also lead to some structural distortions whereby the A ion now requires a smaller site. If t < 0.85, the distorted structures are no longer the perovskite structure anymore, e.g., the ilmenite, $FeTiO_3$, in which both cations are in a 6-coordination environment.

There are also a number of perovskite-like materials, which consist of the basic perovskite cell sandwiched between layers such as oxides of alkaline earth metals. This gives rise to a number of possible stacking sequences. Furthermore, a fairly large amount of partial substitution and non-stoichiometry can be tolerated by perovskite compounds, whereby cations of different valences can replace both A and B ions.

The large varieties of structures and compositions of perovskite materials have attracted considerable interest both in applied and fundamental areas of solid state chemistry, physics, advanced materials, and catalysis. Perovskites find a number of applications that include multilayer capacitors, piezoelectric transducers, and electrostrictive actuators [2]. Synthesis of perovskite compounds can be very challenging because the method of synthesis should be one that produces a material that has all the properties that meet the requirements for end use [38]. More precisely, if the compound has to be mechanically strong for application then it has to be sintered at high temperature during the synthesis process in order to make it very dense and to minimize surface area. On the other hand, if the same compound is to be used for catalytic applications, then the synthetic approach needs to be modified so that a high surface area is maintained in the final compound. Therefore, based on the application of the perovskites, a number of synthetic approaches exist ranging from solid state reactions to soft chemical techniques such as the sol-gel process and the co-precipitation methods.

A class of perovskites which is very common is termed as the layered perovskite compounds. As the name suggests, these materials consist of perovskite slabs which are separated by a metal-oxide layer [39]. The layered perovskites are good candidates for important technological applications, such as non-volatile computer memories, and oscillators and filters in microwave communication devices, etc., because of their very interesting features like photocatalytic activity, ionic conductivity, dielectric, ferroelectric, magnetic, luminescence, and intercalation properties [39]. The layer–structured perovskites and their derivatives differ from normal perovskites by a relative excess of anion. The bismuth containing layered perovskites were first discovered by Aurivillius and are therefore known as the Aurivillius family of compounds [40]. They have the general formula $Bi_2A_{n-1}B_nO_{3n+3}$, in which the A cations can be Bi^{3+}, Ba^{2+}, Sr^{2+}, K^+, Ca^{2+}, Na^+, Pb^{2+}, or many rare earth metal ions, and the B cations can be transition metal ions such as Ti^{4+}, Nb^{5+}, Ta^{5+}, Fe^{3+}, Cr^{3+}, and W^{6+}. The structure is made up of $(Bi_2O_2)^{2+}$ layers which alternate with n $(A_{n-1}B_nO_{3n+1})^{2+}$ perovskite slabs. Compounds with n values ranging from 1 – 5 have been synthesized [41-44]. The compositional flexibility of the perovskite blocks in the Aurivillius structures to incorporate various cations on the A and B sites makes it possible to modify their ferroelectric and related properties based on their chemical composition.

The bismuth layer structured compounds $SrBi_2Ta_2O_9$ [SBT] (an Aurivillius compound with A = Sr^{2+}, B = Ta^{5+}, and n = 2) and $Bi_4Ti_3O_{12}$ [BIT] (with A = Bi^{3+}, B = Ti^{4+}, and n = 3) have attracted much attention recently because of their interesting ferroelectric, piezoelectric, and pyroelectric properties [45-48]. Although structurally similar, SBT and BIT do not have the same ferroelectric properties. SBT is well known

for its fatigue resistance (shows retention of polarization even after being subjected to a large number of repetitive polarization switching cycles) and it is therefore a potential candidate for application in non-volatile ferroelectric memory devices. It has significant advantages over the lead-based ferroelectric materials such as $Pb(Zr_xTi_{1-x})O_3$ (PZT) which suffers from serious fatigue problems [49,50]. It is widely believed that the $(Bi_2O_2)^{2+}$ layers in SBT seemingly play an important role in suppressing fatigue in the material. The net electrical charge of the bismuth oxide layers and their position in the structure compensate for the space charges that cause fatigue by accumulating at the sample-electrode interface [49]. Although BIT has high remnant polarization value attractive for ferroelectric random access memory applications, it is not fatigue-free [51]. This observation is interesting because it points to the fact that the charge compensating role of the $(Bi_2O_2)^{2+}$ layers might not be enough to make the material resist to polarization degradation upon repetitive switching cycles. Using X-ray photoemission spectroscopy (XPS) it was then demonstrated that the oxygen ion stability in the SBT and BIT structures plays an important role in determining fatigue behavior [52]. As can be seen from the structures of SBT and BIT in Figure 1.7 (a) and (b) respectively, the two compounds differ in their chemical compositions and the number of perovskite slabs separating the bismuth-oxygen layers. It was found that the oxygen ions near strontium in the $(SrTa_2O_7)^{2-}$ layer of SBT are more stable than those near bismuth in the $(Bi_2O_2)^{2+}$ layer, which leads to the presence of oxygen vacancies in the bismuth-oxygen layers [52]. In the case of BIT, the oxygen ions in the vicinity of Ti^{4+} are not very stable and could be easily lost so that oxygen vacancies are formed both in the bismuth-oxygen layers and in the perovskite slabs. The oxygen vacancies in the titanium–oxygen octahedra may disrupt

the ferroelectric responses coming from the perovskite blocks, and hence, result in fatigue.

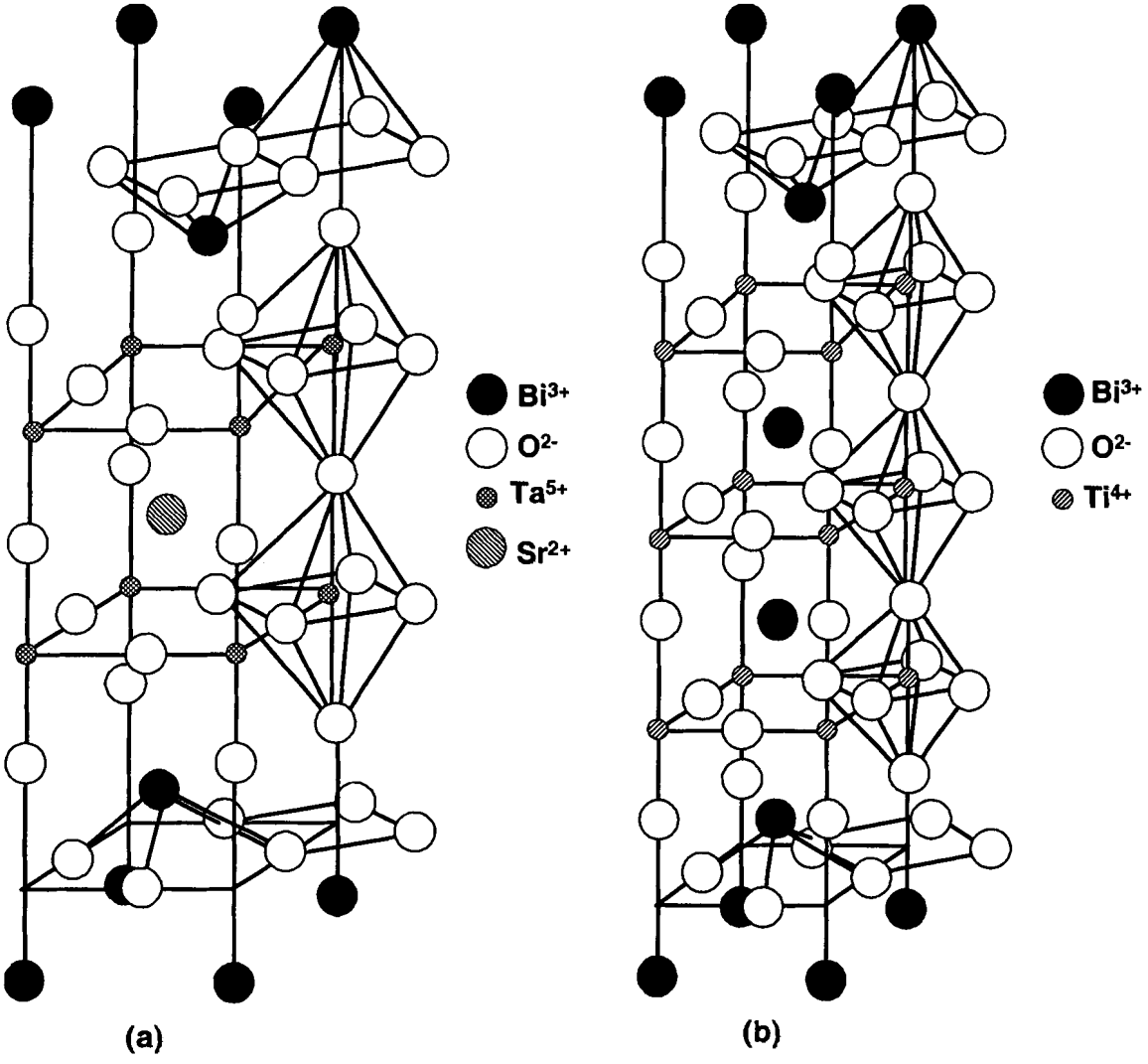

Figure 1.7: Crystal structures of the bismuth-containing layered perovskites (a) $SrBi_2Ta_2O_9$ (SBT) and (b) $Bi_4Ti_3O_{12}$ (BIT).

1.5 Soft Chemical Synthesis – The Sol-Gel and the Co-Precipitation Methods

Soft chemical routes to mixed oxide compounds are based on transformations that take place in solution. Of these chemical techniques, the sol-gel processing has gained considerable attention and popularity recently. Developed in 1845 by M. Ebelman who made the first silica gels, this technique has extensively been employed in the synthesis of inorganic mixed oxides because of the numerous advantages it offers over the conventional solid state reactions [53]. Sol-gel processing has highlighted the importance of chemistry in the fabrication of materials starting from chemical precursors. It was not before 1950 that the first non-silicate ceramics, the perovskites, were synthesized using the sol-gel process. In the last two decades, this soft chemistry technique has attracted considerable interest and has known major development in the synthesis of mixed oxides in the form of glass, ceramics, as well as thin films. Using the sol-gel methodology, the syntheses of high purity submicron powders, electronic and ionic conductors, and ferroelectric and magnetic materials have been accomplished [53,54].

The conventional processing of perovskites and perovskite-related materials is usually carried out by solid state reactions of metal carbonates, hydroxides, and oxides. These reactions require long-time grinding and also high temperature treatment so that the starting ingredients are provided with sufficient energy to come together and react. This process may lead to the formation of multi-phases in the final compound because of incomplete reaction. The final product, if not homogeneous, suffers a decrease in its performance. At the high reaction temperature, there is also loss of volatile components, e.g., PbO volatilization from lead-containing compounds, which changes the

stoichiometry, and degrades the property of the final material. The ability to mix (and dissolve) the starting materials, commonly metal alkoxides, homogeneously in solution is one of the major benefits of the sol-gel processing method [55].

The very first thing in this type of processing is the formation of a homogenous solution containing all the necessary cationic ingredients in the desired stoichiometry. Therefore, it is very important to choose the right solvent that is capable of effectively dissolving all the starting chemicals in question. Once the reactants are well-mixed at the molecular level, the next step towards forming a network of oxide in solution through polymerization of the dispersed constituents becomes a lot easier. Broadly speaking, the sol-gel method consists of polymerization reactions which are based on the hydrolysis and condensation of metal alkoxides $M(OR)_n$, where M is a metal having an oxidation state of n^+ and R is an alkyl group. Briefly, in the first step of the reaction, the metal alkoxide is hydrolyzed by a water molecule. Once the hydrolysis step has been initiated, the next reaction that follows is condensation of the hydrolyzed molecules to produce M–O–M linkages or networks. Further condensation reactions can then take place, leading to the formation of longer chains or oligomers. The processes can be summarized in the reaction sequence in Figure 1.8. The formation of more extended networks in the sol through further polymerization of the chains and oligomers then causes gelation to occur. The homogeneous network of M–O–M units then decomposes at a much lower temperature to give the desired inorganic oxide than is required in solid-state reactions. One of the key features of sol-gel methods is the ability to produce small particle sizes, as small as on the nanometer scale. The precursor powder obtained by the decomposition of

the homogeneous gel is actually much finer than powders obtained by the solid state reactions and this explains the increased reactivity of the former [54].

In summary, when compared to solid state synthesis, the sol-gel process offers better control of stoichiometry and homogeneity, higher purity and reactivity of the precursor powders, and significantly reduced temperature of ceramic densification. By allowing the preparation of stable sols, the sol-gel method also opens opportunities to the fabrication of thin and thick films through, e.g., spin-coating method. However, the main disadvantages of the sol-gel process are the cost of the metal alkoxide precursors, and the complexity in the processing.

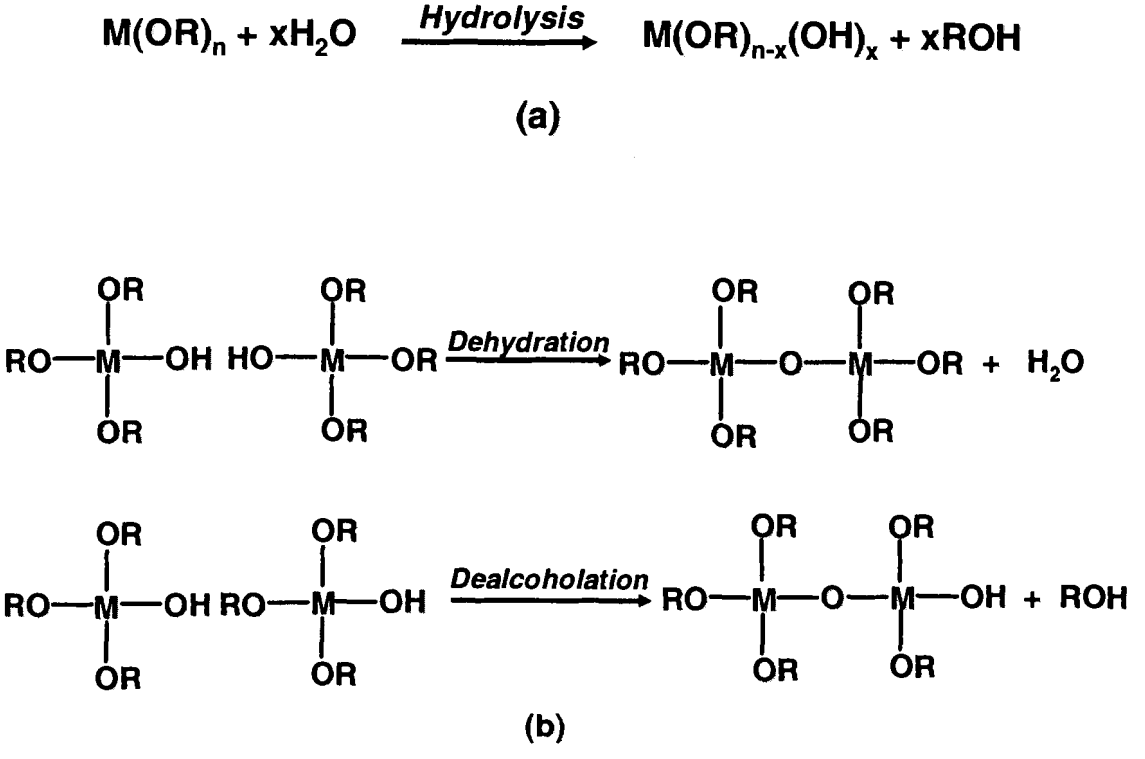

Figure 1.8: (a) Hydrolysis of metal alkoxides, and (b) Condensation of the hydrolyzed species through dehydration or dealcoholation steps.

The sol-gel method is among one of the many soft chemistry methods available for the synthesis of ceramic materials. The co-precipitation method, often referred to as the solid state analogue or a side-branch of the sol-gel process, is another efficient soft chemical route to mixed oxide materials [2]. Briefly, this method begins with a solution of dissolved precursors in a common solvent to which a precipitating agent is added to form a homogeneous and single phase inorganic solid. The precipitate is decomposed at a high temperature to produce the target mixed oxide material. The starting materials can be simple metal salts that can easily be dissolved in water or other appropriate solvents.

Figure 1.9 illustrates the synthesis of the complex metal oxide, $FeCr_2O_4$, by the co-precipitation method. The first step involves dissolving an iron (III) salt and a chromate in water to obtain Fe^{3+} and CrO_4^{2-} ions in solution. These ions are then precipitated in a complex form by an ammonium solution (NH_4^+), and the resulting precipitate can be decomposed at a high temperature into the target $FeCr_2O_4$.

$$Fe^{3+} + 2CrO_4^{2-} + NH_4^+ \longrightarrow \underset{\text{Precursor to } FeCr_2O_4}{NH_4Fe(CrO_4)_2}$$

$$2NH_4Fe(CrO_4)_2 \xrightarrow{1150\ ^oC} 2FeCr_2O_4 + 2NH_3 + H_2O + 7/2\ O_2$$

Figure 1.9: Synthesis of $FeCr_2O_4$ by the co-precipitation method.

1.6 Objectives of this study

The main topic of this research work is the development of new soft chemistry routes for the synthesis of ferroelectric and relaxor ferroelectric materials, and the characterization of the structural physical properties of the materials synthesized. The objectives consist of the following:

(i) Synthesis and characterization of dielectric and ferroelectric properties of (1-x)$Pb(Mg_{1/3}Nb_{2/3})O_3$–$xPbTiO_3$ [PMN–PT] (x = 0.10 and 0.35) ceramics synthesized using sol-gel processing,

(ii) Synthesis of layered perovskite ferroelectric $SrBi_2Ta_2O_9$ (SBT) by two soft chemical techniques, namely a sol-gel route and a co-precipitation method, and characterization of their dielectric and ferroelectric properties.

The rationales of these objectives are given as follows:

1.6.1 Sol-gel method for the synthesis and characterization of (1-x)PMN–xPT ceramics

As already addressed in the previous sections, the solid solutions of (1-x)PMN–xPT embrace a range of compositions and by varying the amount of PT, the material can be fine-tuned for a number of important applications. For instance, compositions with lower PT content behave more like a relaxor and therefore, have very high dielectric constant, and low remnant polarization at room temperature. On the other hand, PMN–PT systems with higher PT content, for example around the MPB, exhibit the largest piezoelectric coefficients [35].

The 0.65PMN–0.35PT composition is, therefore, very interesting because it lies near the MPB and displays exceptional dielectric and piezoelectric properties suitable for advanced electromechanical applications, both in the forms of electroceramics and thin films. It also displays excellent pyroelectric properties that could be exploited in thin-layer devices [26,30]. Moreover, the addition of 35 mol % of PT to PMN increases the T_{max} from -15 °C in PMN to around 175 °C in 0.65PMN–0.35PT, which makes the material suitable for a number of device applications.

On the other hand, 0.90PMN–0.10PT is a typical relaxor ferroelectric material due to the fact that this composition lies more on the PMN side of the phase diagram of the (1-x)PMN–xPT solid solution (Figure 1.6) [34]. This composition also displays a diffuse phase transition temperature (T_{max}) at ~ 40 °C and its dielectric constant at room temperature is very high (ε' ~10, 000). The high dielectric permittivity, narrow hysteresis loop and strong piezoelectric response of the 0.90PMN–0.10PT make it an excellent material for DRAM and multi-layer capacitor applications [25,56].

However, one of the biggest challenges encountered in the processing of PMN and related compounds, including the (1-x)PMN–xPT systems, is to eliminate the formation of a kinetically more favorable, but functionally undesirable pyrochlore phase which degrades the dielectric properties of the perovskite phase [57]. With a view to improving the desirable properties in these materials, a lot of effort has been put into trying to eliminate the unwanted pyrochlore phase of the chemical formula '$Pb_{1.5}Nb_2O_{6.5}$', which is a reaction product between Nb_2O_5 and PbO [57-60]. Therefore, to avoid prior reaction between these two components, the 'columbite route' was proposed for the synthesis of PMN in solid state reactions, and it involves two

calcinations steps [57]. These consist of first reacting MgO with Nb_2O_5 to form the columbite phase, $MgNb_2O_6$, which is then reacted with PbO to produce pure perovskite PMN (to make PMN–PT, $MgNb_2O_6$ is reacted with PbO and TiO_2). Although the columbite method is efficient in eliminating the pyrochlore phase, it still suffers from the drawback of two calcination steps which are both carried out at relatively high temperatures of 1000 °C and 900 °C, respectively. Moreover, to obtain ceramics with good dielectric and ferroelectric properties, sintering of the pressed powder at higher temperatures (> 1200 °C) is very important in order to make high density ceramics. However, at such elevated temperatures, another problem is the loss of PbO because of its high volatility. PbO loss from the sintered ceramics also has the effect of degrading the dielectric properties of the material. Therefore, to prevent the loss of PbO during sintering of ceramics, different methods have been tried which mainly include the use of packing powders, and the addition of an excess amount of the lead starting material to the reaction mixture [61]. Such practices have, to some extent, been successful in stabilizing the perovskite phase up to ~95 %. The use of excess lead can, however, result in PbO remaining at the grain boundaries, and this is known to degrade the properties of the PMN–PT systems [62,63].

Considering the difficulties met in the processing of PMN–PT, it is necessary to develop a method that can produce pyrochlore-free powders that are reactive enough to give high density ceramics at relatively low sintering temperatures, and soft chemical techniques are the answer to this. As discussed earlier (Section 1.5), the sol-gel method has a number of advantages over the conventional solid state reactions such as high homogeneity of the components at the molecular level, good control of stoichiometry,

and low processing temperature due to the high purity and reactivity of the precursor powders. Basically, in a sol-gel reaction the metal-organic precursors (typically alkoxides) need to be dissolved in a common solvent. Hydrolysis and condensation reactions then form extended arrays of M–O–M linkages in the sol or gel which prevent the metal ions from precipitating. This polymerization helps keep the mixture homogeneous. Therefore, a solvent that can chelate efficiently to the metal ions and/or act as a cross-linking agent is of great importance in sol-gel chemistry. Two new sol-gel routes were recently developed in our group for the synthesis of PMN–PT ceramics [64]. These methods use 1,3-propanediol as a solvent, which is believed to act as a crosslinking agent, leading to the formation of large oligomeric species. These methods, named as the 'two-step sol-gel' and the 'one-step sol-gel', were able to produce pure phase PMN–PT powders at relatively low temperatures of 850 °C and 750 °C, respectively. The density of ceramics sintered at 1050 °C reached ~91 % and showed pure perovskite phase.

We thought that developing a new solvent system with more metal ions binding sites and better crosslinking characteristics could improve the quality (uniformity of composition) of the sol and gel, and hence of the powder and ceramics. Therefore, the development of a new sol-gel route for the synthesis and characterization of (1-x)PMN – xPT (x = 0.10, 0.35) ceramics constitutes the first part of this research work. Our main goal is to study the formation of pure phase PMN–PT and to synthesize good quality ceramics with improved dielectric and ferroelectric properties in the materials. A new room temperature sol-gel method has been developed, which uses a polyethylene glycol 200 (PEG) and methanol mixture as solvent. The method takes advantage of the multiple binding sites on the PEG chains (hydroxyl groups and ether oxygen) to stabilize the metal

ions in solution. We have also studied the effect of adding a triol molecule, 1,1,1-tris(hydroxy)methylethane (THOME) to the sol-gel reaction. With its three hydroxyl groups, the THOME molecule is known to act as a good cross-linking agent by binding to up to three metal centers at one time and forming oligomeric species in solution. Our new method not only eliminates the reflux steps involved in conventional sol-gel reactions, but also does not require the use of an excess of the lead starting material in order to obtain pure phase PMN–PT ceramics.

Thermogravimetric analysis and differential thermal analysis (TGA/DTA), powder X-ray diffraction (XRD), Fourrier transform infrared spectroscopy (FTIR), scanning electron microscopy (SEM), dielectric spectroscopy, and ferroelectric testing are employed to study the thermal behavior, the phase formation and transformation, the reaction mechanisms, the microstructure, and the dielectric and ferroelectric properties.

1.6.2 Soft chemistry methods for the synthesis of $SrBi_2Ta_2O_9$ (SBT) ceramics and characterization of properties

A member of the Aurivillius family of the layered perovskites, $SrBi_2Ta_2O_9$ [SBT] has been identified as a 'fatigue-free' ferroelectric material and this characteristic has made it a very attractive candidate for application in non-volatile ferroelectric random access memory (NVFRAM) devices [65-67]. With a polarization retention even after 10^{12} switching cycles, SBT has outweighed the well-known $Pb(Zr_xTi_{1-x})$ [PZT] which has been used for decades in data storage applications [66,68]. Apart from its high lead content, which poses environmental concerns, PZT suffers serious fatigue degradation which leads to deterioration of its performance, accompanied by a shortened device lifetime. Therefore, the advantages of SBT as being both fatigue resistant and lead-free are to capture major interest.

To date, a number of different techniques have been employed for the synthesis of SBT thin films [69-73]. There are, however, few studies available on ceramics of this material, and most of these studies are focused on the solid state synthesis of SBT [74,75]. Solid state reactions are more tedious, requiring relatively high sintering temperature and long reaction times and often lead to secondary phases in the final compound. Recourse has been made to soft chemical routes such as the sol-gel process because of its previously mentioned advantages over the solid state reaction.

Therefore, the second part of this research work is devoted to the development of soft chemical routes for the synthesis and characterization of SBT ceramics. We choose to make ceramics of this compound because less attention has been given to this field and it is also very important to first study the bulk properties of any material to be able to

explore to full capacity the applications of the new method being developed. Given the fact that most sol-gel processes reported so far in the literature for the synthesis of SBT commonly use 2-methoxyethanol, a known teratogen, as solvent, our aim is to design new solution-based methods that use less harmful solvents [76]. In that respect, we have successfully developed two new soft chemical routes namely a sol-gel and a co-precipitation method to synthesize pure phase SBT ceramics at a calcination temperature as low as 750 °C. Ethylene glycol was employed as solvent in the sol-gel process while a mixture of PEG and methanol proved to be the right solvent for the co-precipitation method. Of the two approaches, the sol-gel route produced ceramics with better dielectric and ferroelectric properties, while ceramics obtained from the co-precipitation method interestingly show remarkable preferential grain orientation just through normal sintering procedure.

The phase formation, the microstructure, the dielectric and ferroelectric properties are studied using powder X-ray diffraction (XRD), scanning electron microscopy (SEM), dielectric spectroscopy, and ferroelectric testing, respectively.

1.7 References

1. M. E. Lines, and A. M. Glass, *Principles and Applications of Ferroelectrics and Related Materials*, Clarendon Press, Oxford (1977).
2. A. R. West, 'Basic Solid State Chemistry', 2nd edition, John Wiley & Sons Ltd., (1996).
3. Y. Xu, *Ferroelectric Materials and Their Applications*, North Holland (1991).
4. G. Shirane, and S. Hoshino, *J. Phys. Soc. Jpn.*, **6**, 265 (1951).
5. L. E. Cross, *Ferroelectrics*, **151**, 305 (1994).
6. N. A. Spaldin, *Science*, **304**, 1606 (2004).
7. L. E. Cross, *Ferroelectrics*, **76**, 241 (1987).
8. Z.-G. Ye, *Ferroelectrics*, **184**, 193 (1996).
9. Z.-G. Ye, *Key Engineering Materials*, **155-156**, 81 (1998).
10. A. Bokov, and Z.-G. Ye, *J. Phys.: Condens. Matter,* **12**, L541 (2000).
11. A. Bokov, and Z.-G. Ye, *Phys. Rev. B.*, **65**, 144112 (2002).
12. A. Bokov, and Z.-G. Ye, *Phys. Rev. B.*, **66**, 064103 (2002).
13. G. A. Smolenskii, V. A. Isupov, A. I. Agranovskaya, and S. N. Popov, *Sov. Phys. Solid State*, **2** [11], 2584 (1961).
14. D. Viehland, S. J. Jang, and L. E. Cross, *J. Appl. Phys.*, **68**, 2916 (1990).
15. V. Westphal, W. Kleeman, and M. D. Glinchuk, *Phys. Rev. Lett.*, **68**, 847 (1992).
16. I. E. Myl'nikova, and V. A. Bokov, *Sov. Phys. Crystallography*, **4**, 408 (1959).
17. V. A. Isupov, *Ferroelectrics*, **90**, 113 (1989).
18. G. A. Smolensky, and V. A. Isupov, *Soviet J. Techn. Phys.*, **24**, 1375 (1954).
19. V. A. Isupov, *Ferroelectrics*, **289**, 131 (2003).
20. Y. Yamashita, *Amer. Ceram. Soc. Bull.*, **73** (**8**), 74 (1994).
21. E. Husson, and A. Morell, *Key Engineering Materials*, **68**, 217 (1992).
22. L. E. Cross, S. J. Jang, R. E. Newnham, S. Nomura, and K. Uchino, *Ferrolectrics*, **23**, 187 (1980).
23. K. Uchino, *Ferroelectrics*, **151**, 321 (1994).
24. S. L. Swartz, and T. R. Shrout, *Mater. Res. Bull.*, **17**, 1245 (1982).

25. L. F. Francis, and D. A. Payne, *J. Am. Ceram. Soc.*, **74** [12], 3000 (1991).

26. A. S. Bhalla, R. Guo, and E. F. Alberta, *Materials Letters*, **54**, 264 (2002).

27. S. W. Choi, T. R. Shrout, S. J. Jang, and A. S. Bhalla, *Ferroelectrics*, **100**, 29 (1989).

28. O. Noblanc, P. Gaucher, and G. Calvarin, *J. Appl. Phys.*, **79**, 4291 (1996).

29. A. K. Singh, and D. Pandey, *J. Phys.: Condens. Matter*, **13**, L931 (2001).

30. Z.-G. Ye, B. Noheda, M. Dong, D. Cox, and G. Shirane, *Phys. Rev. B*, **64**, 184114-1 (2001).

31. B. Noheda, D. E. Cox, G. Shirane, J. Gao, and Z.-G. Ye, *Phys. Rev. B*, **66**, 054104 (2002).

32. B. Noheda, D. E. Cox, G. Shirane, J. A. Gonzalo, L. E. Cross, and S. E. Park, *Appl. Phys. Lett.*, **74**, 2059 (1999).

33. J. Kuwata, K. Uchino, and S. Nomura, *Jpn. J. Appl. Phys.*, **21**, 1298 (1982).

34. S. E. Park, and T. R. Shrout, *Mater. Res. Innovations*, **1**, 20 (1997).

35. S. E. Park, and T. R. Shrout, *J. Appl. Phys.*, **82**, 1804 (1997).

36. T. Shrout, Z. P. Zhang, N. Kim, and S. Markgraf, *Ferroelectr. Lett.*, **12**, 63 (1990).

37. S. E. Park, and, W. Hackenberger, *Curr. Opin. Solid State Mater. Sci.*, **6**, 11 (2002).

38. L. G. Tejuca, and J. L. G. Fierro, 'Properties and Applications of Perovskite-type Oxides', Marcel Dekker, Inc. (1993).

39. R. H. Mitchell, 'Perovskites – Modern and Ancient', Almaz Press Inc., Thunder Bay (2002).

40. B. Aurivillius, *Arki. Kemi*, **1**, 463 (1949).

41. D. A. Rae, J. G. Thompson, A. L. Withers, *Acta Crystallogr. B*, **47**, 870 (1991).

42. Ismundar, B. J. Kennedy, Gunawan, Marsongkohadi, *J. Solid State Chem.*, **126**, 135 (1996).

43. M. Kumar, A. Srinivas, G. S. Kumar, and S. V. Suryanarayana, *Solid State Chem.*, **104**, 741 (1997).

44. B. Aurivillius, and P. H. Fang, *Phys. Rev. A.*, **126**, 893 (1962).

45. G. A. Smolenskii, V. A. Isupov, and A. I. Agranoskya, *Sov. Phys. Solid State*, **3**, 651 (1961).

46. G. S. Murugan, and K. B. R. Varma, *J. Electroceram.*, **8**, 37 (2002).

47. A. Fouscova, and L. E. Cross, *J. Appl. Phys.*, **41**, 2834 (1970).

48. V. K. Seth, and W. A. Schulze, *IEEE Transactions on Ultrasonics, Ferroelectrics, and Frequency Control*, **36** (1), 41 (1989).

49. C. A. Paz de Araujo, J. D. Cuchlaro, M. C. Scott, L. D. Mcmillan, and J. F. Scott, *Nature*, **374**, 627 (1995).

50. S. B. Desu, and T. K. Li, *Mater. Sci. Eng. B*, **34**, L4 (1995).

51. P. C. Joshi, and S. B. Krupanidhi, *J. Appl. Phys.*, **72**, 5517 (1992).

52. B. H. Park, S. J. Hyun, S. D. Bu, T. W. Noh, J. Lee, H.-D. Kim, T. H. Kim, and W. Jo, *Appl. Phys. Lett.*, **74** (13), 1907 (1999).

53. Alain C. Pierre, 'Introduction to Sol-Gel Processing', Kluwer Academic Publishers, Boston/Dordrecht/London (1998).

54. D. A. Payne, *J. Sol-gel Sci. Techn.*, **2**, 311 (1994).

55. D. C. Bradley, *Chem. Rev.*, **89**, 1317 (1989).

56. R. E. Newhnam, Q. C. Xu, S. Kumar, and L. E. Cross, *Ferroelectrics*, **102**, 259 (1990).

57. S. L. Swartz, and T. R. Shrout, *Mat. Res. Bull.*, **17**, 1245 (1982).

58. S. L. Swartz, and T. R. Shrout, *Mat. Res. Bull.*, **17**, 1245 (1982).

59. M. Lejeune, and J. P. Boilot, *Ferroelectrics*, **54**, 191 (1984).

60. M. Lejeune, and J. P. Boilot, *Bull. Amer. Ceram. Soc.*, **64**, 679 (1985).

61. Z. Ye, P. Tissor, and H. Schmid, *Mat. Res. Bull.*, **25**, 739 (1990).

62. H.-C. Wang, and W. A. Schulze, *J. Am. Ceram. Soc.*, **73** [4], 825 (1990).

63. H. M. Jang, K.-M. Lee, and M.-H. Lee, *J. Mater. Res.*, **9** [10], 2634 (1994).

64. L. Zhang, 'Synthesis and Characterization of Relaxor-Based Piezo- and Ferroelectric (1-x)Pb(Zn1/3Nb2/3)O3–xPbTiO3 [PZN–PT] and (1-x)Pb(Mg1/3Nb2/3)O3–xPbTiO3 [PMN–PT]', Masters Thesis, Chemistry Department, Simon Fraser University, Burnaby, BC, Canada (2000).

65. J. F. Scott, and C. A. De Araujo Paz, *Science*, **246**, 1400 (1989).

66. C. A. Paz de Araujo, J. D. Cuchiaro, M. C. Scott, L. D. Mcmillan, and J. F. Scott, *Nature*, **374** (13), 627 (1995).

67. J. F. Scott, F. M. Ross, C. A. De Araujo Paz, M. C. Scott, and M. Huffman, *Mater. Res. Soc. Bull.*, **21** (1996).

68. J. J. Lee, C. L. Thio, and S. B. Desu, *J. Appl. Phys.*, **78** (8), 5073 (1995).

69. M. L. Calzada, R. Jimenez, A. Gonzalez, and J. Mendiola, *Chem. Mater.*, **13**, 3 (2001).

70. K. Kato, C. Zheng, J. M. Finder, S. K. Dey, and K. Torii, *J. Am. Ceram. Soc.*, **81** (7), 1869 (1998).

71. S. B. Desu, D. P. Vijay, X. Zhang, and B. P. He, *Appl. Phys. Lett.*, **69** (12), 1719 (1996).

72. M. L. Calzada, A. Gonzalez, R. Jimenez, C. Alemany, and J. Mendiola, *J. Eur. Ceram. Soc.*, **21**, 1517 (2001).

73. M. A. Zurbuchen, J. Lettieri, S. J. Fulk, Y. Jia, A. H. Carim, D. G. Schlom, and S. K. Streiffer, *Appl. Phys. Lett.*, **82** (26), 4711 (2003).

74. J. S. Yang, and X. M. Chen, *Mater. Lett.*, **29**, 73 (1996).

75. J.-K. Lee, B. Park, and K.-S. Hong, *J. Appl. Phys.*, **88** (5), 2825 (2000).

76. G. M. Anilkumar, and Y.-M. Sung, *J. Mater. Sci.*, **38**, 1391 (2003).

CHAPTER 2:
Materials Synthesis and Characterization – Principles and Instrumentation

2.1 Soft Chemical Synthesis of Relaxor Ferroelectric $(1-x)Pb(Mg_{1/3}Nb_{2/3})O_3$–$xPbTiO_3$ (x = 0.10, 0.35), and Ferroelectric $SrBi_2Ta_2O_9$ Ceramics

Sol-gel processing is one of the most common of soft chemical methods that is widely used in the synthesis of mixed oxide materials. The method primarily relies on polymerization reactions of the metal-containing starting materials (usually alkoxides), which are triggered by the solvent molecules. Therefore, the choice of an appropriate solvent is very important in such processes because it has to be the one that is able to dissolve all the starting ingredients and produce a homogeneous solution mixture. The dissolution depends on how well the solvent molecules can exchange with the alkoxy groups on to the metal complexes and contribute in polymerizing them, possibly, into chain structures which bring the cations in solution as close together as possible. Slow drying of this solution then leads to a viscous sol or a gel in which more complex cross-linked structures form through further polymerization reactions. Calcining of the viscous sol or gel at high temperatures to remove all organic moieties leads to the formation of a homogeneous precursor powder which can then be crystallized into the target inorganic phase at considerably lower temperatures than required in solid state reactions.

In the new room-temperature sol-gel route developed in this work for the synthesis of (1-x)PMN–xPT (x = 0.10, 0.35) ceramics, a mixture of polyethylene glycol

200 (PEG200) and methanol proved to be the right solvent for all our starting materials, producing a clear and homogeneous mixture. Polyethylene glycol (PEG) is well-known to be able to stabilize metal ions in solution and keep them from precipitating by binding them through the hydroxyl groups and also through the ether oxygens found in the polymer backbone [1,2]. We also studied the effects of adding a triol molecule, 1,1,1-tris(hydroxy)methylethane (THOME), which is known to help in cross-linking cations and bring them closer together, thus further preventing them from precipitating in the form of hydroxides [3].

For the synthesis of $SrBi_2Ta_2O_9$ (SBT) ceramics, two soft chemical methods, namely a sol-gel and a co-precipitation route, were designed. In the co-precipitation method, the PEG200/MeOH mixture was again the solvent of choice for dissolving all the starting materials before co-precipitating the cations into a homogeneous precursor solid. For the sol-gel process, ethylene glycol was used as solvent and mild reflux conditions were required.

In order to study the potentials of our soft chemical methods developed in this research work, and to understand the effects of reaction parameters and of additives used (e.g., THOME in the case of PMNT) on the sol-gel reactions as well as on the properties of the final materials, a series of characterization techniques have been employed, which are discussed in the following sections.

2.2 Thermogravimetry/Differential Thermal Analysis (TG/DTA)

In solid state chemistry it is particularly important to have knowledge of the temperature at which a solid state reaction takes place and whether the solid decomposes to a different composition(s) or phase(s). This information is useful for the preparation of the desired materials. Methods that are commonly used for the characterization of these reactions include thermal analysis techniques, namely, thermogravimetry (TG) and differential thermal analysis (DTA) [4]. When heat is applied to a compound, two events may take place simultaneously: a thermal change and a weight loss, but the latter does not always occur. Thermogravimetry measures the change in weight of the sample as a function of time or temperature, while differential thermal analysis measures the difference in temperature between an inert reference material and the sample while both are being heated at a constant rate in a suitable atmosphere [4].

In DTA, two thermocouples of the same nature are connected together, i.e., either the positive or negative legs of both thermocouples are electrically connected, meaning that the net electromotive force (EMF) for the two thermocouples is zero at any given temperature. Therefore, an EMF response will only occur when the temperature of one thermocouple differs from the other. In a DTA experiment the sample is put next to one thermocouple and an inert reference material, usually alumina powder (α - Al_2O_3) (because its heat capacity remains constant even up to its melting point of 1930 °C), is put next to the other thermocouple. As both are heated at an equal heat flow, thermal changes can be followed since each thermocouple produces its own EMF as temperature changes. Since no thermal changes take place in the reference, any changes that are detected come from thermal events in the sample. These temperature differences therefore, serve as

reaction indicators. A plot of these temperature differences as a function of temperature gives rise to a curve with peaks that either increase (Exothermic) above or decrease (Endothermic) below the baseline. If evaporation of water (or any type solvents) occurs, an endothermic peak appears on the DTA curve because the process absorbs heat, causing the temperature of the thermocouple next to the sample to go down (or to decay). If a structural change that tends to release heat occurs in the sample, then an exothermic peak will be observed. Schematic representations of a typical DTA set-up, and a DTA curve are shown in Figure 2.1.

As mentioned above, thermogravimetric analysis measures the change in the weight of a sample as a function of increasing temperature [4]. The apparatus consists of an analytical balance, which has a weight-change detector on one side of it. The equipment also has a temperature-controlled furnace, which houses a crucible containing the sample. A change in sample weight is detected and the current in the drive coil changes to counter the displacement of the beam. The change in current is proportional to the change in the weight of the sample. This change is plotted as a function of temperature.

In this study, the thermogravimetric and differential thermal analysis of the viscous (1-x)PMN–xPT (x = 0.10, 0.35) precursor sols obtained by the room temperature sol-gel reactions were simultaneously measured on a Seiko Exstar 6300 TG/DTA Thermal Analyzer. About 13–15 mg of the samples and the Al_2O_3 reference were heated in Pt pans from room temperature to 1000 °C at a heating rate of 5 °C/min.

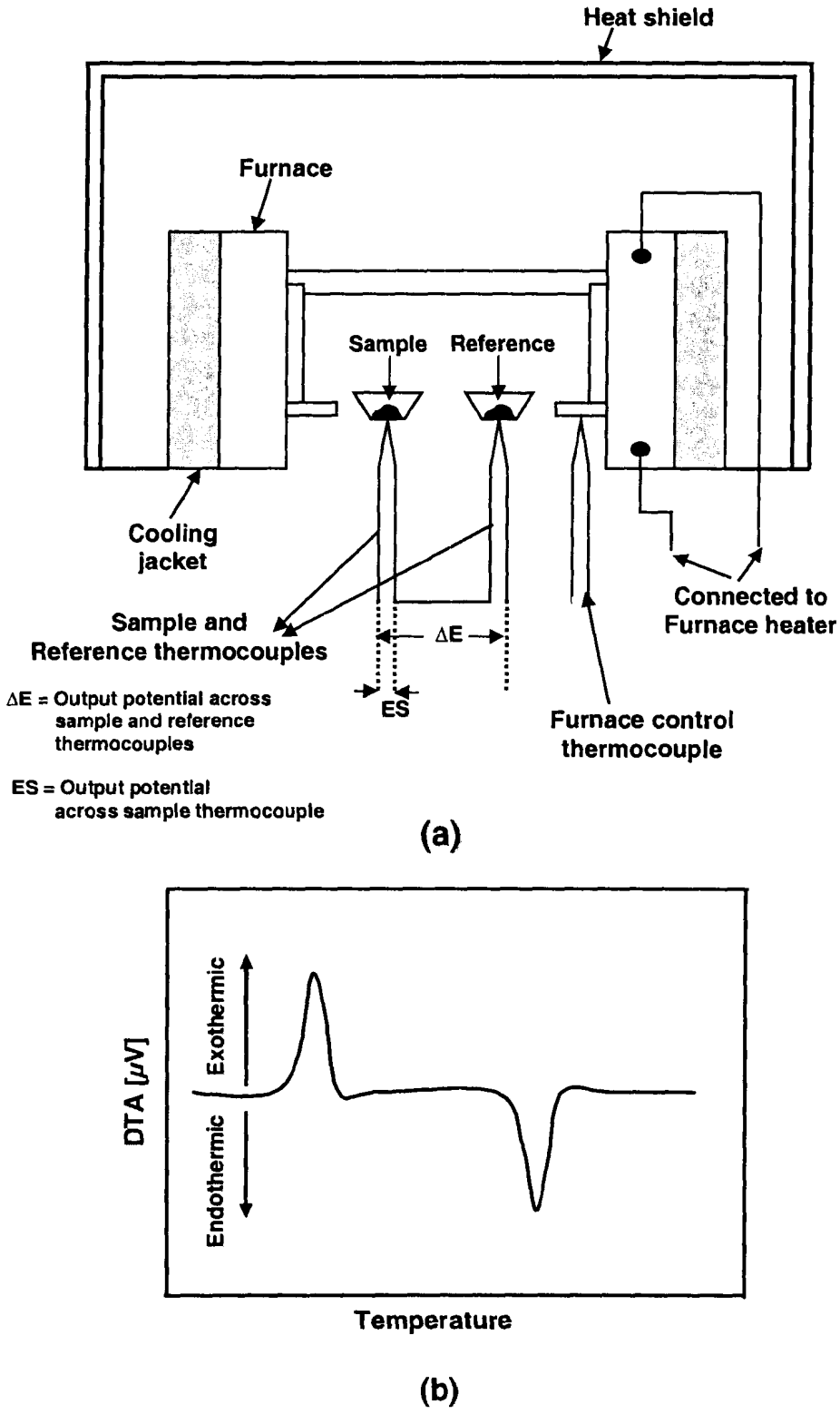

Figure 2.1: (a) Instrumentation for differential thermal analysis (DTA), (b) DTA curve showing exothermic and endothermic peaks.

2.3 X-ray Diffraction

X-rays are electromagnetic radiation. They are of exactly the same nature as light but with much shorter wavelength. While visible light has a wavelength of the order of 4000 – 7000 Å, that of X-rays (used in diffraction) lies in the range of 0.5 – 2.5 Å. They are found between the gamma and ultraviolet rays in the electromagnetic spectrum. This radiation has been of invaluable importance to solid state chemistry in two key aspects of research, namely in the fingerprint identification of crystalline materials and in determining their structure [5,6].

X-rays are produced when electrically charged particles, usually electrons, accelerated through >30 kV and therefore, of sufficient kinetic energy, are rapidly decelerated by collision with a solid body, e.g., a copper target. The electrons hitting the target have sufficient energy to ionize some of the copper 1s electrons, i.e., electrons from the K shell. As this happens, an electron from either of the outer 2p or 3p orbital immediately drops to occupy the vacancy on the 1s level. The energy that is released in this transition appears as X-rays. This is illustrated in Figure 2.2. In the case of copper, the 2p $\rightarrow$ 1s transition produces K_α radiation with a wavelength of 1.5418 Å. The K_α radiation is the one typically used in diffraction experiments because of its high intensity.

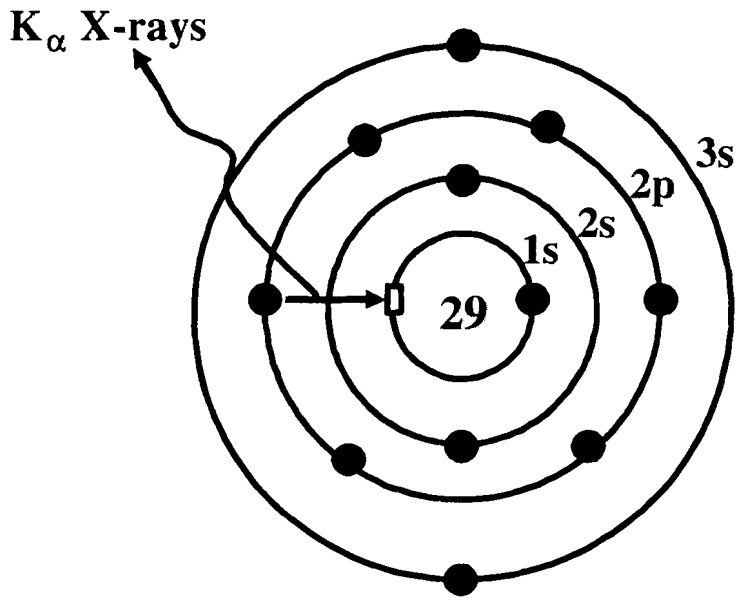

Figure 2.2: The generation of Cu K_α X-rays by ionization of a 1s electron and the subsequent transition of a 2p electron.

The radiation is produced in an X-ray tube comprising of an electron source (the cathode) which is generally a heated tungsten filament, and an anode to which the copper target is attached. The X-ray tube is evacuated to prevent oxidation of the tungsten filament. Less than one part in a thousand of the energy of the incident electron beam goes into production of X-rays, and the rest gets converted into heat that can easily melt the anode. Therefore, constant cooling of the anode is very important and this is achieved by maintaining a continuous water flow around the latter while the X-ray tube is in operation. Beryllium is used to make up the small windows found on the tube walls through which the X-rays leave. The X-rays emerging from the X-ray tube contain the K_α as well as radiation of other wavelengths. Since it is best to have a monochromatic beam of X-rays for most diffraction experiments, and the K_α line is the most intense one, it is

desired to filter out all the other wavelengths. In the case of X-rays emitted from a copper target, a Ni foil is used as filter for this purpose.

In powder X-ray diffraction method, this monochromatic beam of X-rays emerging from the Ni filter is then allowed to strike a finely powdered sample and, depending on the size and shape of the unit cell, and the atomic number and position of the different atoms in the structure, different crystalline materials will produce their own distinct diffraction patterns. In a powder sample the lattice planes are oriented in all possible directions, of which, some are oriented at the Bragg angle, θ, to the incident beam, satisfying the Bragg's law, $2d\sin\theta = n\lambda$, where θ is the angle of incidence, d is the interplanar distance, and λ is the wavelength of the incident beam. Therefore, diffraction occurs for these planes. The diffraction principle and the Bragg's law are explained using Figure 2.3 which shows two X-ray beams, 1 and 2, being reflected from two adjacent planes, A and B. For the reflected beams to be in phase, the extra distance, xyz, travelled by beam 2 must be equal to a whole number of wavelengths. Since

$$\mathbf{xy = yz = d \sin\theta,}$$

$$\mathbf{xyz = 2d \sin\theta,} \text{ and}$$

$$\mathbf{xyz = n\lambda}$$

where, d = the spacing between the two planes, and θ = the angle of incidence (Bragg angle), we obtain the Bragg's law:

$$\mathbf{2d \sin\theta = n\lambda}$$

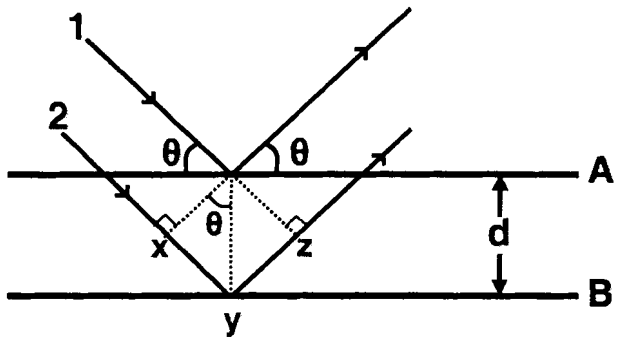

Figure 2.3: Diffraction principle and derivation of Bragg's law.

The diffraction spectra, which are plots of the intensity of the Bragg's peaks as a function of 2θ, are used to identify the compounds and to check the phase purity of the samples. Each crystalline solid has unique characteristic X-ray powder pattern which may be used as a 'fingerprint' for its identification. Compounds of the same structural type do not give rise to the same powder diffraction patterns. This is because they have different unit cell parameters due to their different unit cell size, which make the d-spacing and therefore, the peak positions vary. The intensities of the peaks also vary because of the presence of different types of ions with different atomic numbers, and hence, different X-ray scattering powers. For example, $PbTiO_3$ (PT) and $Pb(Mg_{1/3}Nb_{2/3})O_3$ (PMN) both have the ABO_3-type perovskite structure, but produce different X-ray diffraction patterns because of their different symmetries. The Miller indices, *hkl*, of the diffraction planes, the intensity, I_{hkl}, of the resulting peaks, and the corresponding 2θ values for the tetragonal PT and pseudocubic PMN are given in Table 2.1, and the X-ray diffraction patterns are illustrated in Figures 2.4 (a) and (b), respectively.

$PbTiO_3$ (Tetragonal; a = b = 3.940 Å, c = 4.063 Å)				$Pb(Mg_{1/3}Nb_{2/3})O_3$ (Cubic; a = 4.044 Å)			
2θ	**d_{hkl}**	**I_{hkl}**	**hkl**	**2θ**	**d_{hkl}**	**I_{hkl}**	**hkl**
21.858	4.150	227	001	21.961	4.044	212	100
22.549	3.900	381	100	31.254	2.860	999	110
31.607	2.842	999	101	38.527	2.335	137	111
32.102	2.758	472	110	44.785	2.022	235	200
39.175	2.297	341	111	50.417	1.809	40	210
44.566	2.076	115	002	55.623	1.651	250	211
46.035	1.950	235	200	65.196	1.430	94	220
50.506	1.833	79	102	69.700	1.348	7	221
51.514	1.765	65	201	74.074	1.279	67	310
51.847	1.744	62	210	78.357	1.219	9	311
55.975	1.658	148	112				
56.915	1.608	266	211				
66.005	1.421	98	202				
67.143	1.379	52	220				
69.329	1.384	7	003				
70.718	1.335	42	212				
71.546	1.308	18	221				
71.822	1.300	11	300				
73.945	1.305	49	103				
76.108	1.240	44	301				
76.377	1.233	53	310				
78.456	1.237	16	113				

Table 2.1: X-ray diffraction data for perovskite compounds, $PbTiO_3$ and $Pb(Mg_{1/3}Nb_{2/3})O_3$ [5].

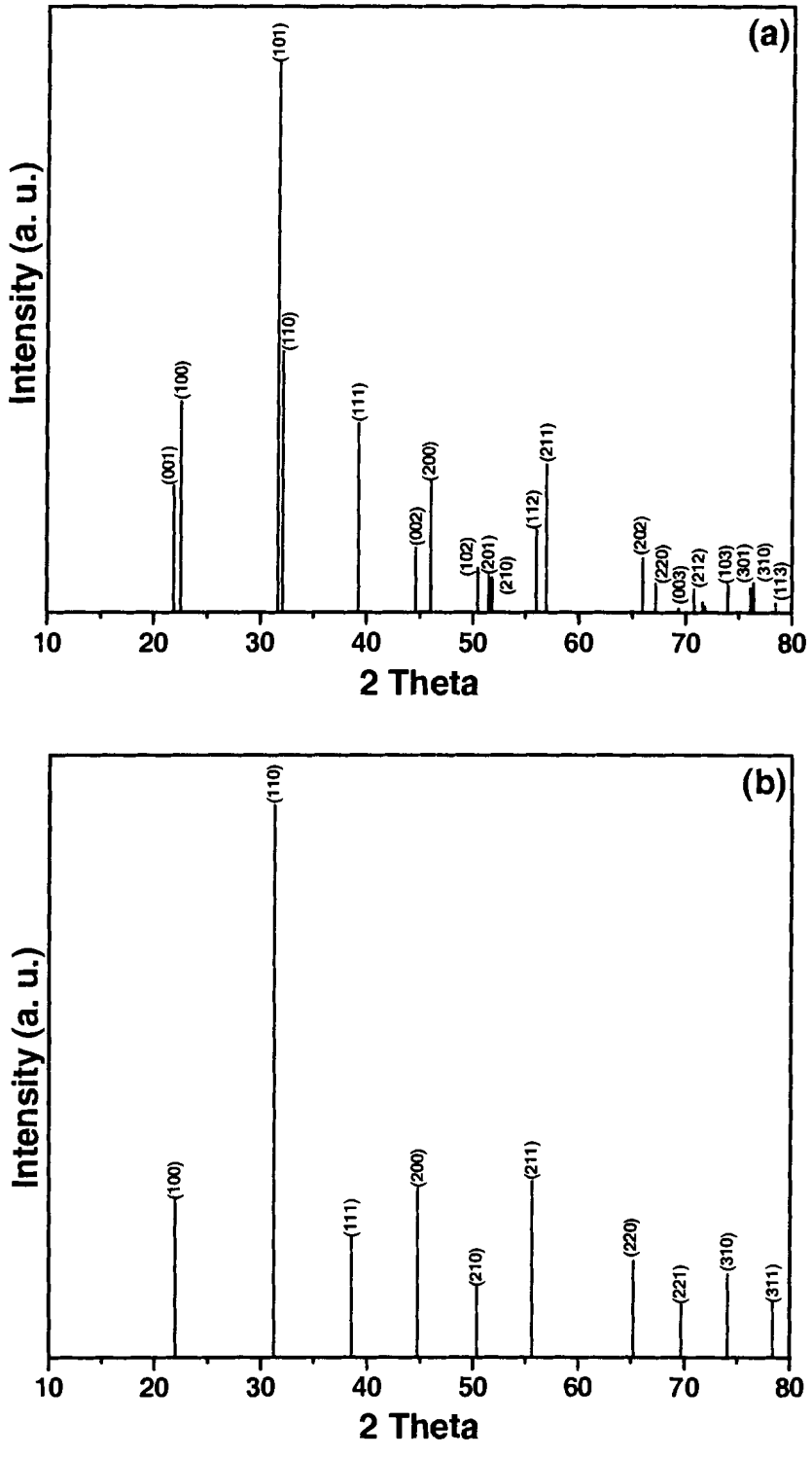

Figure 2.4: X-ray diffraction spectra of (a) tetragonal $PbTiO_3$, and (b) pseudocubic $Pb(Mg_{1/3}Nb_{2/3})O_3$.

In this research work a Philips powder diffractometer using CuK_α radiation (40 kV, 35 mA) was used to check the phases of the 0.65PMN – 0.35PT samples. For the $0.90Pb(Mg_{1/3}Nb_{2/3})O_3$–$0.10PbTiO_3$ [0.90PMN–0.10PT] and $SrBi_2Ta_2O_9$ (SBT) samples, phase formation was determined on a Rigaku X-ray diffractometer which also uses CuK_α radiation (46 kV, 42 mA).

2.4 Infrared Spectroscopy

Infrared radiation occurs between the visible and microwave regions of the electromagnetic spectrum. Bonds in molecules are able to rotate and to vibrate by absorbing infrared radiation. When radiation of frequencies smaller than 100 cm^{-1} is absorbed, it is converted into molecular rotation. Since this absorption is quantized, it gives rise to discrete lines on the molecular rotation spectrum. On the other hand, IR radiation in the range of 10,000 – 100 cm^{-1} is converted into energy of molecular vibration when absorbed by molecules. Again, this absorption is quantized, but the resulting spectra appear as bands instead of lines because a single vibrational energy change results in a number of rotational energy changes. These vibrational-rotational bands occurring between 4000 – 400 cm^{-1} are of particular interest to organic chemistry while the far-IR regions (700 – 200 cm^{-1}) are important to inorganic chemistry [7].

IR spectra are therefore plots of the intensity of the radiation absorbed by specific bonds in the molecule as a function of the frequency or wavelength of the incident radiation. This technique is a very important tool that helps in the elucidation of structural information about a given molecule [7]. Since a given bond will absorb at a particular frequency, a peak-by-peak correlation is excellent evidence for identity. Table 2.2 shows the characteristic absorption frequencies of some common functional groups. Any two different compounds are unlikely to show exactly the same IR spectrum unless they are enantiomers. Either transmittance (T) or absorbance (A) is used to express the band intensities. Transmittance is the ratio of the intensity of radiation transmitted by the sample to that which was incident on the later. Absorbance is the logarithm, to the base 10, of the reciprocal of the transmittance. This is expressed in Figure 2.5.

Functional Group	*Characteristic Absorption Frequencies* (cm^{-1})
Alkyl C-H Stretch	2950 - 2850
Alkenyl C-H Stretch Alkenyl C=C Stretch	3100 - 3010 1680 - 1620
Alkynyl C-H Stretch Alkynyl C≡C Stretch	~3300 2260 - 2100
Aromatic C-H Stretch Aromatic C-H Bending Aromatic C=C Bending	~3030 860 - 680 1700 - 1500
Alcohol/Phenol O-H Stretch	3550 - 3200
Carboxylic Acid O-H Stretch	3000 - 2500
Amine N-H Stretch	3500 - 3300
Nitrile C≡N Stretch	2260 - 2220
Aldehyde C=O Stretch Ketone C=O Stretch Ester C=O Stretch Carboxylic Acid C=O Stretch Amide C=O Stretch	1740 - 1690 1750 - 1680 1750 - 1735 1780 - 1710 1690 - 1630
Amide N-H Stretch	3700 - 3500

Table 2.2: Characteristic IR absorption frequencies for some of the common functional groups [7].

Transmittance, $T = I / I_0$
Absorbance, A = log10 (1/T)

Figure 2.5: Relationship between transmittance and absorbance when electromagnetic radiation passes through a given sample.

In this work, IR spectroscopy was used in order to give an insight of the structural transformation taking place during the transformation of the PMN–PT precursor sol containing metal-organic species to the crystalline inorganic phase. The 0.65PMN–0.35PT sols prepared with and without the triol molecule (THOME) were treated at different temperatures and IR spectroscopy was performed on the resulting powders to investigate the different mechanisms of the thermal reactions and the crystallization of the precursor powders into the perovskite phase. The IR spectra were obtained on a Bomem MB spectrometer. The solid samples were mixed with potassium bromide, ground and pressed into thin pellets for the experiments. As for the liquid samples (sols), small drops were placed in between two sodium chloride disks for the measurements.

2.5 Scanning Electron Microscopy

Scanning Electron Microscopy (SEM) is a powerful tool for unveiling important and useful information about the microstructure of solids. SEM is able to produce very detailed 3-D images at considerably higher magnifications than can be achieved by an optical microscope [5]. The scanning electron microscope uses electrons rather than light waves to create those images. SEM analysis reveals detailed information about ceramic surface texture, grain sizes and shapes, and grain boundaries.

For an SEM experiment, the sample's surface has to be made conducting and this can be achieved either by applying a coating of graphite paste or by sputtering a thin layer of gold on the surface to be scanned. The sample is then mounted on a holder inside the sample chamber and air is pumped out of the chamber in order to create a high vacuum. Once this is achieved, an electron gun placed right on top of the sample emits a high energy electron beam which is focused onto a fine spot on the specimen [8,9]. This focused beam is then made to scan the surface of the sample by moving back and forth. As the high energy electrons hit the surface of the specimen, secondary electrons are ejected from a depth of about 50 – 500 Å. This is the result of interactions between the energetic electrons from the beam and conduction electrons which are weakly bound in the sample. The secondary electrons then hit a detector which counts the electrons and sends the signals to an amplifier and the final image is created based on the number of electrons which are emitted from the different spots on the sample. A schematic representation of the instrumentation involved in a scanning electron microscope is shown in Figure 2.6.

In this work, the mircrostructure and grain size of the 0.65PMN – 0.35PT and SBT ceramics were imaged using a Bausch and Lomb Nanolab 2100 SEM equipment, and a Strata 235 Dualbeam instrument composed of a Field Emission Scanning Electron Microscope and Focus Ion Beam (FESEM/FIB), respectively.

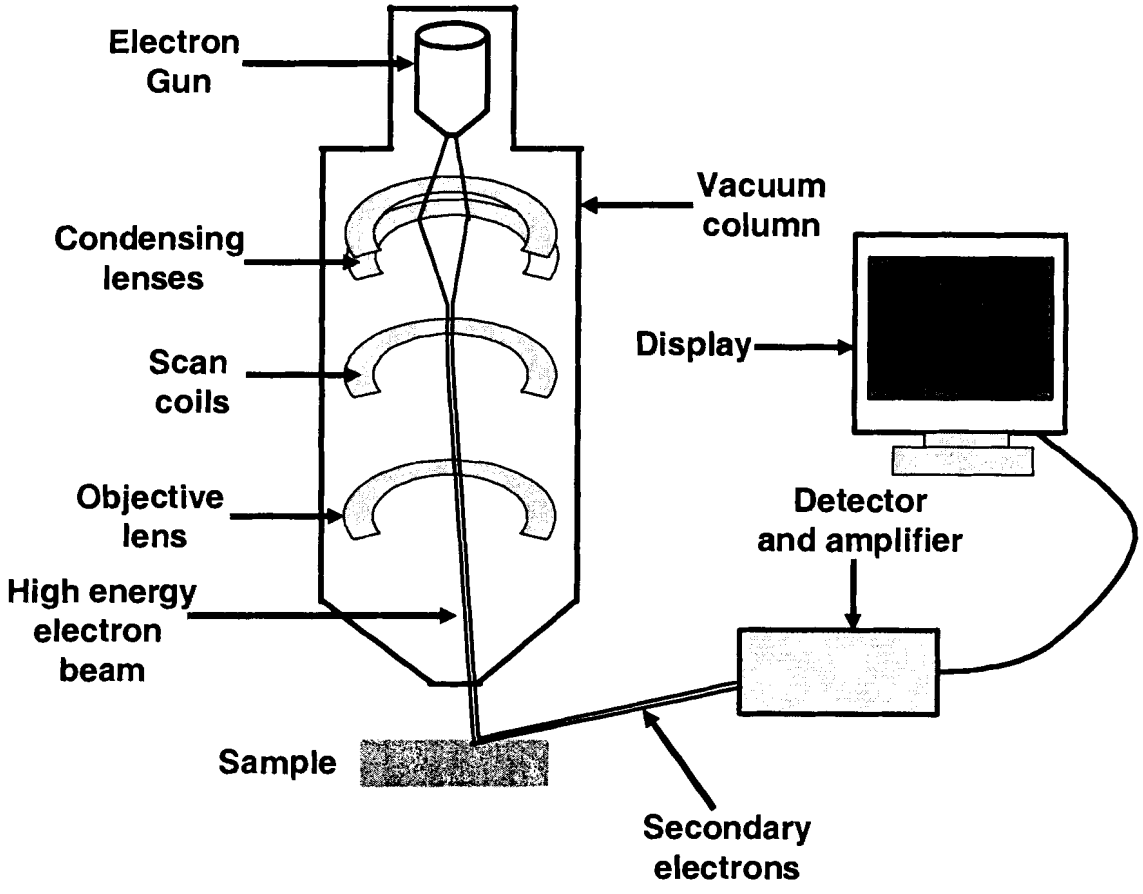

Figure 2.6: Schematic representation of a scanning electron microscope.

2.6 Dielectric Characterization by Means of Impedance Spectroscopy

In order to characterize the microstructure and electrical properties of electroceramics, techniques that can probe or distinguish between the different microstructural regions of a ceramic are required. One of the methods available to measure the electrical properties of ceramics is impedance spectroscopy [10-12]. This technique has gained a lot of importance because it has proved to be very powerful for unravelling the complexities of electroceramics. The frequency dependence of the different parts of an electroceramic allows the overall electrical properties of the material to be separated, thus making them easier to be studied and/or modified. In impedance spectroscopy, an alternating voltage is applied across a sample and a standard resistor, which are in series, and the in- and out-of-phase components of the voltage across the sample are measured. These components are then divided by the magnitude of the current to give the resistive and reactive components of the impedance. The measurements are repeated as a stepwise function of frequency which typically ranges from 10^{-2} to 10^{7} Hz, and the different regions of the material are characterized according to their electrical relaxation times or time constants, by a resistance and a capacitance, usually placed in parallel. The principle of an impedance spectroscopy measurement of an electric material is shown in Figure 2.7.

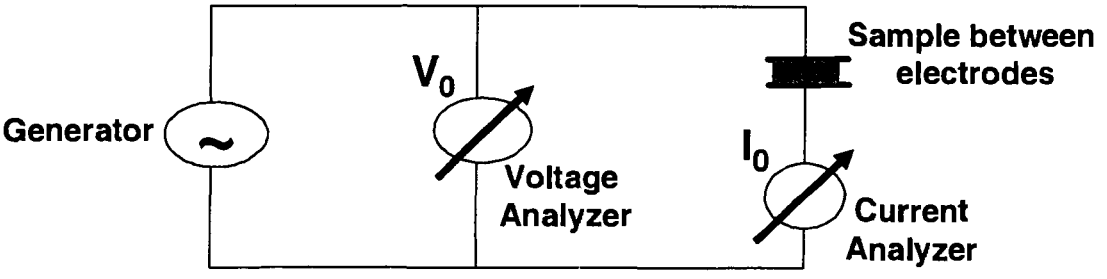

Figure 2.7: Principle of a dielectric (or impedance) measurement.

The sample, usually in the form of a disc, is sputtered with a layer of gold on each side and the electrical wires (gold) are attached using silver paste. As shown in Figure 2.7, a sinusoidal voltage V(t) (equal to $V_0 \sin\omega t$) with a fixed frequency $\omega/2\pi$ is applied to the sample by means of the generator, and this produces polarization in the sample. This voltage causes a current I(t) (equal to $I_0 \sin(\omega t + \varphi)$ to flow through the sample at the same frequency. Generally, there is a phase shift between the resulting current and the applied voltage, which is known as the phase angle, φ. This is graphically represented in Figure 2.8.

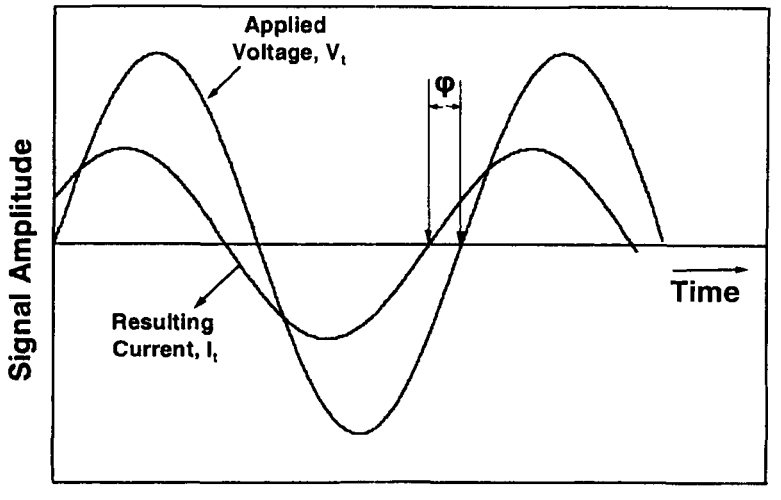

Figure 2.8: Relationship of amplitude and phase difference between applied voltage and resulting current.

By measuring the complex impedance, Z^*, of the sample and by separating it into its real and imaginary parts, Z' and Z", the capacitance, C, and conductance, G, can be calculated as follows:

$$Z^* = Z' + Z''$$

$$= V/I = V_0 \sin\omega t / I_0 \sin(\omega t + \varphi) = 1/G + 1/\omega C$$

The dielectric constant of the sample, which is the real part of the dielectric permittivity, ε', can then be obtained from the impedance measurement.

The permittivity, ε', of a dielectric material is related to its capacitance, C. The application of a voltage, V, to the sample and the flow of a current, I, through it causes the accumulation of a given amount of charges, Q, on the opposite plates of the capacitor, producing an electric field between the plates. The presence of the dielectric material (the sample) between the parallel plates of the capacitor causes a reduction in the effective field, E. This is because the polarization of the material produces an electric field, $E_{polarization}$, which opposes the field of the charges on the plates, E_0. This is illustrated in Figure 2.9. Therefore,

$$E = E_0 - E_{polarization} = \sigma / \varepsilon' \varepsilon_0$$

where, σ = charge per unit area, ε_0 = permittivity of free space, and ε' = the dielectric constant of the material between the capacitor plates.

With

$$E = V/d \ ; Q = CV \ ; \text{ and } \ \sigma = Q/A,$$

$$V = Ed = Q/C$$

Therefore,

$$C = Q/Ed = Q\varepsilon'\varepsilon_0/\sigma d = \varepsilon'\varepsilon_0 A/d$$

where, C = capacitance, A = area of plates, and d = distance separating the plates (or thickness of the dielectric material).

Ferroelectric and relaxor ferroelectric materials cause a considerable lowering of the effective electric field, E, between the capacitor plates. As discussed in Chapter 1 (Sec. 1.1), ferroelectrics have their polarization oriented in different directions, which gives rise to the formation of domains, and within a given domain, all dipoles are oriented in the same direction. The application of an external field then causes domain walls to move as all the dipoles begin to align themselves in the same direction. This leads to a large increase in polarization which results in an electric field, $E_{polarization}$, opposing the applied electric field, E_0. Owing to these non-linear effects, large values of static dielectric constant are observed in these materials. When subjected to an alternating field, a point is reached when at certain frequencies the dipoles which are responsible for polarization can no longer keep up with the oscillation of the electric field. The re-orientation of the dipoles and the reversal of the field therefore become out-of-phase causing a dielectric relaxation, i.e., a decrease in the real part of permittivity, ε'.

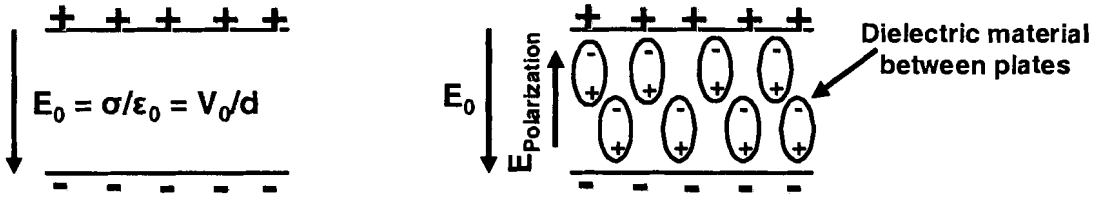

Figure 2.9: Reduction of effective electric field between the plates of a capacitor by a dielectric material.

Impedance spectroscopy was used to study the temperature and frequency dependences of the real part of dielectric permittivity of the ceramics prepared in this research work. The ceramics were sputtered with layers of gold on opposite sides and gold wires were used for electric connection. The dielectric permittivity of the 0.90PMN–0.10PT ceramics was measured on an Alpha Broadband High Resolution Dielectric/Impedance Analyzer (Novocontrol), while the 0.65PMN–0.35PT and $SrBi_2Ta_2O_9$ (SBT) samples were studied using a computer-controlled impedance analyzer (Solartron 1260) in conjunction with a dielectric interface (Solartron 1296).

2.7 Ferroelectric Measurement

The spontaneous polarization present in ferroelectric materials can be reversed by the application of an external electric field, and this forms the basis for the occurrence of the ferroelectric hysteresis loop in these compounds. The principle of ferroelectric hysteresis has been explained in Chapter one (Sec. 1.1). In a ferroelectric hysteresis testing experiment, a voltage is applied to the sample (which is in the form of a capacitor) and the resulting polarization is measured in terms of the amount of charge accumulated on the capacitor plates. The tester is computer-controlled and the software executes the appropriate commands by collecting and processing the data, and displaying the results in the form of the hysteresis loop [13].

For the hysteresis measurement, the opposite surfaces of the sample (usually in the form of a disc) of a given area, A, are coated with a layer of gold to make the electrodes. Gold wires are then attached to the electrodes using silver paste, and the sample is connected to an electrical circuit consisting of a reference capacitor, C_R, as shown in Figure 2.10. A variable power source is used to apply a voltage to the reference capacitor and the sample, and the resulting charge, Q, is measured for each applied voltage. By measuring the voltage, V_R, across the reference capacitor, Q can be determined as follows:

$$\mathbf{Q = C_R V_R}$$

Using the calculated charge and the surface area, A, of the sample the software can then generate the polarization, P, from

$$\mathbf{P = Q/A}$$

and produce a plot of P as a function of the electric field, E (equal to V_S/sample thickness).

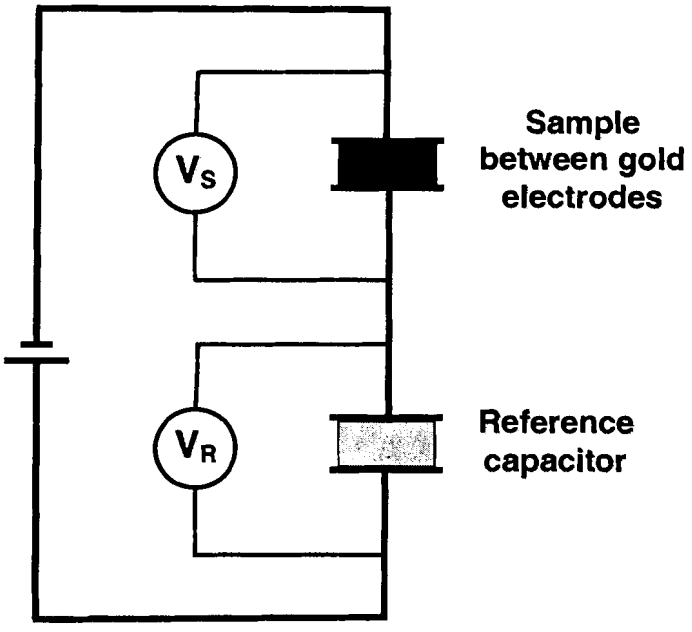

Figure 2.10: Electrical circuit for a ferroelectric hysteresis testing experiment.

The ferroelectric hysteresis loops of the 0.90PMN–0.10PT, 0.65PMN–0.35PT and SBT ceramics prepared in this research work were measured on a RT66A standard ferroelectric testing system at -178 °C for 0.90PMN–0.10PT and room temperature for 0.65PMN–0.35PT and SBT ceramics.

2.8 References

1. M. A. Gülgün, M. H. Nguyen, and W. M. Kriven, *J. Am. Ceram. Soc.*, **82** (3), 556 (1999).

2. N. Uekawa, T. Sukegawa, K. Kakegawa, and Y. Sasaki, *J. Am. Ceram. Soc.*, **85** (2), 329 (2002).

3. N. Sriprang, D. Kaewchinda, J. D. Kennedy, and S. J. Milne, *J. Am. Ceram. Soc.*, **83** (8), 1914 (2000).

4. M. E. Brown, 'Introduction to Thermal Analysis: Techniques and Applications', 2nd Edition, Dordrecht, Boston, Kluwer Academic Publishers (2001).

5. (a) Anthony R. West, 'Basic Solid State Chemistry', 2nd Edition, J. Wiley & Sons, Inc. (1996); (b) M. C. Morris, 'Joint Committee on Powder Diffraction Standards', 1st Edition, Swarthmore, Pa (1976).

6. V. K. Percharsky, and P. Y. Zavalij, 'Fundamentals of Powder Diffraction and Structural Characterization of Materials', Kluwer Academic Publishers, Boston (2003).

7. R. M. Silverstein, and F. X. Webster, 'Spectrometric Identification of Organic Compounds', 6th edition, Wiley, New York, (1998).

8. P. M. Fishbane, S. Gasiorowicz, S. T. Thornton, 'Physics for scientists and engineers', 2nd edition, Prentice Hall Upper Saddle River, New Jersey 07458 (1996).

9. D. A. Skoog, F. J. Holler, and T. A. Nieman, 'Principles of Instrumental Analysis', 5th edition, Harcourt Brace College Publishers (1998).

10. J. Ross Macdonald, 'Impedance Spectroscopy: Emphasizing solid materials and systems', J. Wiley & Sons, Inc. (1987).

11. J. T. S. Irvine, D. C. Sinclair, and A. R. West, *Advanced materials*, **2** [3], 132 (1990).

12. C. Elissalde, and J. Ravez, *J. Mater. Chem.*, **11**, 1957 (2001).

13. RT66A standard ferroelectric testing system manual.

CHAPTER 3:
Phase Formation and Dielectric Properties of $0.9Pb(Mg_{1/3}Nb_{2/3})O_3$–$0.1PbTiO_3$ Ceramics Prepared by a New Sol-Gel Method

K. Babooram, H. Tailor, and Z.-G. Ye*

Department of Chemistry, Simon Fraser University, 8888 University Drive, Burnaby, BC, Canada, V5A 1S6

* Corresponding author. Tel.: +1-604-291-3351; Fax: +1-604-291-3765;

e-mail address: zye@sfu.ca

Reproduced with permission from *Ceramics International*, **30**, 1411-1417 (2004)

ABSTRACT

Ceramics of lead magnesium niobate – lead titanate solid solution, $0.90Pb(Mg_{1/3}Nb_{2/3})O_3$-$0.10PbTiO_3$, have been synthesized by a new room temperature sol-gel route, using polyethylene glycol-200 (PEG) and methanol mixture as solvent. The use of a triol molecule, 1,1,1-tris(hydroxymethyl)ethane (THOME), which is known to serve as a complexing agent in binding together the metal ions in the precursor solution, has been shown to give good dielectric and ferroelectric properties (ε'_{RT} = 25,000, ε'_{max} = 33,000 at T_{max} = 40 °C and P_r = 18 $\mu C/cm^2$ at room temperature) for the stoichiometric PMN–PT ceramics sintered at 1050 °C. A 5% mol excess of lead in the sol-gel process without THOME led to an improvement in the formation of the perovskite phase, but a degradation of the dielectric properties with ε'_{max} = 10,000 and P_r = 11 $\mu C/cm^2$ only.

3.1 Introduction

The relaxor ferroelectric solid solution system (1-x)$Pb(Mg_{1/3}Nb_{2/3})O_3$-x$PbTiO_3$ [(1-x)PMN–xPT] has attracted considerable interest because of its remarkable dielectric and electromechanical properties in the form of ceramics and single crystals [1-3]. $Pb(Mg_{1/3}Nb_{2/3})O_3$ (PMN) is very well known to exhibit typical relaxor ferroelectric behavior characterized by a broad and frequency dependent dielectric maximum and T_{max} (around –15 °C) [4]. Addition of the normal ferroelectric $PbTiO_3$ (PT) to PMN shifts this transition temperature upwards and enhances the dielectric properties of the solid solutions [5, 6]. A morphotropic phase boundary (MPB) appears in a region of 30 – 37 mol % PT with the presence of a rhombohedral, tetragonal, and monoclinic phase [7]. As a result, the (1-x)PMN– xPT system embraces a wide range of compositions which find important and interesting applications in multi-layer dielectric capacitors, piezoelectric devices, and sensors [8]. The PMN–PT system has a higher stability of the perovskite structure and excellent piezo-/ferroelectric properties compared to other relaxor-based systems, such as (1-x)$Pb(Zn_{1/3}Nb_{2/3})O_3$–x$PbTiO_3$ [PZNT] and (1-x)$Pb(Sc_{1/2}Nb_{1/2})O_3$–x$PbTiO_3$ [PSNT] [3]. Being more on the PMN side of the (1-x)PMN-xPT solid solution phase diagram, 0.90PMN-0.10PT is a typical relaxor ferroelectric material with a weak rhombohedral distortion [7]. It exhibits high dielectric permittivity, narrow hysteresis loop and strong piezoelectric response, which, together, make it an excellent material for multi-layered high density capacitors [8]. The composition of 0.90PMN–0.10PT has a diffuse phase transition temperature (T_{max}) at ~40°C and its dielectric constant at room temperature is very high (ε' ~10 000), making it a potential candidate for DRAM and multi-layer capacitor applications [9].

The synthesis of pure perovskite 0.90PMN-0.10PT by conventional solid state reactions can be very challenging due to the formation of a kinetically more stable but undesired impurity phase of pyrochlore structure, which considerably impairs the dielectric properties of the material [10]. As a result, a number of different soft chemical techniques like sol-gel and solution processes have been designed for the synthesis of pure perovskite 0.90PMN-0.10PT [11-13]. The polymeric precursor method, which is based on the Pechini's technique, has become very popular in the making of fine mixed-metal oxide powders [14-16]. This solution process consists of preparing a polymer-cation complex in solution and then converting it into the multi-component oxide by burning away the organic components during high-temperature treatment [17]. The main feature of this method is that it allows a very homogeneous dispersion of the cations in the polymer-cation complexes, which helps in the formation of fine and highly reactive mixed oxide powders [18].

Polyethylene glycol [PEG] has proved to be a very suitable polymer for use in the polymeric precursor method in the preparation of mixed oxide powders and ceramics. The reason for this is the coordination of the ether oxygen atoms in PEG to the metal cations, which allows it to dissolve a number of inorganic salts as well as metal alkoxides. Besides polymer-binding, cross-linking can also greatly help in obtaining a very homogeneous distribution of cations in solutions. Sriprang *et al.* used a triol, 1,1,1-tris(hydroxymethyl)ethane [THOME] as a cross-linking agent for the cations in the synthesis of lead zirconium titanate thin films [19]. They demonstrated that, with its three hydroxyl groups, THOME could bind to up to three metal ions at a time, forming oligomeric species that were then oxidized to form the final mixed oxide component.

In our recent work, we have prepared 0.65PMN-0.35PT ceramics using a room temperature soft chemical route [20]. A 1:2 volume mixture of PEG200 and methanol was used as solvent, and THOME was used as a complexing agent. Pure perovskite phase, high density, high dielectric constant, and excellent ferroelectric properties were obtained in the ceramics prepared from a stoichiometric amount of the lead starting material in the preparation of the sol [See Chapter 4]. A decrease in the ceramic quality in terms of the perovskite phase purity and dielectric properties was observed in those ceramics prepared without using THOME in the reaction. In this work, we report the synthesis of 0.90PMN-0.10PT ceramics by the new room temperature soft chemical route based on polyethylene glycol.

3.2 Experimental

The 0.90PMN–0.10PT ceramics have been prepared by the same soft chemical route used to prepare the 0.65PMN–0.35PT ceramics, the synthesis details of which are outlined in the flowchart in Figure 4.1 (Chapter 4). The starting materials used were lead (II) acetate trihydrate [$Pb(CH_3COO)_2.3H_2O$], magnesium 2,4-pentanedionate dihydrate [$Mg(O_2C_5H_7)_2.2H_2O$], niobium (V) ethoxide [$Nb(OC_2H_5)_5$], and titanium diisopropoxide bis acetyl acetonate [$Ti(OC_3H_7)_2(O_2C_5H_7)_2$] (TIAA). Stoichiometric amounts of $Pb(CH_3COO)_2.3H_2O$, $Mg(O_2C_5H_7)_2.2H_2O$ and 1,1,1–tris(hydroxymethyl)ethane [$C(CH_2OH)_3(CH_3)$] (THOME) were dissolved in a 1:2 volume mixture of polyethylene glycol 200 (PEG) and methanol (MeOH) by simple stirring at room temperature to give a clear, yellow solution. In a separate flask, $Nb(OC_2H_5)_5$, TIAA, and THOME were mixed and stirred in the PEG/MeOH mixture under the same conditions to yield a light orange clear solution. These two solutions were then mixed together and further stirred at room temperature for about 5 – 6 h, at the end of which a clear yellow solution was formed. The volatile organic species were evaporated by rotary evaporator, giving rise to a very viscous precursor sol, which was then burnt at 500 °C for 2 h to form a light orange powder. The powder was then ground in acetone, pressed into discs and treated at various temperatures between 650 – 1050 °C for 8 h. The as-prepared ceramics were abbreviated as 10PEG(S)T. The same procedure was employed to prepare the 0.90PMN-0.10PT ceramics under various conditions: (i) stoichiometric amount of lead (II) acetate and no THOME [10PEG(S)], (ii) 5% mol excess of lead (II) acetate with THOME [10PEG(5)T], and (iii) 5% mol excess of lead (II) acetate and no THOME [10PEG(5)] in order to study

the effects of these chemical parameters on the quality and properties of the resulting ceramics.

The phases of the 0.90PMN–0.10PT samples were checked by X-ray powder diffraction using CuKα radiation (46 kV, 42 mA) on a Rigaku X-ray diffractometer. The decomposition processes of the precursor solutions were investigated by thermogravimetric and differential thermal analyses (TG/DTA) on a Seiko Exstar 6300 TG/DTA Thermal Analyzer. The precursor sols were oxidized by heating from room temperature to 1000 °C at a heating rate of 5 °C/min. The grain size was imaged using scanning electron microscopy (SEM) on a Bausch and Lomb Nanolab 2100 SEM equipment. The temperature and frequency dependences of the dielectric permittivity of the 0.90PMN-0.10PT ceramics were measured on an Alpha High Resolution Dielectric/Impedance Analyzer (Novocontrol). Ferroelectric hysteresis loops were displayed on a RT66A standard ferroelectric testing system by applying a field of E = 23 kV/cm across the ceramics.

3.3 Results and Discussion

3.3.1 Thermogravimetric/Differential Thermal Analysis (TG/DTA)

The best conditions for the pyrolysis of the precursor solutions and for the sintering of the precursor powders were determined by thermal analyses. Figures 3.1 (a) and 3.1 (b) show the DTA/TG curves of the 10PEG(S)T and 10PEG(5) precursor solutions, respectively, from room temperature to 1000 °C at a heating rate of 5 °C/min. Three different weight loss regions can be observed on the TGA curve of the 10PEG(S)T precursor solution. The first one in the region of 45 – 120 °C indicates the volatilization of solvent and/or moisture, which was still present in the precursor solution. A second weight loss appears in the region of 120 -- 325 °C, which can be attributed to the decomposition of PEG chains, the THOME molecules, and the acetate groups present in the sol. The third weight loss occurring between 325 and 545 °C is assigned to the decomposition of the complex structures in the sol, which can be PEG chains and/or THOME molecules bound to the metal centers. This process was accompanied by a strong exothermic peak at 331 °C on the DTA curve. The other exothermic peaks at 345 °C and 428 °C are the result of the decomposition of more complex metal-organic structures or oligomers that were formed from condensation reactions in the precursor solution. The small exothermic peak at 536 °C can be attributed to the formation of the crystalline mixed oxide phase. These observations lead to the conclusion that all the organic moieties present in the precursor solution are oxidized and decomposed at temperatures below ~ 450 °C, after which the resulting matter undergoes a rearrangement of the M–O–M networks to form the crystalline pyrochlore phase at around 536 °C.

The 10PEG(5) precursor solution exhibits similar thermal behavior. The differences here are the absence of the THOME molecule and the presence of a 5 % mol excess of lead in the sol-gel process. Three weight loss regions are also observed on the TG curve shown in Figure 3.1 (b), which are at 42 – 104 °C, 136 – 285 °C, and 288 – 320 °C, corresponding to (i) the volatilization of the solvent and/or moisture present in the precursor solution, (ii) the decomposition of the PEG-cation complexes, and (iii) the decomposition of more complex PEG-metal structures or oligomers, respectively. The exothermic peaks observed on the DTA curve [Fig. 3.1 (b)] at 277 °C, 350 °C, and 417 °C result from the thermal processes associated with the second and third weight losses, respectively. The exothermic peak at 515 °C is assigned to the crystallization of the oxide phases that are a mixture of the perovskite and pyrochlore phases, as revealed by X-ray diffraction [see Sec. 3.3.2]. The first exothermic peak occurs at a temperature (277 °C) lower than in the 10PEG(S)T sol (331 °C). This strongly supports the fact that both the PEG chains and the THOME molecules chelate to the metal centers in the 10PEG(S)T sol, forming more complex structures that decompose at a higher temperature. In the 10PEG(5) sol, however, only the PEG chains can bind to the cations through their end hydroxyl groups and the ether oxygens present in the polymer backbone.

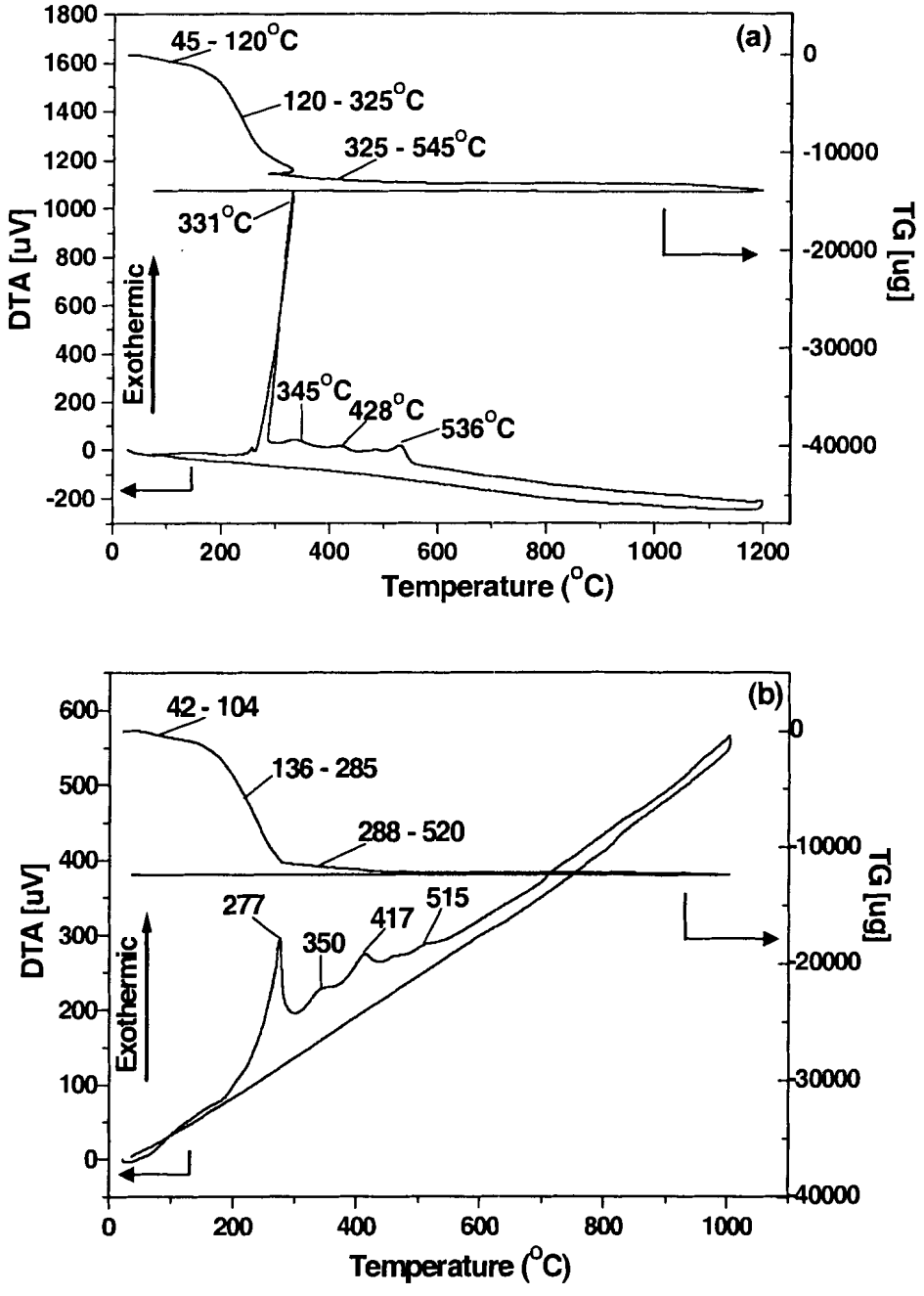

Figure 3.1: TG/DTA curves from room temperature at a heating rate of 5 °C/min for (a) 10PEG(S)T and (b) 10PEG(5) precursor solutions.

3.3.2 Phase Analysis by X-ray Diffraction

Powder X-ray diffraction (XRD) was used to check the phases of all the samples. The XRD patterns of the 10PEG(S)T, 10PEG(S), 10PEG(5), and 10PEG(5)T samples synthesized at different temperatures are shown in Figures 3.2 (a), 3.2 (b), 3.2 (c), and 3.2 (d), respectively. It can be seen that crystallization already occurred at 500 °C in all the samples, with the formation of the pyrochlore phase in the 10PEG(S)T and 10PEG(S) samples, and a mixture of the perovskite and the pyrochlore phases in the 10PEG(5) and 10PEG(5)T samples. Upon heating, the perovskite phase grows at the expense of the pyrochlore phase in all cases. In the 10PEG(5) sample an almost pure perovskite phase appears at 1000 °C, above which, the impure phase seems to grow a bit upon further heating. In the case of 10PEG(S)T and 10PEG(S), the perovskite phase appears as the major phase after thermal treatment at 950 °C and 1000 °C, respectively, but a small amount (<10 %) of pyrochlore phase persists.

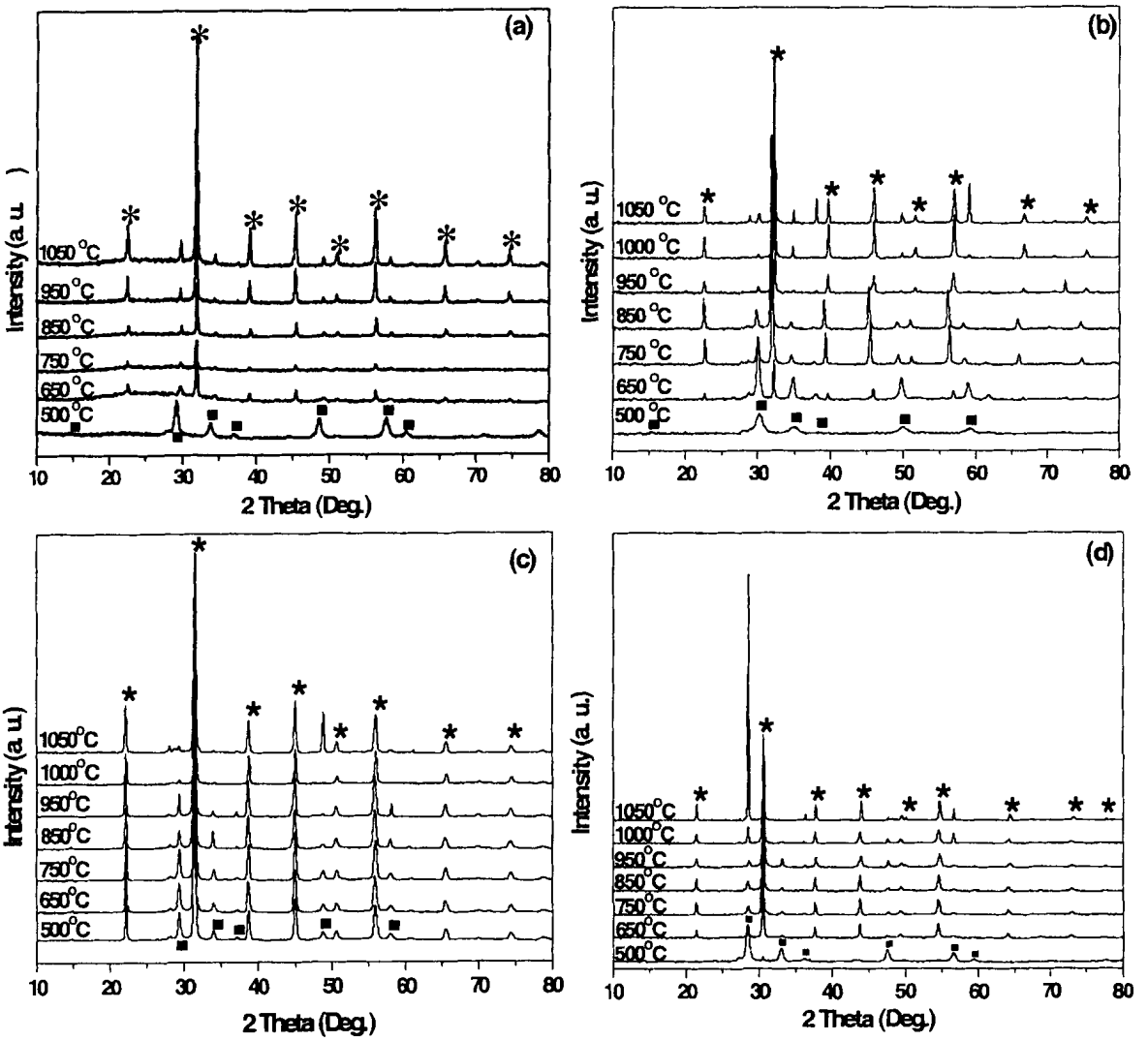

Figure 3.2: X-Ray diffraction spectra at different calcination temperatures of (a) 10PEG(S)T, (b) 10PEG(S), (c) 10PEG(5), and (d) 10PEG(5)T precursor powders. All samples were calcined for a period of 8 h (* Perovskite; ▪ Pyrochlore).

Figures 3.3 (a) and 3.3 (b) show the plots of the amount of perovskite phase formed as a function of the sintering temperature for the 10PEG(S)T and 10PEG(S), and the 10PEG(5) and 10PEG(5)T ceramics, respectively. For 10PEG(S)T [Fig. 3.3 (a)] as the sintering temperature is increased, the amount of perovskite phase also increases from ~75 % at 650 °C to a maximum of ~ 90 % at 950 °C, after which it drops down to ~88 % at 1050 °C. The ceramic relative density, on the other hand, increased from ~85 % at 950 °C to 95 % at 1050 °C. For 10PEG(5) [Figure 3.3 (b)], the sample treated at 500 °C already contains more than 87 % of the perovskite phase. Upon further heating, the amount of the perovskite phase increases to a maximum of ~96 % at 1000 °C and then decreases to ~93 % at 1050 °C with the relative density being ~95 % for both temperatures. These results indicate that the presence of a 5 % excess of lead in the precursor solution improves the formation the perovskite phase by about 2 – 5 % in the 10PEG(5) ceramics as compared to 10PEG(S)T for the same sintering temperature. The 10PEG(5)T sample treated at 500 °C contains ~20 % of the perovskite phase, which increases to a maximum of about 85 % at 750 °C, after which it drops considerably down to only ~25 % [Fig. 3.3 (b)] at 1050 °C. In the case of 10PEG(S), the amount of perovskite phase formed after treatment at 650 °C is about 42 %. This value increases to a maximum of ~91 % at 1000 °C [Fig. 3.3 (a)], dropping to 88 % at 1050 °C. Both ceramics showed a lower calculated density of ~ 90 % compared to the 10PEG(S)T and 10PEG(5) sintered at 1050 °C and 1000 °C, respectively. These results show that a 5 % mol excess of lead in the precursor powder favours the formation of the perovskite phase at a temperature as low as 500 °C in both 10PEG(5) and 10PEG(5)T but the former has considerably more of the perovskite phase. It is interesting to note that the 5 % excess of

lead without THOME results in the highest perovskite phase of 96 %, while the combination of an excess of lead and THOME in the precursor powder leads to a maximum perovskite phase of about 85 % only.

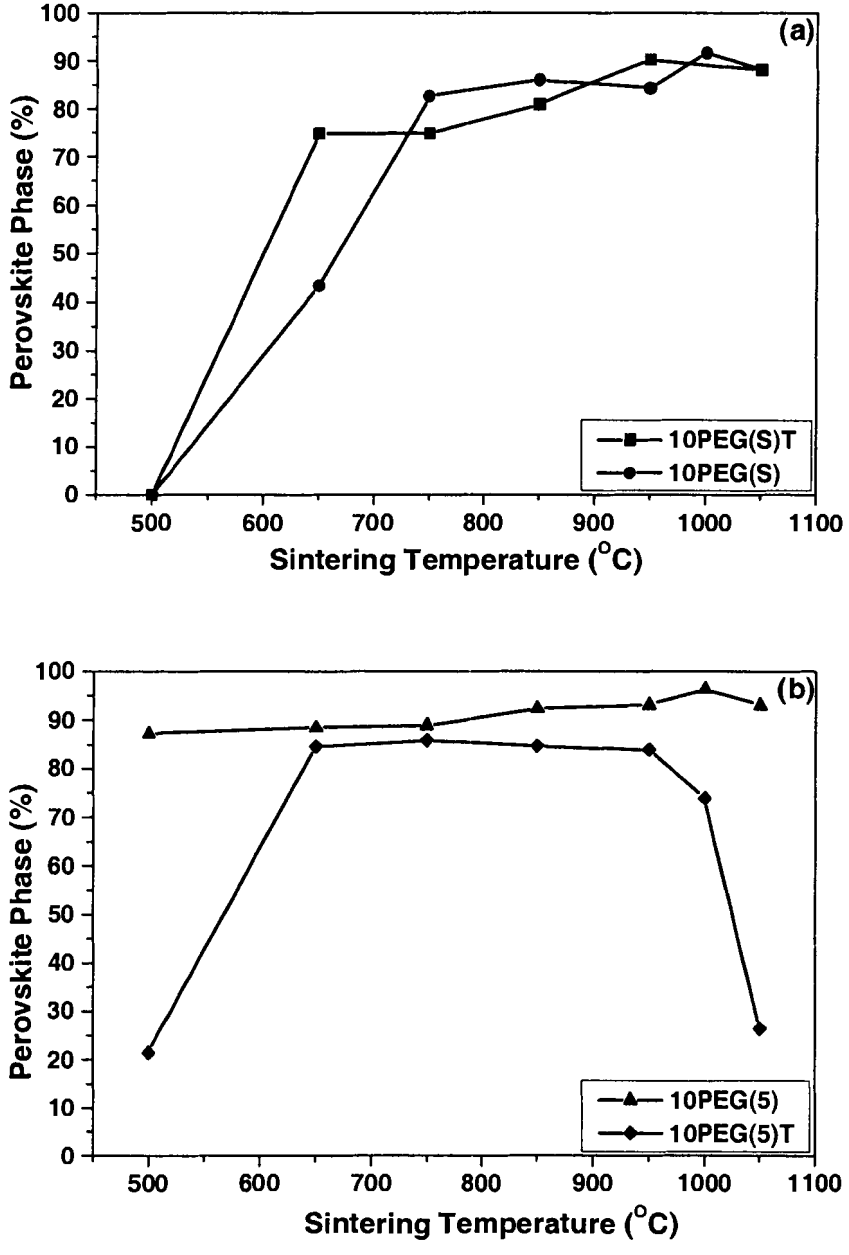

Figure 3.3: Dependence of the amount of perovskite phase formation on the sintering temperature of the (a) 10PEG(S)T and 10PEG(S), and (b) 10PEG(5) and 10PEG(5)T ceramics.

3.3.3 Dielectric Measurements

Figures 3.4 (a) and 3.4 (b) illustrate the temperature and frequency dependences of the real part of the dielectric permittivity (ε') of the 10PEG(S)T and 10PEG(5) ceramics sintered at 1050 °C and 1000 °C, respectively, with a relative density of 95 %. As can be observed from these curves, a ferroelectric to paraelectric phase transition occurs at the Curie temperature (T_C) of ~40 °C for both ceramics. The 10PEG(S)T ceramic shows a room temperature dielectric constant of nearly 25,000, and a maximum value of ε'_{max} ~33,000 at T_{max} ~40 °C (1 kHz). It is worth noting that these dielectric constant values are considerably higher than those obtained by solid state reactions [10], or other sol-gel processes [11]. The room temperature dielectric constant obtained here is the highest value observed so far in 0.90PMN–0.10PT ceramics. On the other hand, the 10PEG(5) ceramic shows a much lower dielectric constant value of ~8,000 at room temperature and an ε'_{max} of ~10,000 at T_{max}. The dielectric measurements of the 10PEG(S) sample sintered at 1000 °C (not shown) gave rise to a room temperature dielectric constant of 12,500 and an ε'_{max} of ~19,700 at a T_{max} ~42 °C.

It is interesting to note here that the 10PEG(S)T ceramic sintered at 1050 °C shows the best dielectric properties even with the lowest amount of perovskite phase (88 %). The high value of dielectric constant in the 10PEG(S)T ceramic can be attributed to the presence of the THOME molecule in the sol-gel process. Its beneficial role in the sol-gel preparation of 0.65PMN–0.35PT ceramics using polyethylene glycol-200 and methanol as solvent has been highlighted in our previous work [20] (See Chapter 4). The presence of three hydroxyl groups on the THOME molecule allows it to complex to metal centers, leading to the possibility of cross-linked or oligomeric species in solution [19].

The benefit of this is an easier formation of M–O–M bonds and their arrangement into a more compact structure after the organic components are burnt off, favouring a denser ceramic with larger grain sizes [as depicted in the 0.65PMN–0.35PT ceramics prepared with stoichiometric lead and THOME (See Chapter 4)] having better dielectric properties. An excess of lead can improve the formation of the perovskite phase to some extent, but it can also degrade the dielectric properties of the resulting ceramic, especially in combination with THOME. This is shown by the considerable lowering of the room temperature dielectric constant and ε'_{max} in 10PEG(5), as compared to 10PEG(S)T. The dielectric properties of the stoichiometric 10PEG(S) without THOME are intermediate between 10PEG(S)T and 10PEG(5). This is probably because the absence of THOME in 10PEG(S) results in smaller grain sizes in the ceramic, hence lowering the dielectric constant. As for the 10PEG(5) ceramic, the presence of an excess of lead might have resulted in the incorporation of PbO in the grain boundaries, causing a considerable decrease in the dielectric properties.

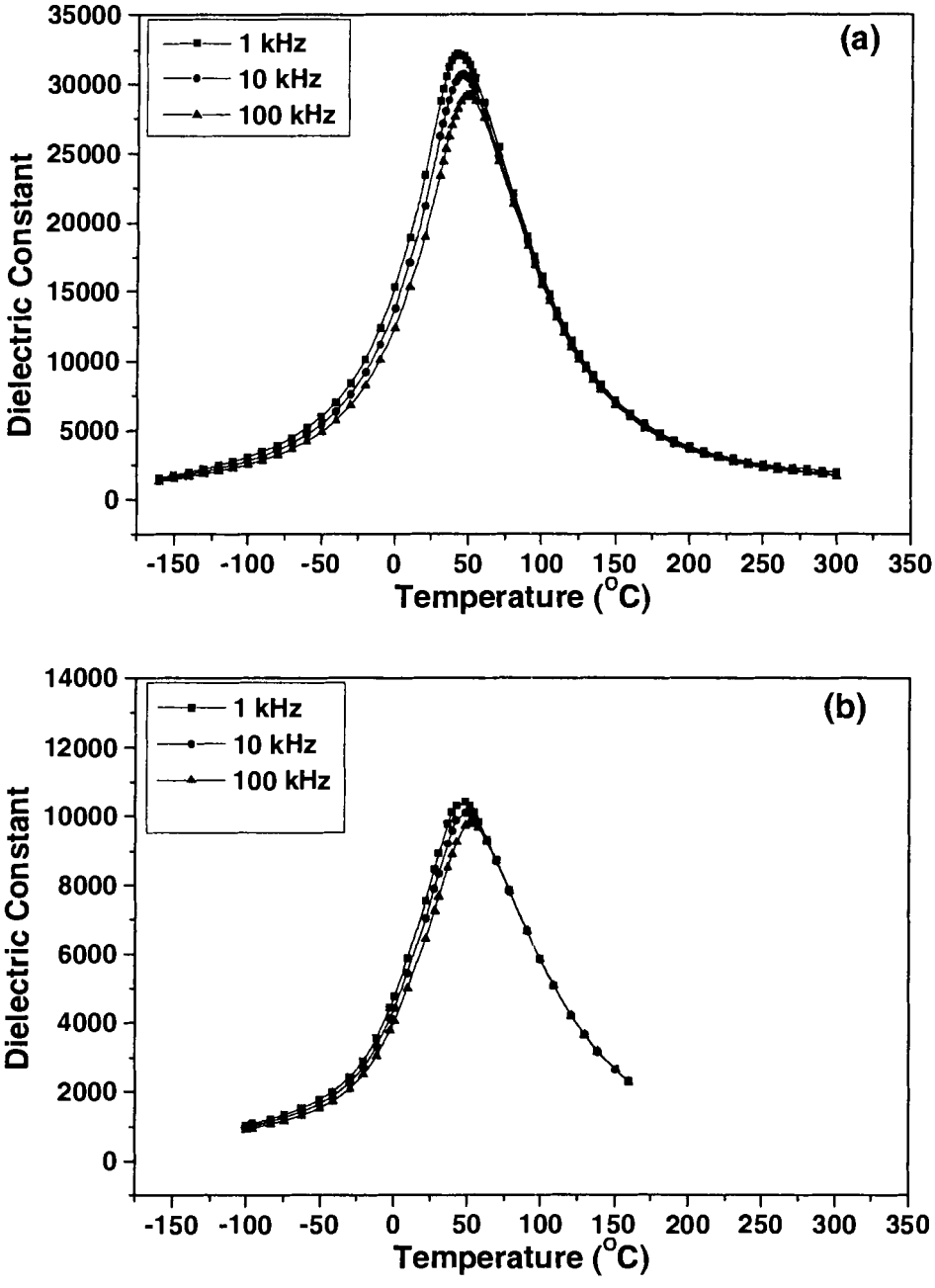

Figure 3.4: Impedance spectroscopic data showing the dependence of dielectric constant as a function of temperature and frequency for (a) 10PEG(S)T and (b) 10PEG(5) ceramics sintered at 1050 °C and 1000 °C for 8 h, respectively.

3.3.4 Ferroelectricity

The ferroelectric hysteresis loops of the 10PEG(S)T and 10PEG(5) ceramics sintered at 1050 °C and 1000 °C are shown in Figures 3.5 (a) and 3.5 (b), respectively. Both ceramics have a coercive field, E_C, of about 7.5 kV/cm. The 10PEG(S)T ceramic shows a well-defined and saturated ferroelectric hysteresis loop with a remnant polarization (P_r) of 18 $\mu C/cm^2$ which is higher than that of 10PEG(5) (P_r = 11 $\mu C/cm^2$). The improved ferroelectric properties of the 10PEG(S)T ceramic can also be attributed to the presence of the THOME molecule in the sol-gel synthesis, leading to a dense morphology and good dielectric properties. These properties make the material promising for applications in advanced electromechanical devices. The presence of excess lead in the 10PEG(5) ceramic is again detrimental as it lowers the P_r of the compound. Ferroelectric hysteresis measurement of a 10PEG(S) sample (not shown) sintered at 1000 °C shows a coercive field of ~7.5 kV/cm and a remnant polarization of 19 $\mu C/cm^2$, which are very close to the results observed in 10PEG(S)T.

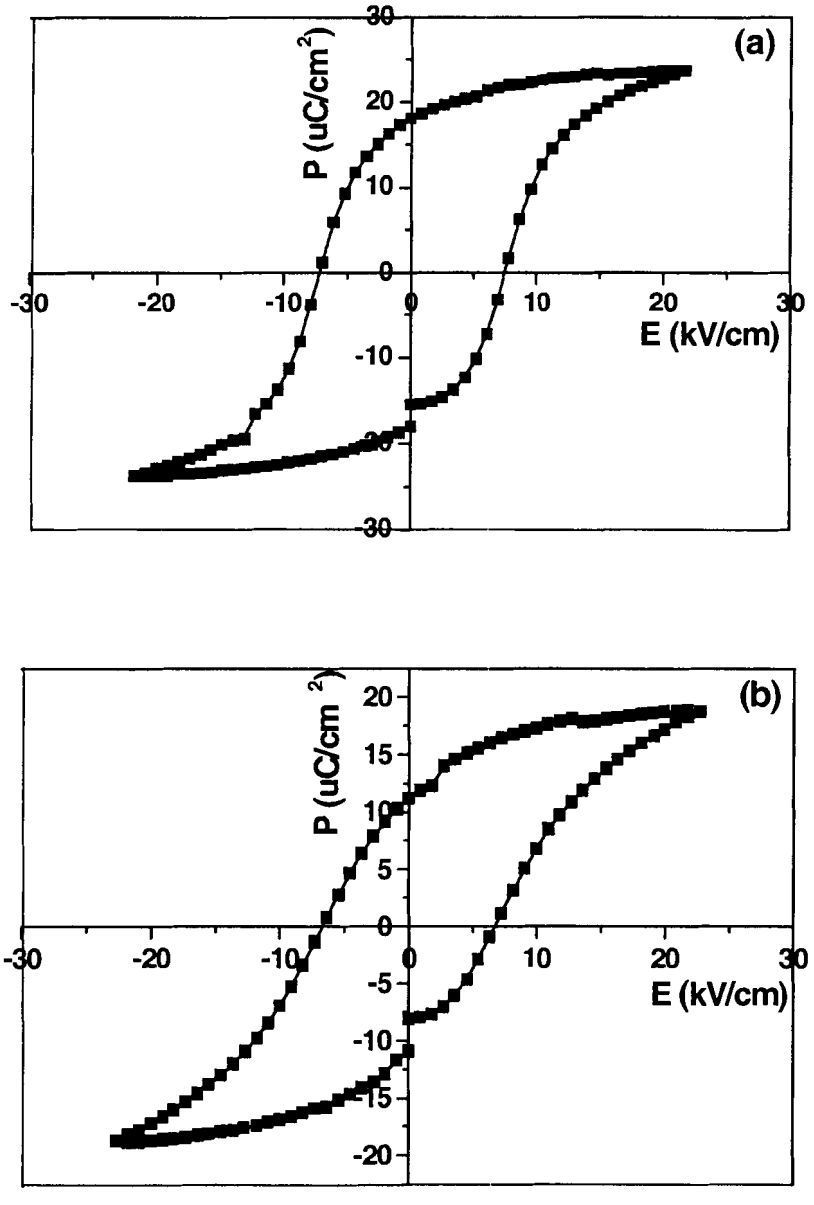

Figure 3.5: Ferroelectric hysteresis loops showing the variation of electrical polarization as a function of applied electric field for (a) 10PEG(S)T and (b) 10PEG(5) ceramics sintered at 1050 °C and 1000 °C for 8 h, respectively.

3.4 Conclusion

Relaxor ferroelectric 0.90PMN–0.10PT ceramics have been synthesized by a new room temperature soft chemical route, which uses polyethylene glycol-200 and methanol as solvent. The effects, on the ceramic quality, of using a complexing agent, 1,1,1-tris(hydroxymethyl)ethane (THOME) and stoichiometric amount of the lead starting material in comparison to using (i) stoichiometric amount of lead and no THOME, (ii) 5 % mol excess of lead and no THOME, and (iii) 5 % mol excess of lead and THOME, have been studied in this work. Stable precursor solutions are obtained from all the sol-gel reactions, which makes the method promising for making thin films. It has been proposed by thermal analysis that the THOME molecule takes part in the sol-gel process, by binding to the metal centers and forming cross-linked or oligomeric species which have an influence on the arrangement of the M–O–M networks in the ceramic precursor powder. The results, summarized in Table 1, show better electrical properties in the ceramics synthesized with stoichiometric amount of lead. On the other hand, the presence of an excess of lead in the ceramics impaired the electrical properties even though it leads to a slightly higher percentage of the perovskite phase. These ceramics show lower values of the room temperature and maximum dielectric constants, and remnant polarization (8,000 and 10,000, and 11 $\mu C/cm^2$, respectively) as opposed to room temperature dielectric constant of 25,000 and ε'_{max} of 33,000, and P_r of 18 $\mu C/cm^2$ in the ceramics prepared with THOME and no excess of lead. Ceramics synthesized from precursor solutions containing stoichiometric amount of lead and no THOME have intermediate room temperature dielectric constant, ε'_{max}, and P_r (12,500, 19,500, and 19 $\mu C/cm^2$, respectively) between the 10PEG(S)T and 10PEG(5). It can clearly be shown from the

results that of the ceramics prepared with stoichiometric lead, the one containing THOME in the sol-gel process has the best dielectric properties. This highlights the important role of the triol molecule in the synthesis of 0.90PMN–0.10PT compounds.

	Phase		Properties				
	Max.% Perovskite	Sintering temperature (°C)	ε' (RT)	ε'max.	Tmax.	Pr (RT)	Rank*
10PEG(S)T	90.3	950	25,000	33,000	40	18	1
10PEG(S)	91.7	1000	12,500	19,700	42	19	2
10PEG(5)	96.4	1000	8,000	10,000	40	11	3
10PEG(5)T	85.9	750	-	-	-	-	4

*** 1: Best; 4: Worst**

Table 3.1: Phase formation and properties of 0.90PMN–0.10PT ceramics prepared under various conditions.

Acknowledgement

This work was supported by Natural Science and Engineering Research Council of Canada (NSERC).

3.5 References

1. S. J. Jang, K. Uchino, S. Nomura, and L. E. Cross, *Ferroelectrics*, **27**, 31 (1980).
2. S.-E. Park, and T. R. Shrout, *J. Appl. Phys.*, **82** [4], 1804 (1997).
3. Z.-G. Ye, and M. Dong, *J. Appl. Phys.*, **87** [5], 2312 (2000).
4. Z.-G. Ye, *Key Eng. Mater.*, **155-156**, 81 (1998).
5. T. R. Shrout, Z. P. Chang, N. Kim, and S. Markgraf, *Ferroelectric Lett.*, **12**, 63 (1990).
6. Z.-G. Ye, Y. Bing, J. Gao, and A. A. Bokov, *Phys. Rev. B.*, **67**, 104104-1 (2003).
7. B. Noheda, D. E. Cox, G. Shirane, J. Gao, and Z.-G. Ye, *Phys. Rev. B*, **66**, 054104 (2002).
8. R. E. Newhnam, Q. C. Xu, S. Kumar, and L. E. Cross, *Ferroelectrics*, **102**, 259 (1990).
9. L. F. Francis, and D. A. Payne, *J. Am. Ceram. Soc.*, **74** [12], 3000 (1991).
10. S. L. Swartz, T. R. Shrout, W. A. Schulze, and L. E. Cross, *J. Am. Ceram. Soc.*, **67** [5], 311 (1984).
11. Ravindranathan, S. Komareni, A. S. Bhalla, and R. Roy, *J. Am. Ceram. Soc.*, **74** [12], 2996 (1991).
12. F. Chaput, J. P. Boilot, M. Lejeune, R. Papiernik, and L. G. Hubert Pfalzgraf, *J. Am. Ceram. Soc.*, **72** [8], 1355 (1989).
13. Y. Narendar and G. L. Messing, *J. Am. Ceram. Soc.*, **80** [4], 915 (1997).
14. M. P. Pechini, U.S. Pat. No. 3,330,697 (1967).
15. P. A. Lessing, *Am. Ceram. Soc. Bull.*, **68**, 1002 (1989).
16. L.-W. Tai, and P. A. Lessing, *J. Mater. Res.*, **7**, 502 (1992).
17. S. C. Zhang, G. L. Messing, W. Huebner, and M. M. Coleman, *J. Mater. Res.*, **5**, 1806 (1990).
18. N. Uekawa, M. Endo, K. Kakegawa, and Y. Sasaki, *Phys. Chem. Chem. Phys.*, **2**, 5485 (2000).
19. N. Sriprang, D. Kaewchinda, J. D. Kennedy, and S. J. Milne, *J. Am. Ceram. Soc.*, **83** [8], 1914 (2000).
20. K. Babooram, and Z.-G. Ye, *Chem. Mater.*, **16**, 5365 (2004).

Chapter 4:
Polyethylene Glycol-Based New Solution Route to Relaxor Ferroelectric $0.65Pb(Mg_{1/3}Nb_{2/3})O_3$–$0.35PbTiO_3$

K. Babooram, and Z.-G. Ye*

Department of Chemistry, Simon Fraser University, 8888 University Drive, Burnaby, BC, Canada, V5A 1S6

* Corresponding author; Tel.: (604) 291-3351; Fax: (604) 291 3765;

email address: zye@sfu.ca

Reproduced with permission from *Chem. Mater.*, **16**, 5365-5371 (2004).

ABSTRACT

A new soft chemical route has been developed for the synthesis of relaxor ferroelectric lead magnesium niobate – lead titanate solid solution (0.65PMN-0.35PT). The method uses a polyethylene glycol (PEG) and methanol mixture as solvent and it has very interesting features. Not only does it allow reactions to be performed at room temperature, but it also does not require an excess amount of the lead starting material to compensate for lead oxide loss during ceramic sintering as is usually the case in conventional synthesis. The effect of using a triol molecule, 1,1,1-tris(hydroxy)methylethane (THOME), which is known to serve as a complexing agent in binding together the metal ions in the precursor solution, has also been studied. Pure perovskite phase was obtained in ceramics sintered at a relatively low temperature of 1040 °C as compared to 1250 °C in solid state reactions. The dielectric constant at room temperature is above 5000 and the value at the Curie temperature reaches up to ~27000 at a frequency of 1kHz. Ferroelectric hysteresis is displayed on a ceramic with an average grain size of 2 μm, giving rise to a remnant polarization (P_r) of 21 μC/cm^2 and a coercive field (E_c) of ~7.5 kV/cm.

4.1 Introduction

The solid solutions between the relaxor ferroelectric lead magnesium niobate, $Pb(Mg_{1/3}Nb_{2/3})O_3$ (PMN), and the normal ferroelectric lead titanate, $PbTiO_3$ (PT), abbreviated as (1-x)PMN–xPT (or PMNT), have gained a lot of interest as potential candidates for dielectric and piezoelectric devices, such as multi-layer capacitors, sensors, and actuators [1-4]. While lower PT contents give rise to materials with high dielectric constants and low remnant polarization suitable for dynamic random-access memory (DRAM) devices, those with higher PT contents have low dielectric constants and high remnant polarization at room temperature. Compositions around the morphotropic phase boundary (MPB) exhibit typical ferroelectric hysteretic character, with a large spontaneous polarization and a low coercive field, showing great potentials for advanced electromechanical applications both in the forms of electroceramics and thin or thick films [5]. Recently, single crystals of (1-x)PMN–xPT solid solutions have been found to exhibit electromechanical performance superior to that of the (1-x)$PbZrO_3$–x$PbTiO_3$ (PZT) ceramics [6,7] which have intensely been used for decades as piezoelectric materials for transducers and actuators [8].

Although most research to date has been concentrated on compounds based on the PZT system because of its high remnant polarizations, certain drawbacks like fatigue and aging have deviated attention towards other materials in the quest for better properties [9]. In that respect, the (1-x)PMN–xPT system stands as a potential candidate as its ceramics have been reported to show high dielectric, piezoelectric, and electrostrictive properties. One of the challenges in making PMNT compounds is to suppress and avoid

the formation of a pyrochlore phase which is kinetically favoured over the perovskite phase, and therefore forms more easily. This phase is functionally undesirable because it impairs the dielectric properties of the materials [10].

Solid state reactions, which are relatively cheap and easy to handle, have been widely used to prepare mixed oxide powders and ceramics, but the failure to achieve homogeneity and single phase in some final products has given rise to a number of powderless processing methods which use liquid precursors rather than powders as starting materials [11]. The latter have gained interest because they offer such advantages as control of homogeneity, stoichiometry, purity, therefore leading to increased reactivity [12]. Among the various routes to homogeneous multi-component oxides that have recently been developed, the polymeric precursor method has drawn a lot of attention [13]. Pioneered by Pechini in the 1960's, this method provides a simple route to oxide powders by first making a solution containing all the cations in the form of polymer-cation complexes in the desired stoichiometry, and then firing this solution to drive off any organic moeties and to form the target oxides [14]. Chelation and entrapment of the cations by the polymer chains gives ceramic powders with better chemical homogeneity and a smaller particle size. This is explained from the fact that chelation considerably lowers the mobility of the cations thereby stabilizing them against precipitation [15], which is the key requirement to obtaining a stable precursor solution that can be used for making thin films.

Several researchers have reported the synthesis of multicomponent ceramic oxides via the oxidation of polyethylene glycol- or poly(vinyl alcohol)-cation complexes [11,13,15-17]. The Pechini method, which uses α-hydroxycarboxylic acids like citric and

lactic acids together with polyhydroxyl alcohols such as ethylene glycol to make a polymer resin, has been modified to some extent to the use of water-soluble sources such as metal nitrates and chlorides. This has now become a very common method because these inorganic salts are more stable than the corresponding alkoxides, and hence, easier to handle. Another way of forming extended structures in solution is by crosslinking the cations using a molecule with several binding sites. Sriprang and co-workers [18] demonstrated this through a triol-based route to PZT thin films in which, 1,1,1-tris(hydroxy)methylethane (THOME) was used as the complexing agent. However, to the best of our knowledge, no application of such a technique has been made to the synthesis of the (1-x)PMN–xPT systems. Commonly, sol-gel processes using alkoxides require refluxing at temperatures usually above 100 °C to allow for hydrolysis and condensation reactions to take place and to form the cross-linked structures.

In this work, we report the sol-gel synthesis of 0.65PMN–0.35PT ceramics using a mixture of polyethylene glycol-200 and methanol as solvent for the starting materials. The PMN/PT ratio of 65/35 has been chosen because this composition lies near the morphotropic phase boundary (MPB) which separates the rhombohedral, monoclinic and tetragonal phases in the (1-x)PMN–xPT phase diagram [2]. For compositions around the MPB, anomalously high pyroelectric and dielectric properties have been demonstrated which could be of high interest in thin-layer devices [3,4]. Single crystals of the MPB composition exhibit excellent piezoelectric properties [6,7]. Moreover, MPB compositions are interesting because of an increase in the maximum phase transition temperature (T_{max}) from ~15 to more than 145 °C when the PT content is increased from zero to the MPB compositions [3,19,20]. Using the polymer/alcohol mixture, we are able

to perform a room temperature reaction to make the precursor solution, as well as to obtain the pure (pyrochlore-free) perovskite phase for the PMN–PT ceramics. Furthermore, this new route to PMNT ceramics does not require the use of an excess of the lead starting material, which is necessary in all conventional and most of soft chemical syntheses in order to compensate for lead oxide loss during sintering at high temperatures. We also compare the difference in the quality of the final ceramics with or without using the triol molecule during the sol-gel synthesis.

4.2 Experimental

4.2.1 Preparation of 0.65PMN-0.35PT Ceramics

Ceramics of $0.65Pb(Mg_{1/3}Nb_{2/3})O_3$–$0.35PbTiO_3$ (0.65PMN–0.35PT) solid solution were synthesized by the method outlined in Figure 4.1. Stoichiometric amounts (corresponding to the 0.65PMN-0.35PT composition) of lead acetate trihydrate [$Pb(O_2C_2H_3)_2.3H_2O$, 2.3898 g, 6.30 mmol], magnesium 2,4-pentanedionate dihydrate [$Mg(O_2C_5H_7)_2.2H_2O$, 0.3564 g, 1.38 mmol], and 1,1,1-tris(hydroxy)methylethane (THOME) [$C(CH_2OH)_3CH_3$, 0.3785 g, 3.15 mmol] were mixed with an excess of polyethylene glycol-200 (PEG200) and methanol mixture (PEG200/MeOH at a 1:2 volume ratio). In a separate reaction flask, niobium ethoxide [$Nb(OCH_2CH_3)_5$, 0.8687 g, 2.73 mmol], titanium di-isopropoxide bis-acetyl acetonate (TIAA) [$Ti(O_2C_5H_7)_2(OCH(CH_3)_2)_2$, 1.0701 g, 2.94 mmol], and THOME (0.1766 g, 1.47 mmol) were also mixed with an excess of PEG200/MeOH (1:2) mixture. Both of these reaction mixtures were kept under stirring condition at room temperature for about 3 hours before they were mixed together and further stirred for about 5 hours to give a clear and homogeneous yellow solution. The latter was then dried in a rotary evaporator in order to remove all organic volatiles and form a viscous solution, which was then heat-treated in a high temperature furnace at 500 °C for 2 hours at a heating and cooling rate of 300 °C/h. At this point, a bright yellow powder was obtained and it was ground in acetone, and pressed into pellets. These were then calcined for a period of 8 h in a Pt/Al_2O_3 double crucible set up containing Pb_3O_4 as a PbO source to prevent any lead oxide loss from the sample during this process. The same reaction was also performed, but without the triol

molecule in order to study the possible influence on the properties of the ceramics. The samples containing the triol were named as PEG(S)T and those without the triol PEG(S), respectively.

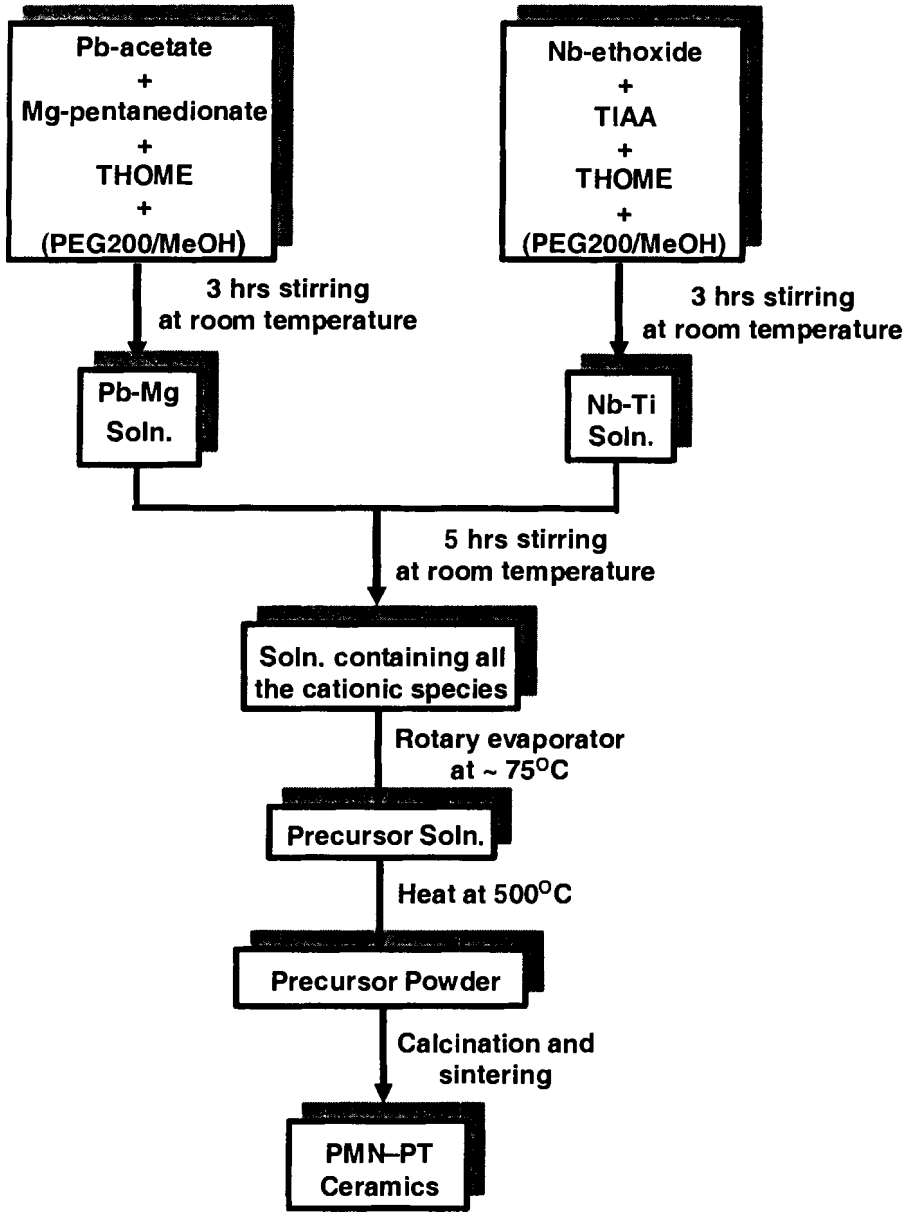

Figure 4.1: Flowchart for the preparation of precursor solutions and ceramics of (1-x)PMN–xPT (x = 0.10 and 0.35).

4.2.2 Characterization of the 0.65PMN-0.35PT Ceramics

Powder X-Ray diffraction (XRD) patterns were obtained on a Philips powder diffractometer using CuKα radiation (40 kV, 35 mA) in order to check the phases formed. The decomposition pathways of the precursor solutions were observed by thermogravimetric and differential thermal analyses (TG/DTA) on a Seiko Exstar 6300 TG/DTA Thermal Analyzer. The precursor solutions were oxidized by heating from room temperature to 1000 °C at a heating rate of 5 °C/min. Fourier transform infrared spectroscopy (FTIR) spectra were obtained on a Bomem MB spectrometer in order to monitor the transformation of the precursor solutions during the thermal reactions leading to the oxides. Grain size was imaged using scanning electron microscopy (SEM) on a Bausch and Lomb Nanolab 2100 SEM instrument, and dielectric permittivity was measured as a function of temperature in a frequency range of 10^2-10^6 Hz on a computer-controlled impedance analyzer (Solartron 1260) in conjuction with a dielectric interface (Solartron 1296). Ferroelectric hysteresis measurements were performed on a RT66A standard ferroelectric testing system.

4.3 Synthesis of 0.65PMN–0.35PT Ceramics

4.3.1 Sol-gel Synthesis

The main challenge at the beginning of this work was to find a proper solvent that would be able to dissolve all the starting materials, especially the magnesium 2,4-pentanedionate which is very difficult to dissolve in such solvents as 2,4-pentanedione, pure methanol, or ethanol. Finally, a 1:2 volume ratio of polyethylene glycol (PEG200) and methanol mixture proved to be successful in obtaining a homogeneous solution mixture containing all four cationic species. An interesting feature here is that this precursor solution to the target 0.65PMN-0.35PT ceramics was formed at room temperature by simple mixing and stirring conditions, thus avoiding the reflux and distillation steps usually required in sol-gel reactions. Moreover, the sol is not moisture sensitive and shows very good stability against precipitation, which makes it a very promising stock solution for depositing thin films. One common practice in the synthesis of lead-based ceramic oxides is to use an excess amount of lead starting material in order to compensate for any loss in terms of PbO during the calcining and sintering processes at high temperatures. In this respect, another benefit of this solvent system is that it facilitates the synthesis of the PMN-PT compound of pure perovskite phase without the need for an excess amount of the lead acetate. However, it has been found that an excess of the PEG200/methanol mixture is necessary in order to keep the solutions from precipitating during the synthesis process.

The triol molecule, 1,1,1-tris(hydroxy)methylethane (THOME), was initially employed in the synthesis of the precursor solutions with a view of improving the quality

of metal oxides because of its high metal-complexing ability, as demonstrated by Sriprang et al. [18], who observed an improvement in the quality of lead zirconium titanate thin films when THOME was employed in the sol-gel synthesis of the precursor solution. At the same time, it is also very well known that polyethylene glycol also chelates and entraps metal ions very efficiently in solution and this helps in the formation of the pure phase of multi-component ceramic oxides when the solution is fired at high temperatures [11]. Based on this consideration, we also performed the reactions without THOME in order to study its role in the synthesis process of the 0.65PMN–0.35PT ceramics. This resulted in ceramics containing about 5 % pyrochlore phase, with considerably lower dielectric constant and remnant polarization values.

4.3.2 X–Ray Diffraction (XRD)

The formation of different phases in all the samples was monitored using X-ray powder diffraction. As can be seen from the XRD patterns in Figures 4.2 (a) and 4.2 (b), the PEG(S)T and PEG(S) powders are already in the crystalline form after treatment at 500 °C, with the presence of a pyrochlore phase. In the case of PEG(S)T [Fig. 4.2 (a)], as temperature is increased further, the perovskite phase grows at the expense of the pyrochlore one, until a pure perovskite phase is obtained for the pellet calcined at 1040 °C. A very good ceramic density of ~ 96 % of the theoretical value was obtained after sintering at 1140 °C for 8 hrs. For the PEG(S) samples the perovskite phase is predominant over the pyrochlore phase as the temperature is increased above 500 °C, but as can be seen from Fig. 4.2 (b), a small amount of pyrochlore phase still subsists after heat treatment at 1040 °C for 8 hrs. As a result, the ceramics are not 100% pure perovskite although the density also reaches ~ 96%.

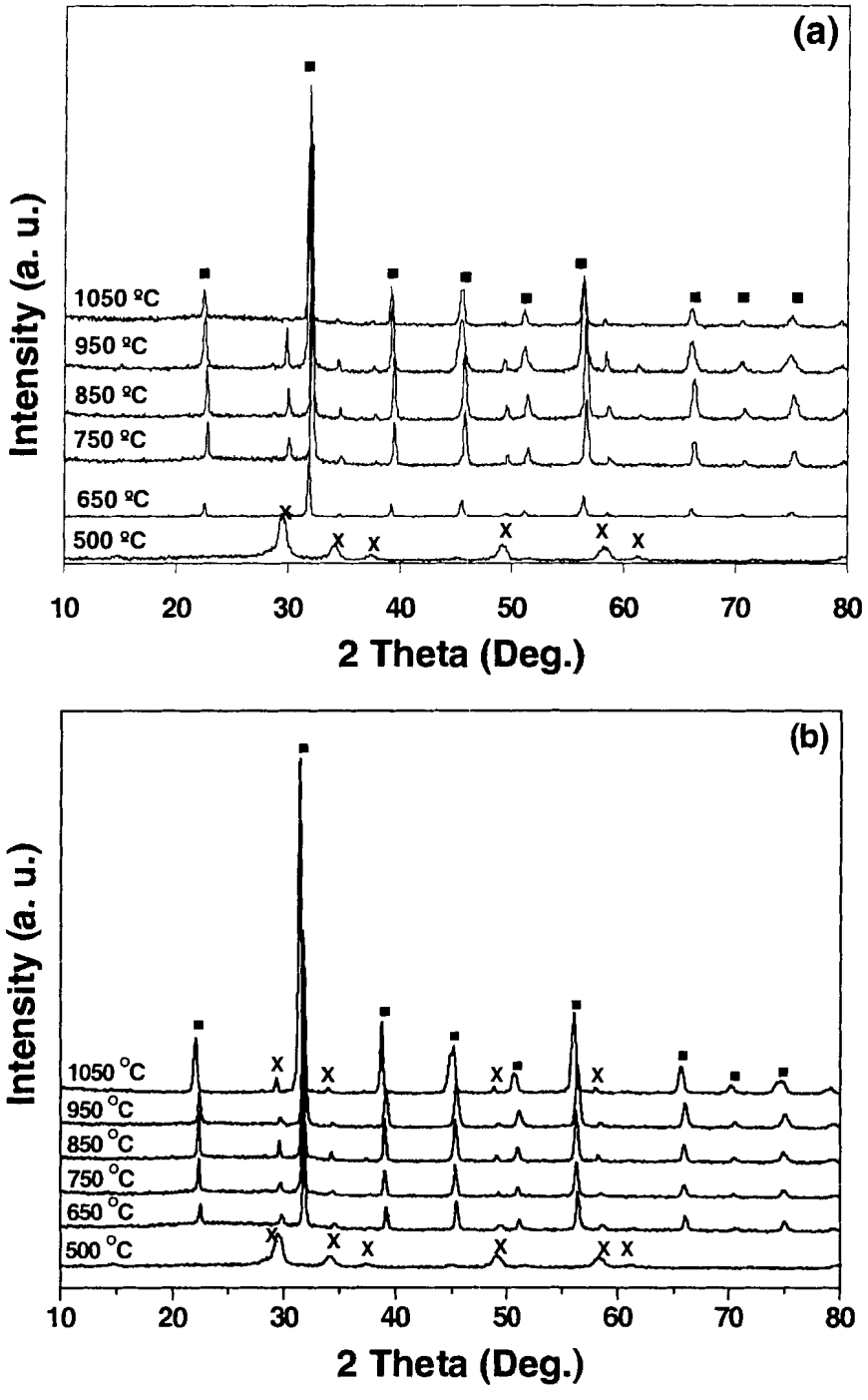

Figure 4.2: X-Ray diffraction spectra at room temperature of the (a) PEG(S)T and (b) PEG(S) precursor powders calcined at different temperatures for a period of 8 h (x pyrochlore; ▪ perovskite).

4.4 Mechanisms of the Reactions

4.4.1 Thermogravimetric/Differential Thermal Analysis (TG/DTA)

To determine the best conditions for the pyrolysis of the precursor solutions and the sintering of the precursor powders and to study the mechanisms of the reactions, thermal analyses were performed. Figures 4.3 (a) and 4.3 (b) show the thermogravimetric analysis / differential thermal analysis (TGA/DTA) curves of the PEG(S)T and PEG(S) precursor solutions, respectively, measured from room temperature up to 1000 °C at a heating rate of 5 °C/min. On the TGA curve of the PEG(S)T solution [Figure 4.3 (a)] three different weight loss regions can be identified. The initial weight loss in the region of 46 – 130 °C corresponds to the volatilization of solvent and/or moisture still present in the precursor solution. A second weight loss in the region of 157 – 330 °C results from the decomposition of the PEG chains as well as of THOME molecules and the acetate groups present in the sol. The strong and sharp exothermic peak at 331 °C arises from the decomposition of the PEG chains and the THOME molecules that were bound to the cations in the precursor solution, in the form of a self-combustion reaction. In separate DTA experiments on a sample of PEG200 (as illustrated in Figure 4.4), oxidation and decomposition peaks were observed below 300 °C. It should also be noted that the endothermic peaks that show up on the DTA curve of pure THOME at 197 °C, and 261.5 °C and 273.8 °C (shown in Figure 4.5), corresponding to the melting and the decomposition of the molecule, respectively, are absent on the DTA curve of the PEG(S)T sol. This indicates that the THOME has also taken part in the precursor solution formation by binding to the metal centers. Therefore, the strong exothermic peak at 331

°C on the DTA of the PEG(S)T sol must result from the decompositions of the PEG chains and of the THOME molecules that interacted with the cations. The fact that they were bound to the metal ions in the precursor solution increased their molecular weights and thereby shifted their decomposition points to a higher temperature than for the free chains or molecules. The final weight loss observed between 347 and 560 °C refers to the decomposition of more complex metal-organic moieties or oligomers that could form in the solution through the linking up of chains during the condensation reactions. This process is accompanied by the weak exothermic peaks observed at 346 °C and 430 °C. The other exothermic peak that appears at 537 °C can be attributed to the formation of a crystalline mixed oxide phase [21]. This crystallization process is also confirmed by X-ray diffraction patterns that show the formation of a pyrochlore phase in a powder heat-treated at 500 °C [See Sec. 4.3.2 (b)]. All these observations lead to the conclusion that all the organic components of the precursor solution are burnt off at temperature below ~ 450 °C, after which, the resulting matter crystallizes into the pyrochlore phase through rearrangement of the random M-O-M networks present.

The thermal analyses on the PEG(S) precursor solution are given in Figure 4.3 (b). The only difference in this solution as compared to PEG(S)T is the absence of THOME as one of the starting materials in the sol-gel process. The results are similar: three different weight loss regions are found on the TGA curve in the temperature ranges of 40 – 100 °C, 150 – 286 °C, and 292 – 485 °C, corresponding to the evaporation of solvent and/or moisture from the precursor solution, the decompositions of the PEG-cation complexes and more complex PEG-cation structures, and the formation of crystalline mixed oxide phase, respectively. The exothermic peaks observed on the DTA

curve at 278 °C, and 335 °C and 418 °C result from the thermal events associated with the second and third weight losses, respectively. The exothermic peak at 471 °C is attributed to the crystallization of the pyrochlore phase, which is confirmed by X-ray diffraction [See Sec. 4.2 (b)]. The presence of this phase was detected in a powder synthesized at 500 °C, i.e., lower than that of the PEG(S)T sample. It can be seen that the presence of THOME in the PEG(S)T precursor solution increases the temperature of formation of the pyrochlore phase, i.e., from 471 °C in PEG(S) to 537 °C. This is attributed to the fact that THOME was also bound to the cations in the presence of PEG in the PEG(S)T solution. As a result, the mechanisms of decomposition of the metal-organic complexes in PEG(S)T and PEG(S) during the high-temperature heat treatment become different, thereby making the rearrangements of the metal-oxygen-metal network also proceed through different pathways. This may be the main reason why pure perovskite phase has been obtained in PMN–PT ceramics made from the PEG(S)T precursor solution, while some pyrochlore still exists in the ceramics synthesized from the PEG(S) solution. Therefore, THOME is shown to play a key role in the formation of the PMNT ceramics.

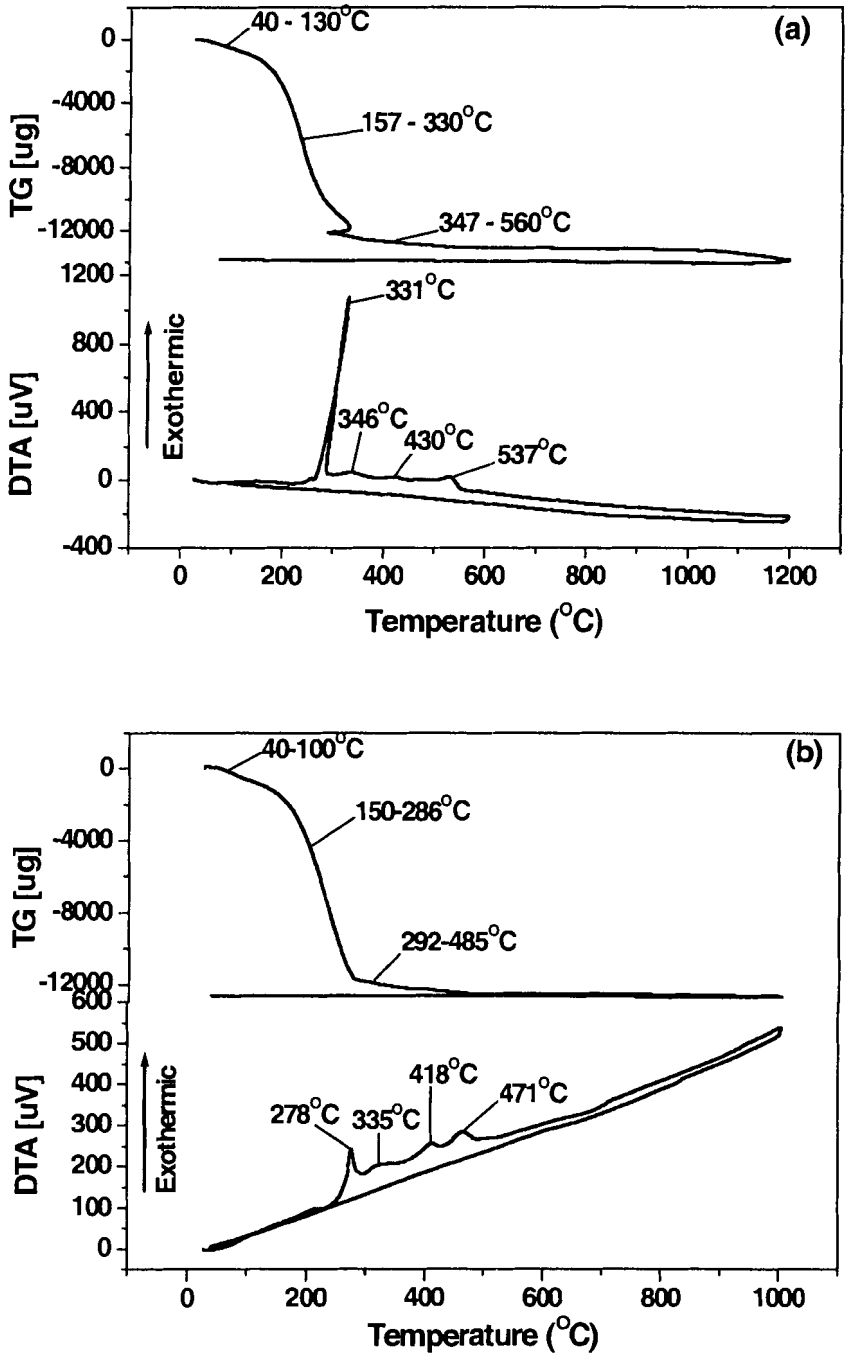

Figure 4.3: TG/DTA curves from room temperature at a heating rate of 5 °C/min for (a) PEG(S)T and (b) PEG(S) precursor solutions.

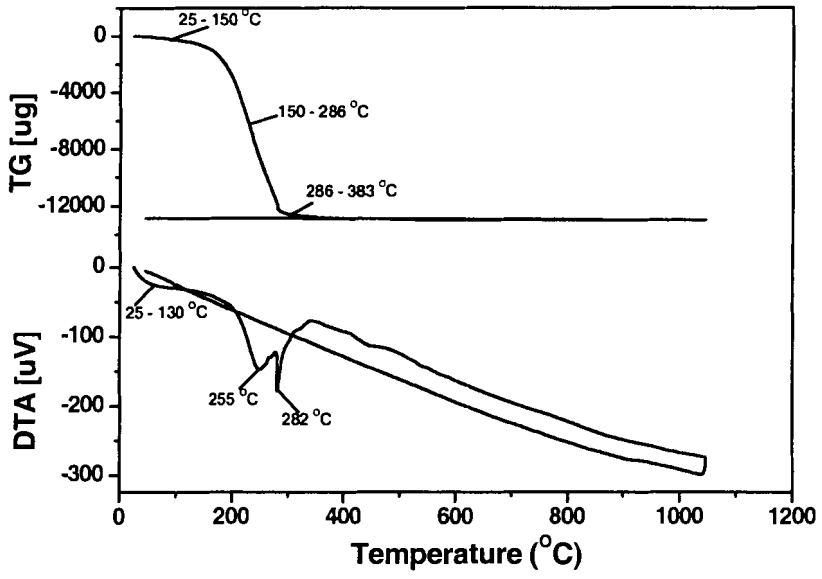

Figure 4.4: TG/DTA curves from room temperature to 1000 °C at a heating rate of 5 °C/min for polyethylene glycol 200 (PEG200).

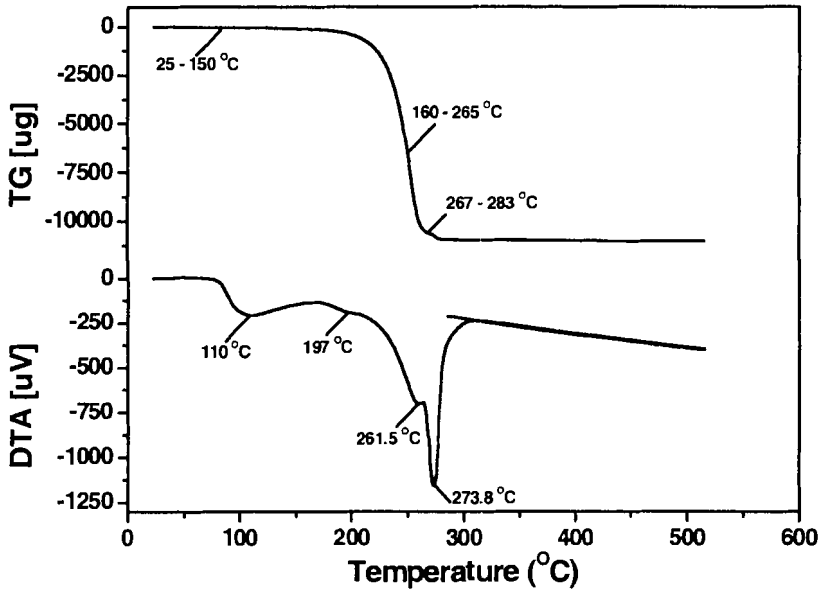

Figure 4.5: TG/DTA curves from room temperature to 500 °C at a heating rate of 5 °C/min for THOME.

4.4.2 Fourier Transform Infrared Spectroscopy (FTIR)

Figure 4.6 shows the FTIR spectra of the initial PEG(S)T and PEG(S) precursor solutions at room temperature, and the resulting products after these solutions were treated at different temperatures of 300, 500, 750, and 1040 °C for a period of 2 hrs. The frequency region of the spectra is from 4000 – 200 cm^{-1}. The spectra clearly show the decomposition of the organometallic species present in the precursor solutions as well as their rearrangements into the inorganic crystalline phases. The room temperature spectra for the PEG(S)T and PEG(S) solutions are very similar. The peaks in the region of 1100 – 1000 cm^{-1} and 700 – 300 cm^{-1} are due to the C-O and the M-O vibrations, respectively [22]. These peaks appear at 1100, 1030 and 662 cm^{-1} in PEG(S)T and 1111, 1030 and 662 cm^{-1} in PEG(S). The absorption peaks in the region of 3200 – 2800 cm^{-1} are assigned to the O-H and the C-H vibrations coming from the excess solvent present [23]. These two spectra also contain peaks from other organic moieties such as carbonyl (~1722 cm^{-1}), acetate (1578 cm^{-1}) and acetylacetonate (1460 and 1350 cm^{-1}) groups which come from the starting materials. After the heat treatment of these precursor solutions at 300 °C, most of the peaks from the organic moieties (O-H: 3376 cm^{-1}, C-H: 2895 cm^{-1}, C=O: 1722cm^{-1}, C-O: 1100cm^{-1}, conjugated C=C: 1578cm^{-1}) [22,23] disappear, indicating the breaking down of the bonds and the decomposition of these species. The peaks that show up at 2363 and 1629 cm^{-1} for the PEG(S)T sample treated at 300 °C can be assigned to the C=O and C≡O stretching of carbon dioxide and carbon monoxide molecules trapped in the pores of the powder, respectively. Similar results were obtained for the PEG(S) sample treated under the same conditions.

As the treatment temperature is increased to 500 °C, some differences appear between the PEG(S)T and the PEG(S)T spectra. The peaks at 1622, 1337 and 1112 cm^{-1} practically merge together into a broad peak on the PEG(S)T spectrum, while they remain distinct on the PEG(S) spectrum. The other remarkable difference is the intense broad peak at 682 cm^{-1} for the PEG(S)T sample, which is assigned to metal-metal and metal-oxygen bonds formed as the organic components burn away and the M-M and M-O networks rearrange themselves towards a more ordered crystalline structure. On the PEG(S) spectrum the two peaks at 596 and 398 cm^{-1} almost merge into a broad one. This clearly points to the existence of different arrangements of metal-oxygen-metal networks in these two samples, resulting from the effect of THOME present in the synthesis of the PEG(S)T sol. After the treatments at 750 and 1040 °C, all the organic moieties have completely been eliminated and the absorption peaks are solely from the M-M and M-O bonds both for PEG(S)T and PEG(S).

At 750 °C, both samples still contain some pyrochlore phase as shown by the XRD patterns in Figures 4.3 (a) and (b). However, the IR spectra of the PEG(S)T and PEG(S) samples treated at this temperature, show difference in the peak positions indicating different arrangements of the metals and oxygen ions in these two powders. After the treatment at 1040 °C, the complete disappearance of the sharp peak at 1629 cm^{-1} and the shift of the 742 cm^{-1} peak to 636 cm^{-1} on the PEG(S)T spectrum provide evidence that the powder has transformed into the pure perovskite phase, while the PEG(S) powder still retains some pyrochlore. This can be supported by the negligible shift in the peak from 390 cm^{-1} to 386 cm^{-1} (from 750 °C to 1040 °C) on the PEG(S) spectrum. Therefore, it can be seen that the IR and XRD data match, supporting the fact that pure perovskite

phase is obtained at 1040 °C in ceramics synthesized from precursor solutions containing THOME.

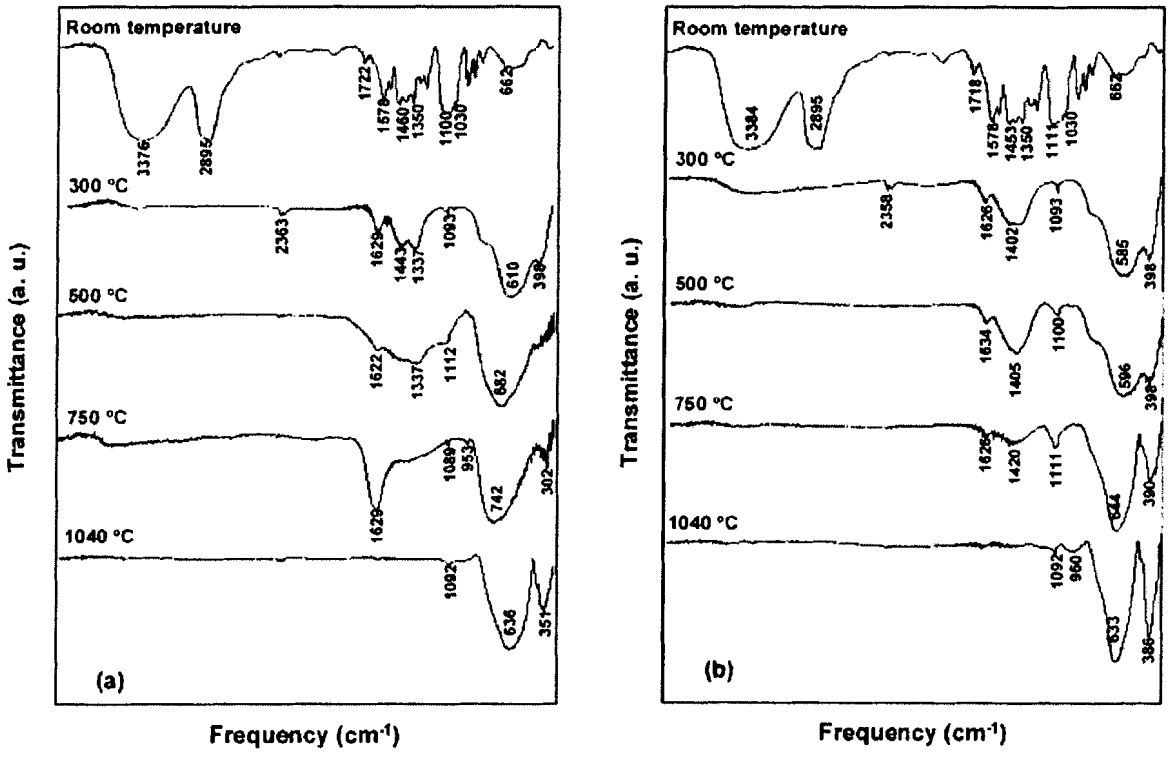

Figure 4.6: FT-IR spectra of the (a) PEG(S)T and (b) PEG(S) precursor solutions at room temperature and of the resulting products after treatment at various temperatures.

4.5 Characterization

4.5.1 Microstructures by Scanning Electron Microscopy (SEM)

The SEM images of microstructure and grain morphology of the PEG(S)T and PEG(S) ceramics sintered at 1140 °C are given in Figures 4.7 (a) and 4.7 (b), respectively. As can be seen from these images, both samples show a relatively uniform grain size distribution but they differ remarkably from each other in their average grain sizes. While the PEG(S)T ceramic shows an average particle size of >2 μm, that of PEG(S) ceramic is found to be ~0.8 μm only. It is worth mentioning that this soft chemical technique is able to produce ceramics which have much finer grain size than for those derived from the conventional solid state synthesis where grain size is usually >10 μm [23]. The results also point out that the use of THOME in the synthesis of the ceramic precursor solution gives rise to a larger particle size as compared to the ceramic obtained from the THOME-free reaction.

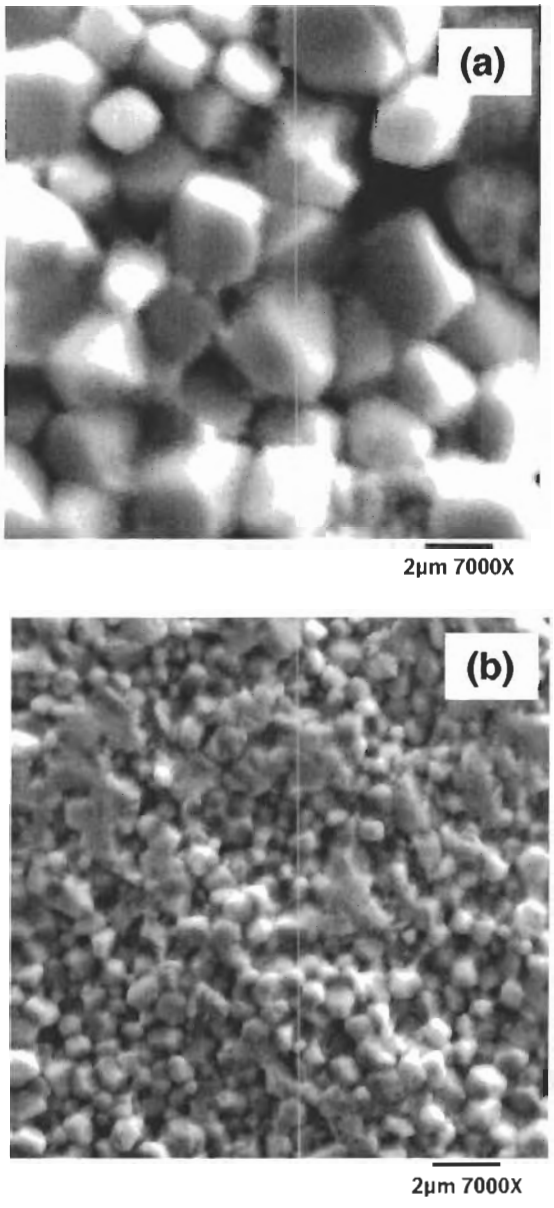

Figure 4.7: Scanning electron microscopy images of (a) PEG(S)T and (b) PEG(S) ceramics sintered at 1140 °C for 8 h.

4.5.2 Dielectric Properties

Figures 4.8 (a) and 4.8 (b) illustrate the temperature and frequency dependences of the real part of dielectric permittivity (ε') of the PEG(S)T and PEG(S) ceramics sintered at 1140 °C. The peak at ~175 °C in both figures indicate the Curie temperature (T_C) of the ferroelectric to paraelectric phase transition upon heating. For the PEG(S)T ceramic, the dielectric constant reaches above 5,000 at room temperature, which is significantly higher than the values in the range of 2,000 – 3,000 usually obtained in PMN–PT ceramics prepared via solid state reactions [23]. A maximum value of the dielectric constant (ε'_{max}) of ~27,000 is attained at the T_C at a frequency of 1 kHz. The weak anomaly observed around 100 °C corresponds to the morphotropic phase transition [3]. The dielectric constant increases sharply just before it peaks at the T_C, indicating a 1st order phase transition. The PEG (S) ceramic, however, shows a much lower dielectric constant of ~2,500 at room temperature, with a ε'_{max} of ~9,000 only at the same T_C of ~175 °C. As discovered before, after sintering at 1140 °C for 8 hrs, the PEG(S)T ceramic shows the pure perovskite phase. The PEG(S) sample, however, contains ~5% of the impure, undesired pyrochlore phase which explains the much lower dielectric constant in it, even though both ceramics have a high relative density of ~96 %. In addition, the dielectric peak for the PEG(S) ceramic becomes much broadened, which can be explained by the particle sizes of the respective ceramics. It was shown by S. Chattopadhyay *et al.* [24] that a decrease in the particle size of nanocrystalline ferroelectric lead titanate, prepared by co-precipitation, leads to a broadening of the peak in the dielectric constant versus temperature curve and lowers the value of the ε'_{max}. Since the grain size is much smaller in the PEG(S) sample (Figure 4.7), its dielectric peak

becomes broadened with a low ε'_{max}. This observation leads to the conclusion that THOME used in the synthesis of the precursor solution plays a very important role not only in favouring the formation of the pure perovskite phase, but also in substantially improving the dielectric properties of the PMN–PT ceramics.

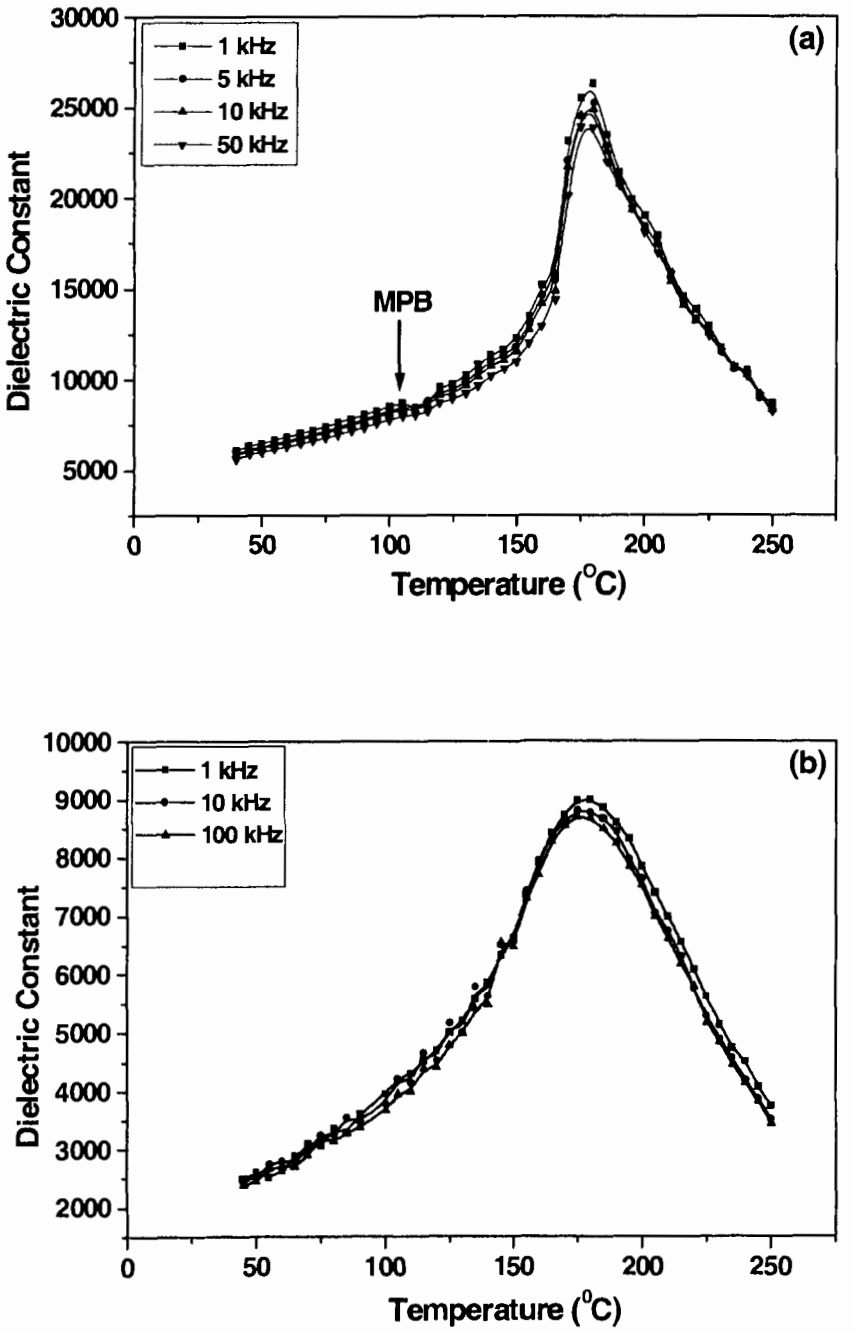

Figure 4.8: Impedance spectroscopic data showing the dependence of dielectric constant as a function of temperature and frequency for (a) PEG(S)T and (b) PEG(S) ceramics sintered at 1140 °C for 8 h.

4.5.3 Ferroelectricity

The polarization versus electric field relations of both the PEG(S)T and PEG(S) ceramics sintered at 1140 °C exhibit hysteresis loops as displayed in Figures 4.9 (a) and 4.9 (b), indicating typical ferroelectric behaviour. The PEG(S)T ceramic shows excellent ferroelectric properties as compared to the PEG(S) ceramic with a well-defined and saturated hysteresis loop and a higher remnant polarization (P_r). It shows a remnant polarization value of 21 $\mu C/cm^2$ and a coercive field of ~7.5 kV/cm. The PEG(S) ceramic, on the other hand, displays a much smaller remnant polarization of 7.5 $\mu C/cm^2$ and a slightly larger coercive field of ~10 kV/cm, and the polarization is still unsaturated even at a field of ~30 kV/cm. The improved ferroelectricity found in PEG(S)T ceramics can be attributed to the effect of the THOME. As discussed above, the triol molecule favours the formation of pure perovskite phase in the PEG(S)T ceramic, hence bringing about better dielectric and ferroelectric properties than the PEG(S) compound.

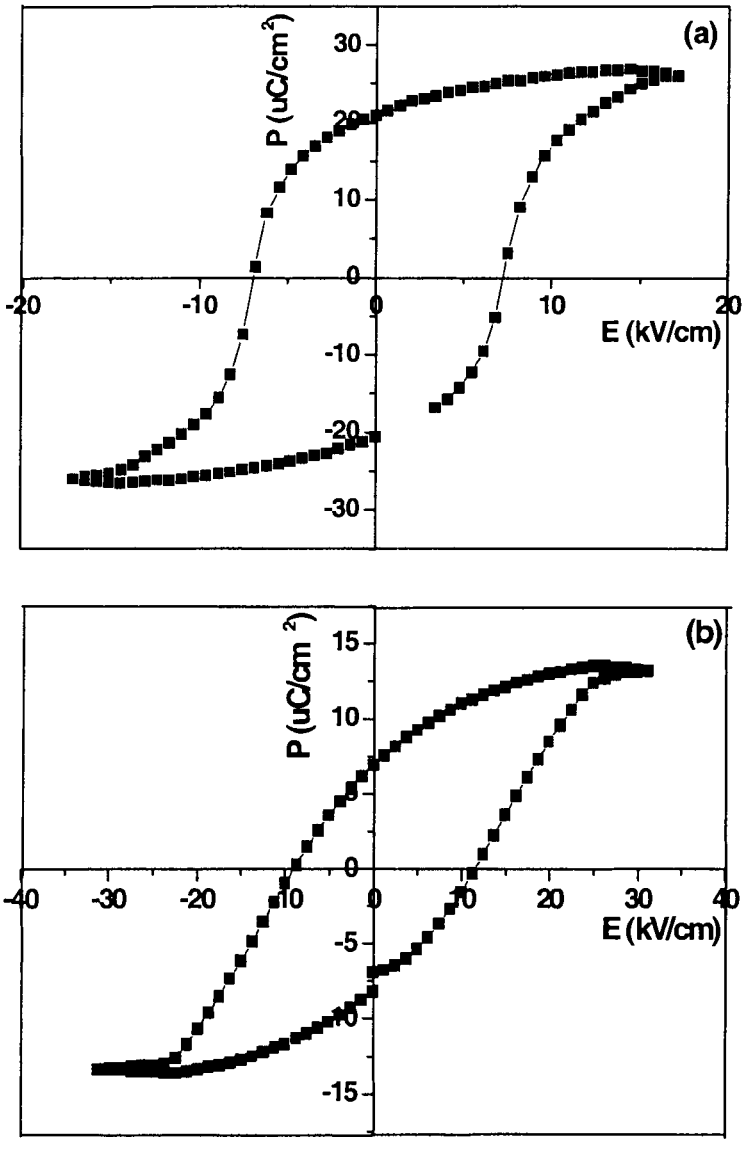

Figure 4.9: Variation of electric polarization as a function of applied electric field for (a) PEG(S)T and (b) PEG(S) ceramics sintered at 1140 °C for 8 h, showing ferroelectric hysteresis loops.

4.6 Conclusions

A new solution method for the synthesis of 0.65PMN-0.35PT ceramics has been developed in this study. It has been shown that by using polyethylene glycol and methanol as solvent, a sol that is very stable to air can be obtained at room temperature. The formation of this sol does not require refluxing and distillation steps that are usually required in conventional sol-gel reactions. More interestingly, the sol-gel reaction is carried out using only stoichiometric amounts of the lead starting material, which gives rise to pure and high density ceramics after sintering, with very good dielectric and ferroelectric properties. The positive effects of the triol molecule, 1,1,1-tris(hydroxymethyl)ethane (THOME) on the synthesis and performance of the perovskite PMN-PT ceramic, have been demonstrated in this work which are related to its nature as a very good metal complexing agent [18]. With three hydroxyl groups in its structure, the THOME molecule can bind to up to three metal centers at a time, thereby forming linear oligomeric species in solution. This has an influence on the arrangement of the M–O–M networks in the precursor powder. Evidence of the presence of different M–O–M arrays in the precursor powder when THOME was used or not in the sol-gel process has been revealed by IR studies. The presence of THOME in the system during the precursor solution synthesis has not only led to the formation of a pure perovskite phase, but also greatly improved the dielectric and ferroelectric properties of the PMN-PT ceramics with a maximum dielectric constant, ε'_{max} of ~27,000 and a remanent polarization, P_r = 21 $\mu C/cm^2$, as compared to ε'_{max} = 9,000 and P_r = 7.5 $\mu C/cm^2$ for the ceramics prepared without THOME. The higher maximum dielectric constant with a sharp peak in the ε'

versus temperature curve is associated with a larger grain size (>2 μm) in the ceramic prepared with THOME, as revealed by SEM. On the other hand, the ceramics prepared without THOME showed a finer particle size (<1 μm) and a broad maximum in the dielectric peak. The excellent ferroelectric properties of PEG(S)T ceramics make the material a very promising candidate for applications in advanced electromechanical devices.

Acknowledgements

This work was supported by Natural Science and Engineering Research Council of Canada (NSERC).

4.7 References

1. L. E. Cross, *Ferroelectrics*, **76**, 241 (1987); L. E. Cross, *Ferroelectrics*, **151**, 305 (1994); Z.-G. Ye, *Key Eng. Mater.*, **155-156**, 81 (1998); Z.-G. Ye, *Curr. Opin. Solid State Mater. Sci.*, **6** [1], 35 (2002).

2. B. Noheda, D. E. Cox, G. Shirane, J. Gao, and Z.-G. Ye, *Phys. Rev. B*, **66**, 054104 (2002); Z.-G. Ye, B. Noheda, M. Dong, D. Cox, and G. Shirane, *Phys. Rev. B.*, **64**, 184114 (2001).

3. S. W. Choi, T. R. Shrout, S. J. Jang, and A. S. Bhalla, *Ferroelectrics*, **100**, 29 (1989).

4. T. R. Shrout, Z. P. Chang, N. Kim, and S. Markgraf, *Ferroelectric Letters*, **12**, 63 (1990).

5. J. H. Park, D. H. Kang, and K. H. Yoon, *J. Am. Ceram. Soc.*, **82** [8], 2116 (1999).

6. R. F. Service, *Science*, **275**, 1878 (1997).

7. S.-E. Park, and T. R. Shrout, *J. Appl. Phys.*, **82** [4], 1804 (1997).

8. B. Jaffe, W. R. Cook, and H. Jaffe, *Piezoelectric Ceramics*; Academic Press: London (1971).

9. L. F. Francis, and D. A Payne, *J. Am. Ceram. Soc.*, **74** [12], 3000 (1991).

10. A. Nijmeijer and H. Kruidhof, *J. Am. Ceram. Soc.*, **80** [10], 2717 (1997).

11. M. A. Gülgün, M. H. Nguyen, and W. M. Kriven, *J. Am. Ceram. Soc.*, **82** [3], 556 (1999).

12. D. A. Payne, *J. Sol-Gel Sci. Technol.*, **2**, 311 (1994).

13. N. Uekawa, T. Sukegawa, K. Kakegawa, and Y. Sasaki, *J. Am. Ceram. Soc.*, **85** [2], 329 (2002).

14. M. P. Pechini, *U.S. Pat. No. 3,330,697* (1967).

15. M. H. Nguyen, S-J. Lee, W. M. Kriven, *J. Mater. Res.*, **14** [8], 3417 (1999).

16. N. Uekawa, M. Endo, K. Kakegawa, and Y. Sasaki, *Phys. Chem. Chem. Phys.*, **2**, 5485 (2000).

17. Y. Shimizu, and T. Murata, *J. Am. Ceram. Soc.*, **80** [10], 2702 (1997).

18. N. Sriprang, D. Kaewchinda, J. D. Kennedy, and S. J. Milne, *J. Am. Ceram. Soc.*, **83** [8], 1914 (2000).

19. K. R. Udayakumar, J. Chen, P. J. Schuele, L. E. Cross, V. Kumar, and S. B. Krupanidhi, *Appl. Phys. Lett.*, **60** [10], 1187 (1992).

20. Y. Lu, G.-H. Jin, M. Cronin-Golomb, S.- W. Liu, H. Jiang, F.-L. Wang, J. Zhao, S.-Q. Wang, and A. J. Drehman, *Appl. Phys. Lett.*, **72** [23], 2927 (1998).

21. R. Thomas, S. Mochizuki, T. Mihara, and T. Ishida, *J. Mater. Res.*, **17** [10], 2652 (2002).

22. D. L. Pavia, G. M. Lampman, and G. S. Kriz, 'Introduction to Spectroscopy', 2nd Edition, Harcourt Brace College Publishers, Washington (1996).

23. L. Zhang, 'Synthesis and Characterization of Relaxor-Based Piezo- and Ferroelectric (1-x)$Pb(Zn_{1/3}Nb_{2/3})O_3$-x$PbTiO_3$ [PZN-PT] and (1-x)$Pb(Mg_{1/3}Nb_{2/3})O_3$-x$PbTiO_3$ [PMN-PT]', Masters Thesis, Simon Fraser University, Burnaby, BC, Canada (2000).

24. S. Chattopadhyay, P. Ayyub, V. R. Palkar, and M. Multani, *Phys. Rev. B*, **52** [18], 13177 (1995).

CHAPTER 5:
Synthesis and Characterization of $SrBi_2Ta_2O_9$ Ceramics by New Soft Chemical Techniques

Abstract

Ferroelectric ceramics of strontium bismuth tantalate, $SrBi_2Ta_2O_9$ (SBT), have been synthesized in pure perovskite phase by two new soft chemical techniques, namely a sol-gel process and a co-precipitation method. The sol-gel process utilizes ethylene glycol as solvent while the co-precipitation technique uses of a polyethylene glycol 200 (PEG) and methanol mixture as solvent. The microstructure and properties of the ceramics have been studied and discussed. The sol-gel derived ceramics sintered at 1200 °C for 8 hrs show good dielectric and ferroelectric properties with a relative density of 96 %, $\varepsilon' = 227$ and $P_r = 7.6\ \mu C/cm^2$ at room temperature, and $\varepsilon'_{max} = 950$ at $T_C = 330$ °C. In comparison, the SBT ceramics prepared under the same conditions, using the co-precipitation method show a plate-like microstructure with preferential grain orientation along the [00$\underline{1}$0] direction, a relative density of 85 %, a dielectric constant, $\varepsilon' = 235$ and a remnant polarization of 3.7 $\mu C/cm^2$ at room temperature, and a maximum dielectric constant ε'_{max} of 850 at $T_C = 330$ °C. The sol-gel derived ceramics show superior dielectric and ferroelectric properties than the ceramics prepared by the solid state reactions ($\varepsilon'_{max} \approx 500$; $P_r = 4.5\ \mu C/cm^2$), which can be attributed to a denser and more homogeneous microstructure with a better distribution of grain orientations, thus eliminating the preferential grain orientation along the non-polar [00$\underline{1}$0]-direction.

5.1 Introduction

Growing interest and attention are being invested in the study of ferroelectric materials with a view to applications in non-volatile random access memory devices [1-3]. In this respect, $Pb(Zr_xTi_{1-x})O_3$ [PZT] appeared first to be a promising candidate. However, PZT have been faced with serious problems such as fatigue, leakage current and aging, which may significantly degrade the performance of the material and the lifetime of the devices [4,5]. Among these problems fatigue, a decrease in the switchable polarization as the number of read/write cycles is increased, is a major issue. Therefore, a great amount of effort has been put into searching for alternatives to PZT. $SrBi_2Ta_2O_9$ [SBT] has emerged as a candidate for non-volatile ferroelectric memory applications [1-3]. A member of the Aurivillius family [6] of compounds with the general formula $(Bi_2O_2)^{2+}(A_{n-1}B_nO_{3n+1})^{2-}$, where n = 2 represents the number of corner-sharing perovskite units, SBT has a layered structure in which $(Bi_2O_2)^{2+}$ layers are sandwiched between the perovskite units. SBT has been identified as a fatigue-free material that can retain its remnant polarization even up to 10^{12} switching cycles, and also has very good data retention of up to 10 years [2-3, 7-8].

There have been a large number of reports on the synthesis and characterization of SBT thin films in the literature. These films were deposited using a number of different techniques, namely sol-gel, pulsed laser deposition (PLD), and metallorganic chemical vapor deposition (MOCVD) [9-13]. Single crystals of SBT were recently grown in our laboratory from high-temperature solutions using a new composite flux and an improved growth process [14]. As far as SBT ceramics are concerned, they were mostly

synthesized using conventional solid state reaction in which relatively high sintering temperature, exceeding 1200 °C, and/or long sintering time (12 – 30 hrs.) were required [15-18]. In solid state reactions, the oxide components are mixed together and thoroughly ground in order to achieve good mixing. Then, high temperature is needed so that the components of the mixture have sufficient thermal energy to overcome the atomic/ionic diffusion barriers for reaction. In most cases, the final product ends up being inhomogeneous with some impure phase(s) present. As a result, material chemists have turned to an alternative soft chemical technique: the sol-gel process. Developed in 1845 by M. Ebelman, this technique has extensively been employed in the synthesis of inorganic mixed oxides because of the many advantages it offers over solid state reactions [19]. The ability to mix (and dissolve) the constituents homogeneously in solution is one of the major benefits of the sol-gel processing method. Once this is achieved, the next step is to progressively form a metal-oxygen network in solution through the polymerization of the dispersed constituents. This network then decomposes giving rise to the desired inorganic oxide at a much lower temperature than required in a solid-state reaction. Basically, the sol-gel process offers better control of stoichiometry and homogeneity, and higher purity and reactivity of the precursor powders [20]. Most of the sol-gel methods documented so far in the literature for the synthesis of SBT make use of 2-methoxyethanol as the solvent because of its versatility in dissolving a range of the alkoxide starting materials [10, 21-23]. However, 2-methoxyethanol is also a potential teratogen causing potential birth defects, and its use in sol-gel processes should be limited, if not prohibited.

This work focuses on researching alternative new soft chemical routes that require mild conditions and which utilize less harmful reagents to synthesize SBT ceramics. We report the successful synthesis of SBT ceramics by two new soft chemical techniques, namely, the sol-gel and co-precipitation methods. While the sol-gel method employs ethylene glycol as solvent, the co-precipitation route makes use of a polyethylene glycol 200 (PEG-200) and methanol mixture as solvent. The properties of the SBT ceramics obtained by these two different soft chemical methods are compared and discussed. Based on the successful room temperature sol-gel synthesis of the relaxor ferroelectric (1-x)$Pb(Mg_{1/3}Nb_{2/3}O_3$ – $xPbTiO_3$ [(1-x)PMN-xPT] (x = 0.10, and 0.35) in PEG-200 [24, 25], the usefulness of this solution is once again proven in completely dissolving all the starting materials of SBT at room temperature, allowing thereby a homogeneous co-precipitation of the cations using an oxalate solution. Recently, there have been a few reports in the literature on and emulsion process, which may be a promising chemical route to fine ceramic powders [26-28]. Basically, this method involves the mechanical dispersion of an aqueous medium, consisting of inorganic salts, into an organic phase. Different kinds of surfactants are also used in order to stabilize the emulsion before the cations are finally co-precipitated to give the stoichiometric precursor powder. In the co-precipitation method reported here, the use of PEG-200 eliminates the need of a surfactant by stabilizing all the cations in solution, possibly through interactions between the metals and both the ether oxygen and terminal hydroxyl groups present in the PEG chains [29].

Ferroelectric bismuth-containing layer-structured perovskites generally have their major component of spontaneous polarization along the a-axis, with much smaller values

of polarization lying along the c-direction. Other properties such as dielectric and piezoelectric properties are also anisotropic in a similar way (i.e., the best properties are obtained in a-oriented grains) [30]. For this reason, many researchers have tried to achieve grain control in these layer-structured ferroelectric perovskites. The most commonly used grain orientation technique in the literature is the hot-forging method which results in the spontaneous polarization being in the grain-oriented c-plane [31-34]. As a result, enhanced dielectric, piezoelectric, and pyroelectric properties have been observed in the hot-forged bismuth layered ceramics. It has been shown by Desu *et al.* [11] that highly c-axis oriented SBT thin films exhibit a decrease in polarization and coercive field as opposed to randomly oriented polycrystalline films. Therefore, it is desirable to synthesize SBT ceramics and thin films with preferred grain orientation, if possible, along the a-axis, for improved properties.

The co-precipitation method developed in this work leads to ceramics with some degree of preferred grain orientation along the c-axis and therefore a lower remnant polarization value, while the sol-gel derived ceramics have higher dielectric constant and P_r values. This is a very interesting feature of the newly designed sol-gel process which minimizes grain orientation along the c-axis without the need of special grain orientation techniques, thereby improving the dielectric and ferroelectric properties of the SBT ceramics. Figure 5.1 illustrates grain orientation in two ceramics, each having their grains oriented in some preferred direction with respect to the plane of the ceramic.

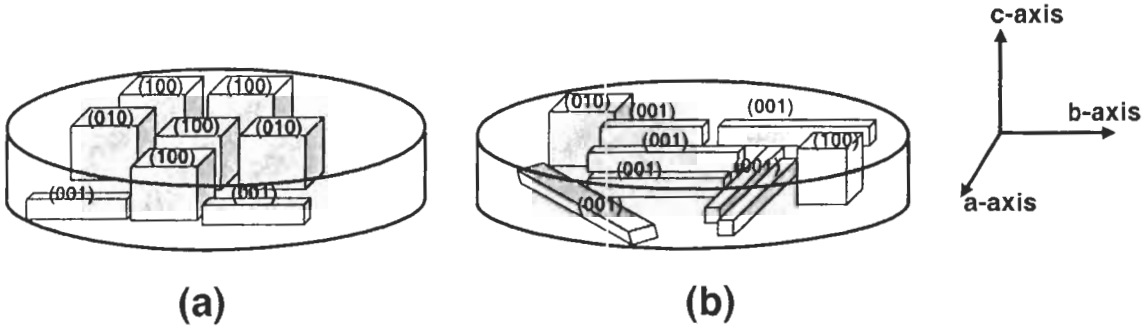

Figure 5.1: Ceramics with preferred grain orientation: (a) grains are preferentially oriented in the ab-plane, (b) grains are preferentially oriented along the c-axis in the (001) direction.

5.2 Experimental

5.2.1 Synthesis of SBT by an Ethylene Glycol-Based Sol-Gel Method

In the first part of this work, $SrBi_2Ta_2O_9$ (SBT) ceramics were synthesized by a sol-gel route using ethylene glycol [$HO(CH_2)_2OH$] as solvent. The synthetic procedure of SBT ceramics by the sol-gel method is outlined in Figure 5.2, in which the metal alkoxides, strontium acetate [$Sr(OOCCH_3)_2.0.5H_2O$], bismuth (III) acetate [$Bi(OOCCH_3)_3$], and tantalum (V) ethoxide [$Ta(OCH_2CH_3)_5$] were used as starting materials. The key to a successful sol-gel reaction is to find the right solvent that can readily dissolve all the starting ingredients. The next step is to hydrolyze and polymerize them through condensation reactions. In this sol-gel method ethylene glycol has proved to be a very good solvent for all our starting materials. This is because the presence of two terminal hydroxyl groups in the molecule makes it easy for ethylene glycol to readily exchange with the alkoxy groups on the metals in a first step. Once this is achieved, the hydrolyzed metal alkoxides can then undergo condensation reactions which lead to the progressive formation of metal-oxygen oligomers and polymers in solution. The possible hydrolysis and condensation of strontium acetate in ethylene glycol are illustrated in Figure 5.3. Similar reactions are possible between the other two metal alkoxides (bismuth acetate and tantalum ethoxide) and ethylene glycol. When all the solutions are mixed together in a final step, further hydrolysis and condensation occur, leading to the formation of an extended and/or cross-linked metal-oxygen-metal network.

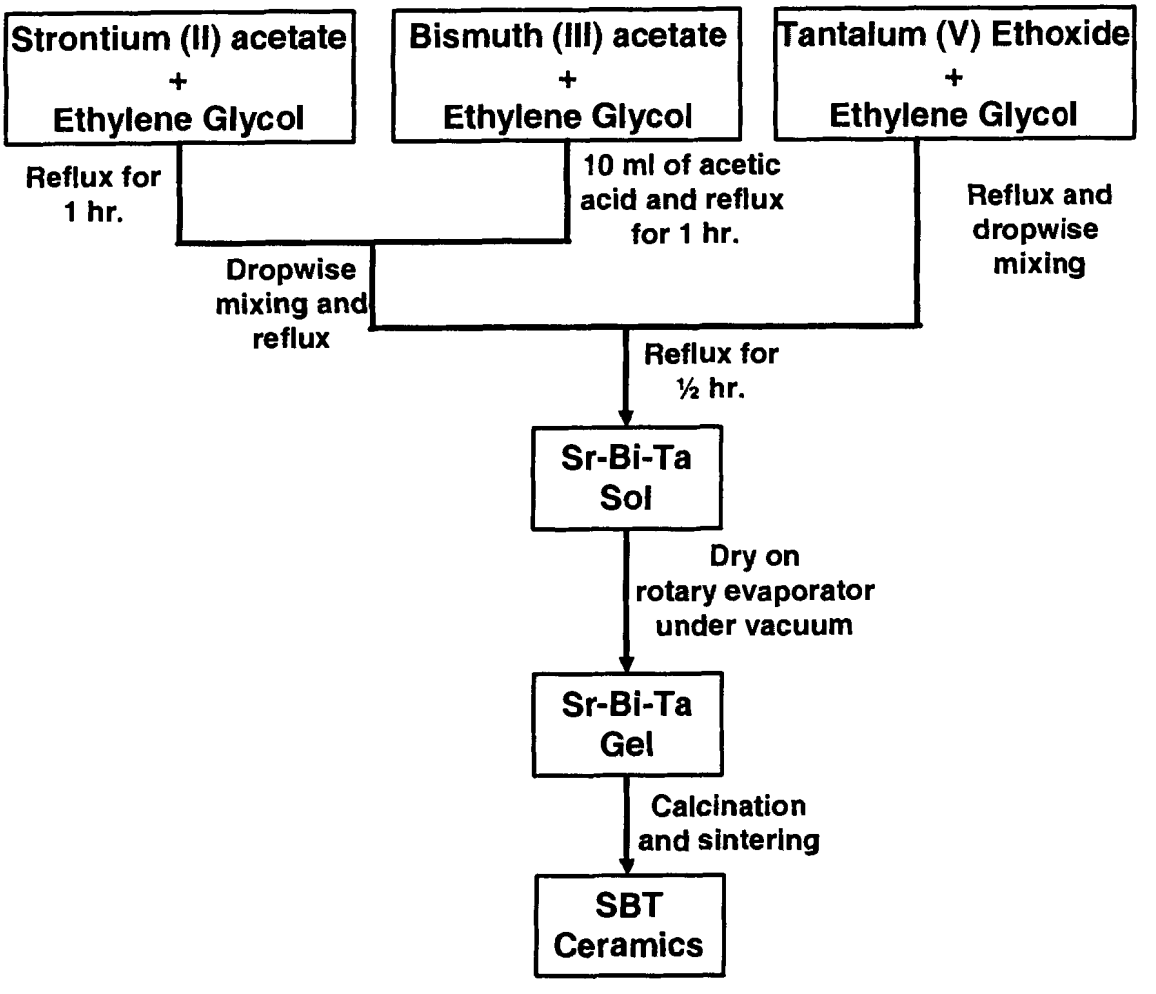

Figure 5.2: Flowchart for the synthesis of SBT ceramics by the sol-gel process.

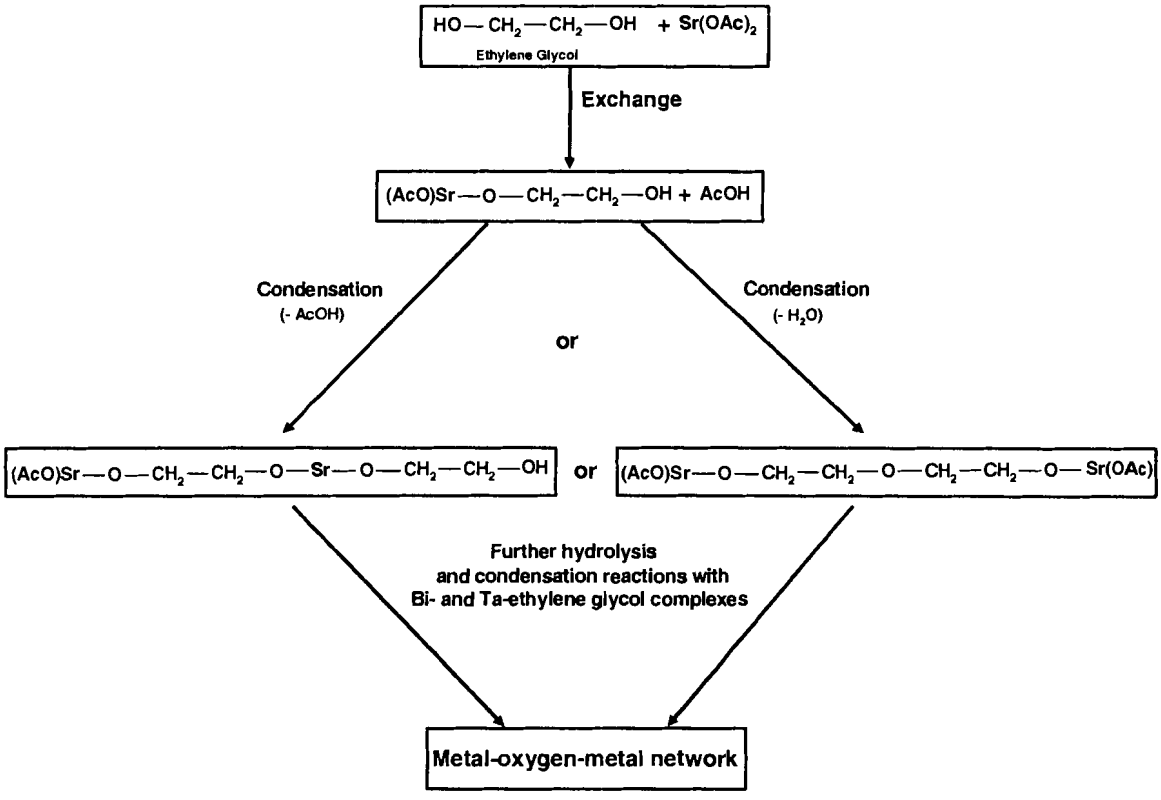

Figure 5.3: Proposed possible hydrolysis and condensation reactions of strontium acetate [$Sr(OAc)_2$] in ethylene glycol [$HO(CH_2)_2OH$].

Stoichiometric amounts of strontium acetate and bismuth (III) acetate were refluxed separately in ethylene glycol for ~1 h to give respective clear, colourless solutions. About 5 mL of acetic anhydride was also added to the flask containing bismuth in order to clear the white precipitate, which forms during reflux. The strontium and bismuth solutions were then mixed together and refluxed for ~1 h. In a separate flask, tantalum (V) ethoxide was refluxed in ethylene glycol for ~½ h and the resulting clear, colourless solution was then added dropwise to the Sr-Bi mixture with constant stirring and refluxing for another ½ h. A colourless sol was finally obtained, which was then dried using a rotary evaporator under vacuum. The resulting white gel was fired at 750 °C for 4 h to produce a white powder, which was examined by X-ray diffraction to confirm the perovskite SBT phase. This product was then mixed with a few drops of polyvinyl alcohol (PVA) solution (5% w/v) as a binding agent and ground to a fine powder after the water (from the binder solution) had evaporated. The powder was pressed into pellets, which were then sintered at different temperatures and for different times, (a) 1000 °C for 8 h, (b) 1200 °C for 4 h, and (c) 1200 °C for 8 h, to obtain dense SBT ceramics. These as-prepared ceramics are abbreviated as SG1000(8), SG1200(4), and SG1200(8), respectively.

5.2.2 Synthesis of SBT by a Polyethylene Glycol-Based Co-precipitation Method

The procedure for the synthesis of SBT ceramics by the precipitation method is illustrated in Figure 5.4. Strontium acetate [$Sr(OOCCH_3)_2.0.5H_2O$], bismuth (III) nitrate [$Bi(NO_3)_3.5H_2O$], and tantalum (V) chloride [$TaCl_5$] were used as starting materials (obtained from Sigma Aldrich Chemicals and Alfa Aesar), and a mixture of polyethylene glycol 200 (PEG) (obtained from Sigma Aldrich Chemicals) and methanol was used as solvent. This solvent system is very efficient in dissolving all the starting metal salts used in this experiment at room temperature. As stated earlier (Sec. 5.1), PEG was chosen because of its ability to interact with metal ions and hence stabilize them in solution. A precipitating agent is added to co-precipitate the cations into a homogeneous solid.

Stoichiometric amounts of the reagents were mixed with 100 mL of a 1:2 volume mixture of PEG and methanol. The mixture was stirred until a clear colourless solution was obtained. Figure 5.5 is a possible picture of the interactions between the ether oxygen and the terminal hydroxyl groups present in the PEG chains, and the cations in this solution. An oxalate solution was prepared by dissolving oxalic acid in aqueous ammonium hydroxide and 50 mL of this solution was added to the Sr-Bi-Ta mixture in order to co-precipitate all the cations. This mixture was stirred for ~2 h and filtered. The white precipitate obtained was stirred in distilled water (50 mL, 3-4 times) and decanted to remove residual chloride. It was filtered again and washed thoroughly with distilled water and finally dried at 100 °C. The dried homogeneous powder was calcined at 750 °C for 4 h after which a few drops of PVA (5% w/v) were added. It was then ground to a fine powder, pressed into pellets, and sintered at higher temperatures for different times:

(a) 1000 °C for 8 hrs, (b) 1200 °C for 4 hrs, and (c) 1200 °C for 8 hrs, to produce dense SBT ceramics, which are abbreviated: PR1000(8), PR1200(4), and PR1200(8), respectively.

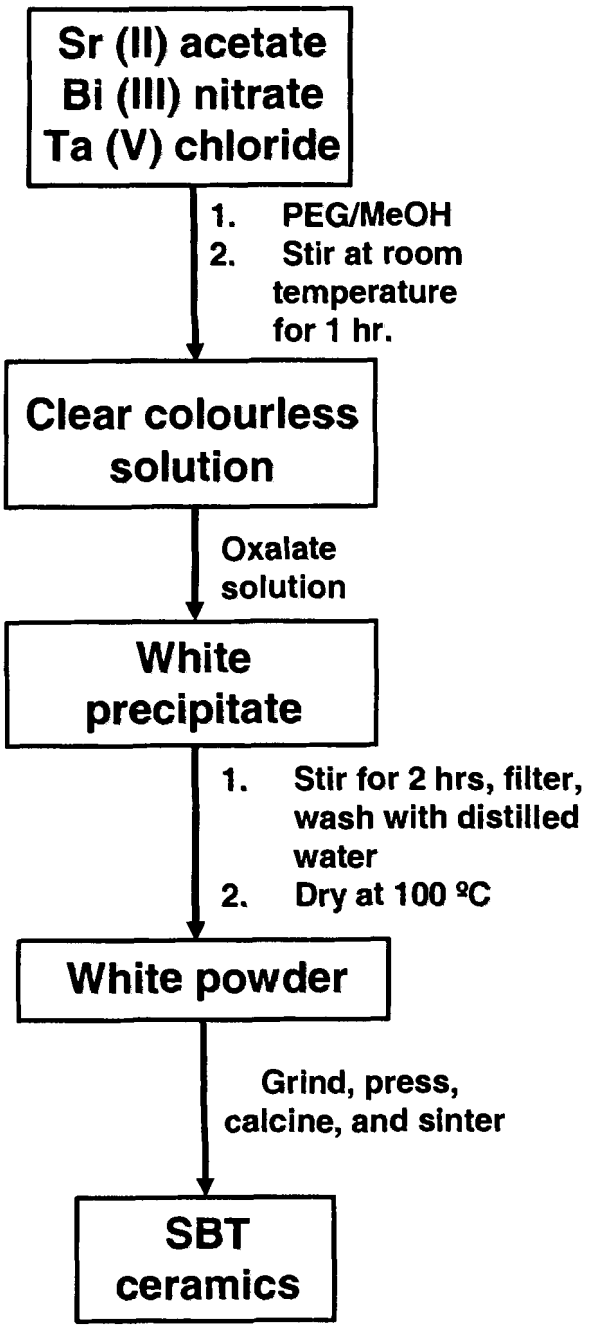

Figure 5.4: Flowchart for the synthesis of SBT ceramics by the co-precipitation method.

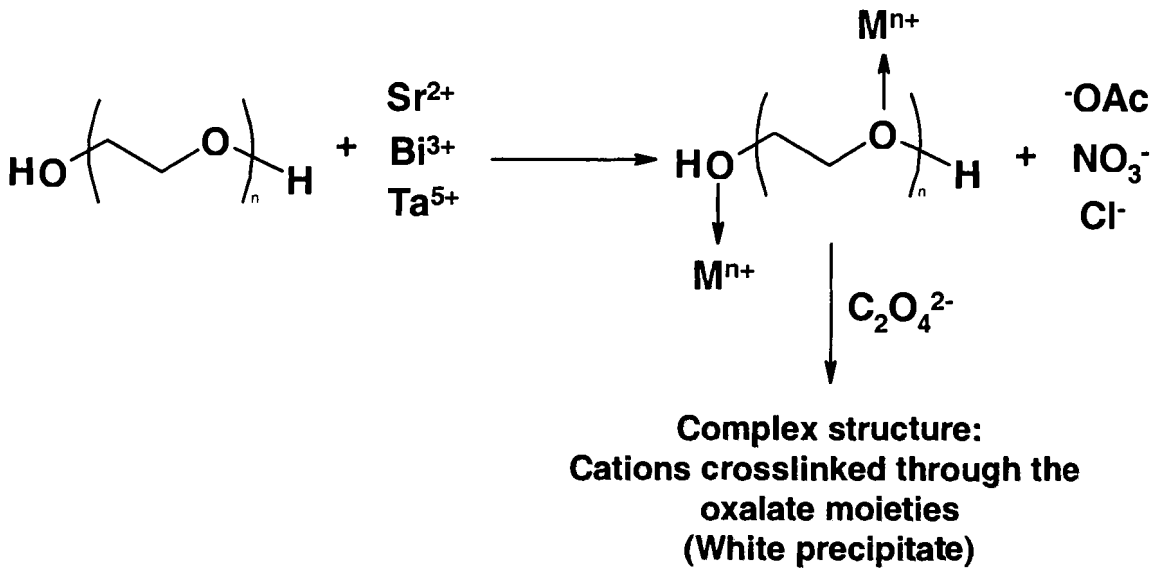

Figure 5.5: Proposed possible interactions between the PEG chains and the metal ions in solution before their co-precipitation by the oxalate ions.

X-ray powder diffraction using Cu Kα radiation (46 kV, 42 mA) was carried out on a Rigaku X-ray diffractometer in order to analyze the phases of the samples. The temperature and frequency dependence of the dielectric permittivity of the ceramics were measured using a computer-controlled impedance analyzer (Solartron 1260) in conjunction with a dielectric interface (Solartron 1296). Ferroelectric hysteresis measurements were performed on an RT66A standard ferroelectric testing system. Gold layers rather than silver were deposited on the ceramics surface for the purpose of electrical measurements because silver was found by Sih et al. [35] to diffuse into SBT ceramics, influencing their electrical properties as well as their T_C. The microstructure was imaged and the grain size determined using scanning electron microscopy (SEM) on a Strata 235 Dualbeam instrument composed of a Field Emission Scanning Electron Microscope and Focus Ion Beam (FESEM/FIB).

5.3 Results and Discussion

5.3.1 Phase analysis by X-ray diffraction

Phases in all the samples were analyzed using powder X-ray diffraction (XRD). The XRD patterns of the SBT ceramics synthesized by the sol-gel process and the precipitation method, and sintered at different temperatures for different times, are shown in Figure 5.6. It is clearly seen from Figure 5.6 (a) that the precursor powder obtained from the sol-gel method is crystalline at 500 °C but not a completely formed perovskite SBT phase. Upon calcination at 750 °C for 4 h this powder converts into the pure SBT phase. The XRD also shows the perovskite phase is still stable to sintering at higher temperatures of 1000 °C and 1200 °C.

As for the ceramics prepared by the co-precipitation method, the precursor powder obtained at room temperature proved to be amorphous, as shown in the inset of Figure 5.6 (b). Pure SBT phase is only obtained after calcination at 750 °C for 4 h which are the same conditions as in the case of the sol-gel process. Once again, the pure SBT phase is stable to sintering at higher temperatures, indicating no degradation of the compound. One important observation from the XRD patterns in Figure 5.6 (b) is the considerable increase in intensity of the (00$\underline{1}$0) peak for the PR1200(8) ceramic. This is an indication of an increase in preferred grain orientation along the (00$\underline{1}$0) direction upon increasing the sintering temperature and time to 1200 °C and 8 h, respectively. Interestingly, this is not the case for the ceramics obtained from the sol-gel process. As shown below, this difference in grain orientation is confirmed by microstructural analysis and is found to affect the properties of the ceramics obtained by these two different methods.

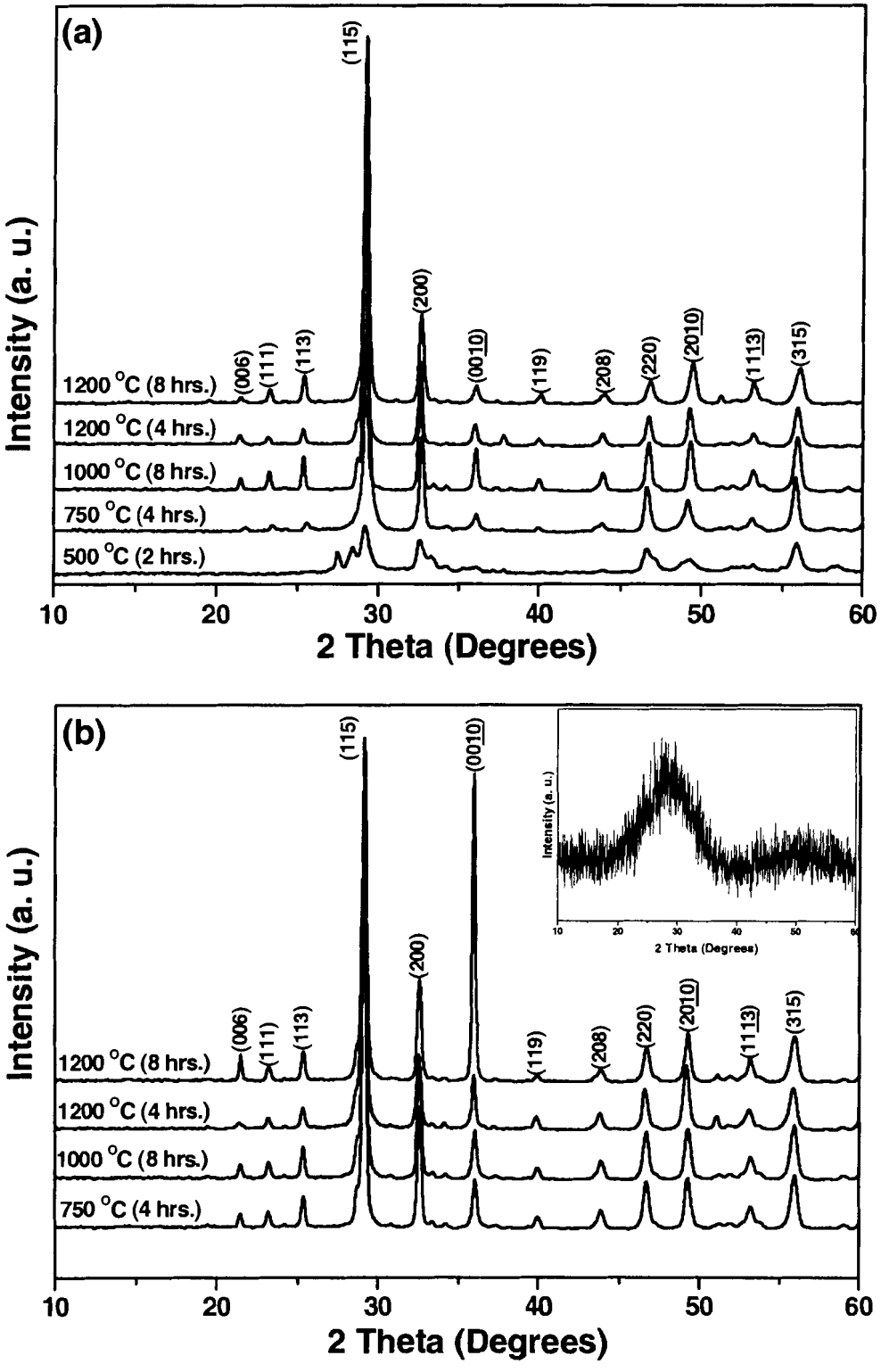

Figure 5.6: XRD patterns of SBT samples prepared by (a) the sol-gel process, and (b) the precipitation method, and sintered at different temperatures for different times. The inset in (b) is the XRD pattern of the precursor powder obtained in the co-precipitation method.

5.3.2 Microstructure by Scanning Electron Microscopy

Scanning electron microscopy (SEM) images of SG1000(8), SG1200(4), SG1200(8), PR1000(8), PR1200(4), and PR1200(8) are shown in Figures 5.7 (a) – (f). The ceramics synthesized by the sol-gel process show a dense microstructure [Figures 5.7 (a) – (c)], with apparent grain growth as the sintering temperature increases. The appearance of this dense microstructure is consistent with the measured relative density of the ceramics, ranging from ~93 % (for the ceramic sintered at 1000 °C) to ~96 % (for those sintered at 1200 °C). SG1000(8) has an average grain size of about 1 μm [Fig. 5.7 (a)]. With an increase in the sintering temperature to 1200 °C, the ceramics are clearly densified while the grain size increases only slightly (2-3 μm), giving rise to a dense and homogeneous microstructure with comparatively isotropic grain morphology [Figure 5.7 (c)]. This indicates that no significant preferential grain growth has occurred in the sol-gel derived SBT ceramics, in agreement with the X-ray diffraction pattern [Figure 5.6 (a)].

In the case of ceramics obtained from the co-precipitation method, rod-like grains of ~2 – 3 μm long and ~0.6 μm diameter are observed in PR1000(8) with a relatively loose microstructure [Figure 5.7 (d)], corresponding to a lower calculated relative density (~ 65 %). Sintering at higher temperature leads to a denser microstructure in the PR1200(4) and PR1200(8) ceramics [Figures 5.7 (e) and (f)], which is consistent with increased densities of 80 % and 85 %, respectively. PR1200(4) noticeably contains some plate-like grains of ~2 – 4 μm long (wide), and about 1 μm thick. PR1200(8) ceramic contains many plate-like grains up to ~8 μm long (or wide) and ~1 – 2 μm thick. This plate-like structure results from a preferential grain growth in the a-b plane due to

the layered structure, with weaker bonding between the perovskite slabs along the c-axis, which gives rise to the plates of (00$\underline{1}$0) plane, as confirmed by the increase in the intensity of the corresponding peak in the XRD pattern of PR1200(8) [Figure 5.6 (b)].

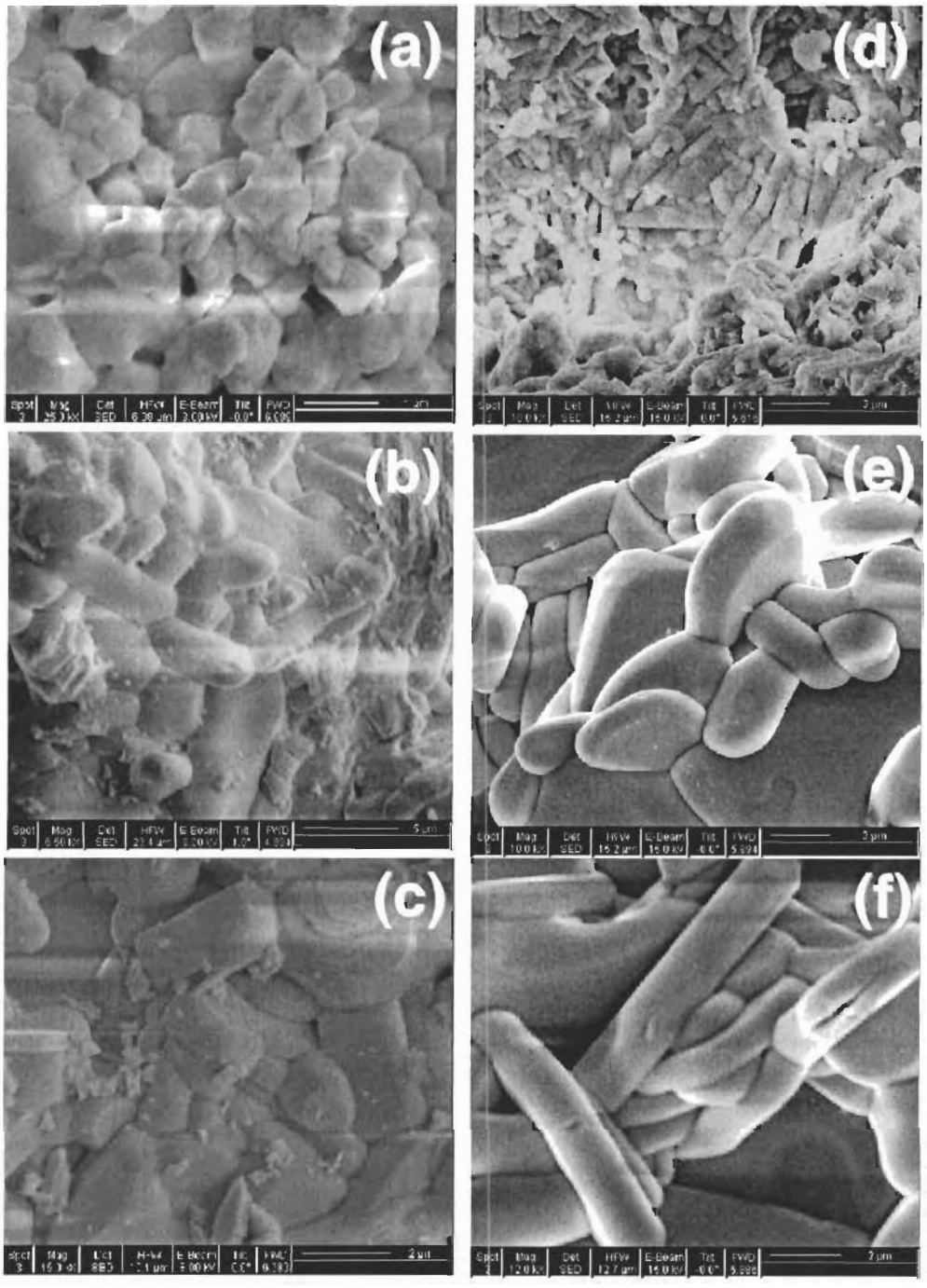

Figure 5.7: Scanning Electron Microscopy images of SBT ceramics; (a) SG1000(8), (b) SG1200(4), (c) SG1200(8), (d) PR1000(8), (e) PR1200(4), and (f) PR1200(8).

5.3.3 Dielectric Measurements

The temperature and frequency dependences of the real part of the dielectric permittivity (ε') of the SBT ceramics prepared by the sol-gel and the co-precipitation methods are illustrated in Figures 5.8 (a) – (c) and Figures 5.8 (d) – (f), respectively. All the ceramics show a peak of dielectric constant, indicating the ferroelectric to paraelectric phase transition at the Curie temperature, T_C. From Figures 5.8 (a) - (c), it can be seen that the SG1000(8) ceramic [(a)] shows a permittivity maximum (ε'_{max}) of about 600 at a frequency of 1 kHz while SG1200(4) and SG1200(8) exhibit an ε'_{max} value of about 950 at the same frequency [(b) and (c)]. In addition, the dielectric peaks for the SG1200(4) and SG1200(8) ceramics are slightly broadened. The room temperature dielectric constant, ε'_{RT}, is 142 in SG1000(8) and it increases to 227 in both SG1200(4) and SG1200(8). T_C is found to decrease from 365 °C to 330 °C when the sintering temperature is increased from 1000 °C to 1200 °C. The results also show that for the ceramics sintered at 1200 °C, increasing the sintering time from 4 hrs to 8 hrs does not affect the dielectric properties of the material by much, nor does it further decrease the T_C.

Similar trends are observed in ceramics prepared from the co-precipitation method. From Figures 5.8 (d) – (f), we can also see a decrease in T_C from 380 °C to 330 °C as the sintering temperature is increased from 1000 °C to 1200 °C. The T_C of 330 °C observed in the PR1200(8) ceramic with (00$\underline{1}$0) preferred orientation is close to the value of 320 °C found in (001) platelets of SBT single crystals prepared in our laboratory by Sih *et al.* [14]. Interestingly, PR1000(8) shows a significant frequency dispersion of the

dielectric permittivity as well as a much broader transition compared to PR1200(4) and PR1200(8).

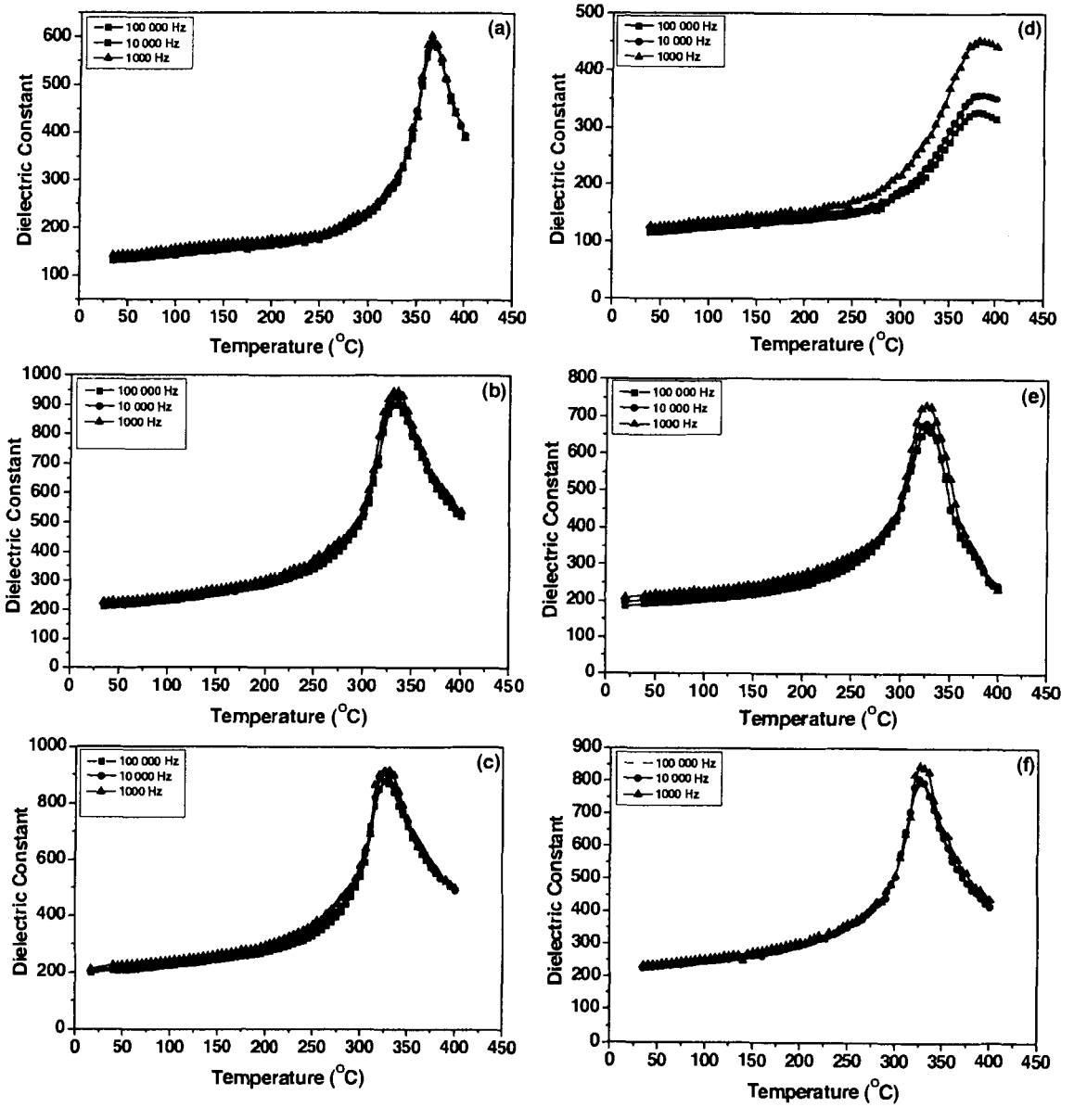

Figure 5.8: Dependences of the real part of the dielectric permittivity on temperature and frequency for SBT ceramics prepared by the sol-gel process, and the co-precipitation method: (a) SG1000(8), (b) SG1200(4), (c) SG1200(8), (d) PR1000(8), (e) PR1200(4), and (f) PR1200(8).

The room temperature dielectric constant values are found to be 125, 215, and 235 for PR1000(8), PR1200(4) and PR1200(8), respectively, which are comparable to those observed for ceramics obtained by the sol-gel method. On the other hand, ε'_{max} ($\approx$ 455) for PR1000(8) is lower than ε'_{max} ($\approx$ 600) of SG1000(8). A slight increase in maximum permittivity value occurs upon increasing the sintering temperature and time, giving rise to the ε'_{max} values of 750 and 850 for PR1200(4) and PR1200(8), respectively. The ε'_{max} values measured in all the sol-gel derived ceramics [SG1000(8), SG1200(4), and SG1200(8)] and the co-precipitation derived ceramics sintered at 1200 °C [PR1200(4) and PR1200(8)] are higher than the values of ~ 400 - 500 reported in the literature for the SBT ceramics synthesized by the conventional solid state reactions [35-37]. The dielectric properties of the ceramics obtained by our sol-gel and co-precipitation methods are compared in Table 5.1 with both those of single crystals [14, 38] and ceramics prepared the solid state reactions.

Table 5.1: Comparison of the dielectric properties of SBT prepared by different methods.

Method	ε'_{RT} (100 kHz)	ε'_{max} (100 kHz)	T_C (°C)
Sol-Gel*	207	900	330
Co-precipitation*	219	800	330
Single Crystals [14]**	135	127	320
Single Crystals [38]***	105	130	355
Single Crystals [38]****	110	1325	355
Solid State Reactions[35]	~100	~ 500	315

* This work.

** Single crystals with dominant (001) orientation and about 1-3% of (113) orientation.

*** Perfectly c-oriented single crystals.

**** Single crystals oriented in the ab-plane.

The enhanced dielectric properties in the sol-gel derived ceramics can be attributed to an increase in density and a more homogeneous microstructure without preferentially oriented grains. The decrease in T_C with increasing sintering temperature for the ceramics prepared by the sol-gel method and the co-precipitation technique is believed to arise from partial loss of Bi_2O_3 due to volatilization. The dielectric and ferroelectric properties of SBT are known to be highly dependent on its stoichiometry [15,18]. A decrease in T_C is an indication of a decrease in the stability of the ferroelectric phase. A change in the stoichiometry of SBT through the loss of bismuth oxide can trigger this effect. The broadening of the dielectric peaks in the sol-gel derived ceramics when the sintering temperature is increased from 1000 °C to 1200 °C [Figures 5.8 (b) and (c)] can also be due to the change in stoichiometry caused by bismuth oxide volatilization. The ceramics may contain regions or grains with varying bismuth content leading to a variation in composition, and hence, broadening of the dielectric peak. The frequency dispersion observed in the ceramic prepared by the co-precipitation method and sintered at 1000 °C for 8 h [Figure 5.8 (d)] can be attributed to the relatively low density (65 %) of the ceramics.

To estimate the extent of loss of bismuth oxide from the SBT ceramics during sintering, the weight loss of the samples was monitored. Table 5.2 summarizes the variation of the percentage weight loss for the ceramics obtained by the sol-gel and the co-precipitation methods. As can be seen from the results, the weight loss increases as the sintering temperature and time are increased for all the ceramics. For the sol-gel derived samples the weight loss increases from 1.73 % in SG1000(8) to 6.48 % in SG1200(4) and 8.65 % in SG1200(8). It is reasonable to suggest that the loss of bismuth oxide from these

ceramics causes a change in the composition from $SrBi_2Ta_2O_9$ to $SrBi_{2-2\delta}Ta_2O_{9-3\delta}$, according to the following equation [35]:

$$\mathbf{SrBi_2Ta_2O_9 \rightarrow SrBi_{2-2\delta}Ta_2O_{9-3\delta} + \delta Bi_2O_3}$$

Oxygen vacancies are formed in the $(Bi_2O_2)^{2+}$ layer because the oxygen ions in this layer are less stable than those in the perovskite blocks [39]. The interlayer bonding between the perovskite slabs is expected to weaken as a result of increased anionic repulsion between them, causing a lengthening of the c-axis and resulting in the destabilization of the ferroelectric phase and thereby a lowering of the T_C [14]. This is indeed observed in the non-stoichiometry, δ, created in the SBT ceramics by the Bi_2O_3 loss as shown in Table 5.2. Similar observations are made in the case of ceramics prepared by the co-precipitation method, which exhibit a higher weight loss under the same conditions (Table 5.2). The high weight loss observed in PR1000(8) may be due to the smaller initial grains [Figure 5.7 (d)] which have a larger specific surface area. This gives rise to a more reactive surface which results in a higher volatilization of Bi_2O_3. The PR1000(8) ceramic shows a very diffuse dielectric maximum at a temperature higher than the T_C of SG1000(8) probably due to its porous and anisotropic microstructure. The results also suggest that the value of T_C stabilizes at ~330 °C after the weight loss exceeds about 6 % in the ceramics prepared by both soft chemical methods.

Table 5.2: Variation of weight loss of ceramics with sintering temperature and its effect on T_C and the stoichiometry for ceramics prepared by the sol-gel and the co-precipitation methods.

Sintering Temperature and time	% Weight Loss		Non-Stoichiometry (δ)		T_C (ºC)	
	SBT by Sol-gel	SBT by Co-precipitation	SBT by Sol-gel	SBT by Co-precipitation	SBT by Sol-gel	SBT by Co-precipitation
1000(8)	1.73	3.70	0.038	0.080	365	380
1200(4)	6.48	7.83	0.141	0.170	330	330
1200(8)	8.65	8.97	0.188	0.195	330	330

5.3.4 Ferroelectric measurements

Typical ferroelectric behaviour is exhibited in SG1000(8), SG1200(4), and SG1200(8) ceramics by the dielectric hysteresis loops displayed in Figures 5.9 (a) – (c), respectively. The values of the remnant polarization and coercive field are extracted and shown in Table 5.3. They are compared with values reported in the literature for ceramics prepared from solid state reaction processes, and for single crystals. An increase in the remnant polarization (P_r), and a decrease in the coercive field (E_C) are found with increasing sintering temperature and time. P_r increases from ~3.40 $\mu C/cm^2$ in SG1000(8) to 6.0 $\mu C/cm^2$ in SG1200(4), and to 7.6 $\mu C/cm^2$ in SG1200(8). SG1200(4) and SG1200(8) show an E_C of 23 kV/cm and 22 kV/cm, respectively, while SG1000(8) has the highest coercive field E_C = 34.5 kV/cm, and its polarization is only saturated at a field as high as ~100 kV/cm.

Figures 5.9 (d) – (e) illustrate the ferroelectric hysteresis loops of PR1200(4) and PR1200(8), respectively. PR1200(4) and PR1200(8) yield almost the same values of the P_r and E_C: 3.5, and 3.7 $\mu C/cm^2$ and 19.5, and 21 kV/cm, respectively. However, the P_r values for these ceramics obtained from the co-precipitation method are only half of those observed in ceramics prepared by the sol-gel process and sintered under the same conditions.

The lower P_r values observed in the ceramics prepared by the co-precipitation method can be due to the preferred orientation along the [00$\underline{1}$0] direction of the grains, as depicted in the XRD pattern of the PR1200(8) ceramic [Figure 5.6 (b)]. The spontaneous polarization in SBT is known to be parallel to the a-axis because the O – Ta – O chains in the a-b plane have high polarizability and hence, is responsible for the polarization [2].

Therefore, the polarization measured in ceramics containing more grains with the polarization oriented along the a-axis parallel to the field direction is larger than in those containing mostly the grains with c-axis along the field direction (i.e., perpendicular to the electrode surfaces) [40, 41]. The XRD spectra clearly show that the grains are preferentially oriented along the c-direction in the PR1200(8) ceramic, which is confirmed by the microstructure in Figure 5.7 (f). Moreover, the measured densities of the SG1200(4) and SG1200(8) ceramics are much higher than those of PR1200(4) and PR1200(8) which is another reason for their higher P_r values. The relationship between the high preferential orientation, relatively low density, and low P_r value observed in the PR1200(8) ceramic is consistent with the previous report that excessive directional grain growth in SBT and $BaBi_2Ta_2O_9$ ceramics leads to a lower density resulting from a loosely packed microstructure [17, 42]. Therefore, the sol-gel derived ceramics have shown a better grain orientation, and thus achieve the purpose of 'grain control' in SBT by minimizing the c-oriented grains.

Table 5.3: Comparison of the ferroelectric properties of ceramics synthesized by the sol-gel process and the co-precipitation method with literature data on single crystals and ceramics prepared by the solid state reaction.

Samples	Sol-Gel method			Co-precipitation		Single crystals [14]*	Single crystals [38]**	Solid state reaction [43]
	1000(8)	1200(4)	1200(8)	1200(4)	1200(8)			
E_C	34.5	23	22	19.5	21	1	22	30
P_r	3.4	6.0	7.6	3.5	3.7	0.01	14	4.5

* Single crystals with dominant (001) orientation and about 1-3% of (113) orientation.
** Single crystals oriented in the ab-plane.

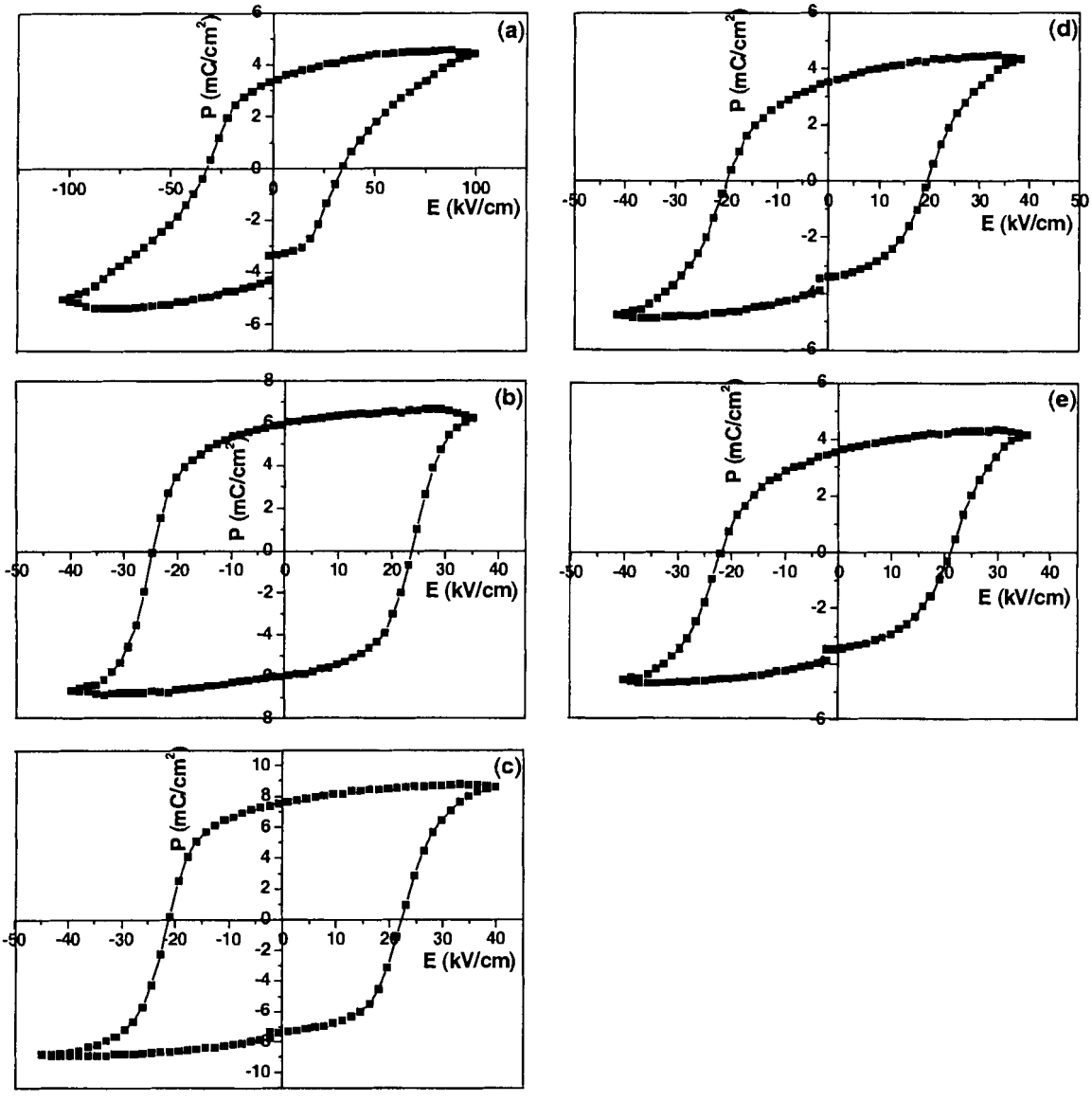

Figure 5.9: Ferroelectric hysteresis loops of SBT ceramics derived from the sol-gel process, and the co-precipitation method; (a) SG1000(8), (b) SG1200(4), (c) SG1200(8), (d) PR1200(4), and (e) PR1200(8).

5.4 Conclusions

Pure SBT ceramics of layered perovskite structure have been successfully synthesized by two new soft chemical routes – a sol-gel process and a co-precipitation method. The sol-gel route employs ethylene glycol to dissolve the starting materials and the co-precipitation method makes use of a PEG-200 and methanol mixture for the same purpose. Ceramics obtained by these two different methods under different processing conditions were systematically investigated. It is found that the sol-gel derived ceramics are much denser (93 – 96 % of theoretical density) and also have smaller and more homogeneous grain sizes when compared with those obtained from the co-precipitation process ($\leq$ 85 % of theoretical density). Ceramics made from the co-precipitation method also tend to have a microstructure with plate-like anisotropic grains preferentially oriented parallel to the (00$\underline{1}$0) plane. The preferential grain orientation occurs when the sintering temperature and time are increased to 1200 °C and 8 hrs, and it is possibly the reason for a lower measured density.

The maximum dielectric constant values, ε'_{max}, in the sol-gel derived ceramics are higher than in ceramics prepared by the co-precipitation method under the same sintering conditions. It is worth noting that the ε'_{max} values of 950 in SG1200(8) and 850 in PR1200(8) are higher than in ceramics prepared by the solid state reactions ($\varepsilon'_{max} \sim 500$). In the ceramics synthesized by both the soft chemical techniques the Curie temperature, T_C, decreases when the sintering temperature is increased from 1000 °C to 1200 °C. The decrease in T_C can be explained by partial Bi_2O_3 volatilization at higher sintering temperatures, which destabilizes the ferroelectric phase. This observation is confirmed by

the loss in weight of the ceramics during sintering, which increases with an increase in temperature and time.

The ferroelectric properties of the ceramics made from the sol-gel method are superior to those derived from the co-precipitation technique, showing a larger P_r of 6.0 $\mu C/cm^2$ and 7.6 $\mu C/cm^2$ for ceramics sintered at 1200 °C for 4 hrs and 8 hrs, respectively. The lower remnant polarization values of 3.5 $\mu C/cm^2$ and 3.7 $\mu C/cm^2$ found in PR1200(4) and PR1200(8) are possibly due to the c-oriented plate-like structures, especially in PR1200(8). Overall, the sol-gel process produces ceramics with much better dielectric and ferroelectric properties because it allows a more homogeneous grain distribution by reducing c-oriented grains in the materials, thus achieving 'grain-control'. This method therefore shows promising potential for depositing SBT thin films with minimized c-axis orientation and hence, improved remnant polarization, which is a key performance parameter for non-volatile memory applications.

5.5 References

1. J. F. Scott, and C. A. De Araujo Paz, *Science*, **246**, 1400 (1989).
2. C. A. Paz de Araujo, J. D. Cuchiaro, M. C. Scott, L. D. Mcmillan, and J. F. Scott, *Nature*, **374** (13), 627 (1995).
3. J. F. Scott, F. M. Ross, C. A. De Araujo Paz, M. C. Scott, and M. Huffman, *Mater. Res. Soc. Bull.*, **21** (1996).
4. J. F. Chang, and S. B. Desu, *J. Mater. Res.*, **9**, 955 (1994).
5. W. L. Warren, D. Dimos, B. A. Tuttle, R. D. Nasby, and G. E. Pike, *Appl. Phys. Lett.*, **65**, 1018 (1994).
6. B. Aurivillius, *Arki. Kemi*, **1**, 463 (1949).
7. S. B. Desu, and T. K. Li, *Mater. Sci. Eng. B*, **34**, L4 (1995).
8. J. J. Lee, C. L. Thio, and S. B. Desu, *J. Appl. Phys.*, **78** (8), 5073 (1995).
9. M. L. Calzada, R. Jimenez, A. Gonzalez, and J. Mendiola, *Chem. Mater.*, **13**, 3 (2001).
10. K. Kato, C. Zheng, J. M. Finder, S. K. Dey, and K. Torii, *J. Am. Ceram. Soc.*, **81** (7), 1869 (1998).
11. S. B. Desu, D. P. Vijay, X. Zhang, and B. P. He, *Appl. Phys. Lett.*, **69** (12), 1719 (1996).
12. M. L. Calzada, A. Gonzalez, R. Jimenez, C. Alemany, and J. Mendiola, *J. Eur. Ceram. Soc.*, **21**, 1517 (2001).
13. M. A. Zurbuchen, J. Lettieri, S. J. Fulk, Y. Jia, A. H. Carim, D. G. Schlom, and S. K. Streiffer, *Appl. Phys. Lett.*, **82** (26), 4711 (2003).
14. B. Sih, J. Tang, M. Dong, and Z.-G. Ye, *J. Mater. Res.*, **16** (6), 1726 (2001).
15. J.-K. Lee, B. Park, and K.-S. Hong, *J. Appl. Phys.*, **88** (5), 2825 (2000).
16. J. S. Yang, and X. M. Chen, *Mater. Lett.*, **29**, 73 (1996).
17. G. S. Murugan, and K. B. R. Varma, *J. Electroceram.*, **8**, 37 (2002).
18. Y. Shimakawa, Y. Kubo, Y. Nakagawa, T. Kamiyama, H. Asano, and F. Izumi, *Appl. Phys. Lett.*, **74** (13), 1904 (1999).
19. Alain C. Pierre, 'Introduction to Sol-Gel Processing', Kluwer Academic Publishers, Boston/Dordrecht/London (1998).
20. D. A. Payne, *J. Sol-Gel Sci. Technol.*, **2**, 311 (1994).

21. C. H. Luck, C. L. Mak, and K. H. Wong, *Thin Solid Films*, **298**, 57 (1997).

22. G. M. Anilkumar, and Y.-M. Sung, *J. Mater. Sci.*, **38**, 1391 (2003).

23. Y. Kim, H. K. Chae, K. S. Lee, and W. I. Lee, *J. Mater. Chem.*, **8**, 2317 (1998).

24. K. Babooram, H. Tailor, and Z.-G. Ye, *Ceramics International*, **30**, 1411 (2004).

25. K. Babooram, and Z.-G. Ye, *Chem. Mater.*, **16**, 5365 (2004).

26. S. D. Ramamurthi, Z. Xu, and D. A. Payne, *J. Am. Ceram. Soc.*, **73** [9], 2760 (1990).

27. G. H. Maher, C. E. Hutchins, and S. D. Ross, *Am. Ceram. Soc. Bull.*, **72** [5], 72 (1993).

28. C.-H. Lu, and S. K. Saha, *J. Am. Ceram. Soc.*, **83** [5], 1320 (2000).

29. N. Uekawa, M. Endo, K. Kakegawa, and Y. Sasaki, *Phys. Chem. Chem. Phys.*, **2**, 5485 (2000).

30. R. Ramesh, and D. G. Schlom, *Science*, **296**, 1975 (2002).

31. K. Sakata, T. Takenaka, and K. Shoji, *Ferroelectrics*, **22**, 825 (1978).

32. T. Takenaka, and K. Sakata, *Jpn. J. Appl. Phys.*, **19**, 31 (1980).

33. T. Takenaka, and K. Sakata, *Ferroelectrics*, **118**, 123 (1991).

34. V. K. Seth, and W. A. Schulze, *IEEE Transactions on Ultrasonics, Ferroelectrics, and Frequency Control*, **36** [1], 41 (1989).

35. B. Sih, A. Jung, and Z.-G. Ye, *J. Appl. Phys.*, **92** [7], 3928 (2002).

36. Y. Wu, M. J. Forbess, S. Seraji, S. J. Limmer, T. P. Chou, and G. Cao, *J. Appl. Phys.*, **89** (10), 5647 (2001).

37. J. S. Kim, C. Cheon, H. Shim, C.H. Lee, *J. Eur. Ceram. Soc.*, **21** [10-11], 1295 (2001).

38. H. Amorin, V. V. Shvartsman, A. L. Kholkin, and M. E. V. Costa, *Appl. Phys. Lett.*, **85** (23), 5667 (2004).

39. B. H. Park, S. J. Hyun, S. D. Bu, T. W. Noh, J. Lee, H.-D. Kim, T. H. Kim, and W. Jo, *Appl. Phys. Lett.*, **74** (13), 1907 (1999).

40. G. A. Smolenskii, V. A. Isupov, and A. I. Agranovskya, *Sov. Phys. Solid State*, **3**, 651 (1961).

41. E. C. Subbarao, *J. Phys. Chem. Solids*, **23**, 665 (1962).

42. C. H. Lu, and B. K. Fang, *J. Mater. Res.*, **13**, 2262 (1998).

43. A. Kitamura, C. W. Lee, Y. Noguchi, and M. Miyayama, *Key Eng. Mater.*, **248**, 3 (2003).

CHAPTER 6:
General Conclusions

This research work deals with the study of the synthesis and characterization of the ceramics of the relaxor-ferroelectric solid solution, $(1-x)Pb(Mg_{1/3}Nb_{2/3})O_3–xPbTiO_3$ [(1-x)PMN–xPT] (x = 0.10 and 0.35), and the layer-structured ferroelectric, $SrBi_2Ta_2O_9$ (SBT). The excellent piezoelectric properties recently discovered in the single crystal form and the high dielectric constant of the (1-x)PMN–xPT system make it very attractive for a wide range of applications namely, in multi-layered capacitors and electromechanical transducers. On the other hand, SBT is a promising candidate for non-volatile ferroelectric memory devices because of its excellent fatigue resistance and good data retention. It is therefore desirable to investigate the bulk properties of these materials in the form of ceramics which can be the cost-effective alternative to single crystals. However, the many difficulties encountered in the solid state synthesis of the (1-x)PMN–xPT ceramics to stabilize the perovskite phase, have required better methods of synthesis. As for the SBT system, the synthesis of ceramics by conventional solid state reactions required high temperature and long reaction time, and the soft chemical routes developed previously to synthesize thin films and ceramics made use of harmful solvents such as 2-methoxyethanol which is a teratogen.

Therefore, the main objectives of this thesis was to design new soft chemical methods that use less harmful solvents for the synthesis of pure (1-x)PMN–xPT (x = 0.10 and 0.35) and $SrBi_2Ta_2O_9$ ceramics, and to study the effects of these methods on the

phase formation, microstructure, and dielectric and ferroelectric properties of these materials. The following has been achieved in the course of this research study.

6.1 (1-x)Pb($Mg_{1/3}Nb_{2/3}$)O_3–x$PbTiO_3$ [(1-x)PMN–xPT] (x = 0.10 and 0.35) Ceramics by a Polyethylene-Glycol Based Sol-Gel Route

A room-temperature sol-gel method has been developed for the first time for the successful synthesis of (1-x)PMN–xPT (x = 0.10 and 0.35) ceramics. The method uses a mixture of polyethylene glycol 200 (PEG200) and methanol as solvent, which have proved to be very efficient in dissolving all the starting materials at room temperature, thus eliminating the refluxing steps commonly required in sol-gel reactions. PEG is also environmentally less harmful and therefore, a much better solvent compared to other hazardous compounds such as 2-methoxyethanol. The PEG molecules can bind to the metal ions through the ether oxygen found in the polymer chain and also through the terminal hydroxyl groups in solution. The other advantage of this new method is that it allows the formation of pure 0.65PMN–0.35PT ceramics without the need for an excess of the lead starting material in the sol-gel reaction as was the case in conventional syntheses in which up to 10 – 15 mol % excess of lead oxide is added in order to compensate for the PbO loss during sintering. The effects of the addition of a complexing agent, 1,1,1-tris(hydroxy)methylethane (THOME), to the sol-gel reaction have also been studied. Thermal analysis has shown that with the presence of three hydroxyl groups in the molecule, THOME serves as a good metal-binding agent, helping in the formation of cross-linked or oligomeric structures in both the 0.65PMN–0.35PT and 0.90PMN–0.10PT sol or gel, and these influence the arrangement of the M–O–M networks in the ceramic precursor powder. IR spectroscopic studies performed on the 0.65PMN–0.35PT

precursor powder have revealed that different M–O–M arrays are present depending on whether THOME was used in the sol-gel reaction or not.

Therefore, this sol-gel method combines the metal binding ability of both PEG and THOME to stabilize the metal ions against precipitation, leading to the formation of a very stable sol. Such a stable sol has not only given rise to the ceramics of good quality, but also shows to be very promising for the deposition of (1-x)PMN–xPT thin films, a work worth being followed up naturally in the near future.

This room-temperature sol-gel process has led to the synthesis of high-density (1-x)PMN–xPT ceramics with very good dielectric and ferroelectric properties, which are achieved by the just one heat treatment of the precursor powder without the addition of any sintering agent. Among the series of 0.90PMN–0.10PT ceramics synthesized with different amounts of lead oxide (stoichiometric or 5 % mol excess), and in the presence or absence of THOME, the one prepared with the stoichiometric amounts of lead oxide and THOME shows the best dielectric and ferroelectric properties. It has a high relative density of 95 % and shows a room temperature dielectric constant, ε'_{RT} of ~25,000 at 1 kHz which is the highest value known for 0.90PMN–0.10PT ceramics. The ceramics show typical relaxor ferroelectric behaviour with diffuse and frequency-dispersive dielectric peaks at T_{max} ~40 °C. The maximum dielectric constant, ε'_{max}, reaches ~33,000 at 1 kHz which is the highest value ever reported for 0.90PMN–0.10PT ceramics. The ceramics also display well-defined and saturated ferroelectric hysteresis loops with a remnant polarization (P_r) of 18 $\mu C/cm^2$ at the temperature of liquid nitrogen, arising from an electric field-induced ferroelectric state.

The 0.65PMN – 0.35PT ceramics synthesized with the stoichiometric amount of lead oxide and THOME also show much better phase purity, and dielectric and ferroelectric properties than the one prepared without THOME. Pure perovskite phase is obtained at a relatively low sintering temperature of 1040 °C. The ceramics exhibit a room temperature dielectric constant, $\varepsilon'_{RT} > 5{,}000$, an ε'_{max} of ~27,000 occurring at the T_C of 175 °C, and a remnant polarization, P_r, of 21 $\mu C/cm^2$ (measured at room temperature). It is worth noting that the ε'_{RT} and ε'_{max} values obtained for the 0.65PMN–0.35PT ceramics are remarkably higher than those observed in the ceramics of the same composition synthesized by solid state reactions. The microstructural features of the 0.65PMN–0.35PT ceramics, as revealed by SEM, show a larger grain size for the ceramic synthesized with THOME, leading to the higher maximum dielectric constant value and a sharp peak in the ε' versus temperature curve as opposed to a broad maximum in the dielectric peak of the ceramic prepared without THOME.

The excellent dielectric and ferroelectric properties of the 0.90PMN–0.10PT and 0.65PMN–0.35PT ceramics synthesized by this new room temperature sol-gel process make these materials very promising for applications in advanced electromechanical transducer devices.

6.2 $SrBi_2Ta_2O_9$ Ceramics by Soft Chemical Methods

Two new soft chemical methods, namely, a sol-gel process and a co-precipitation method have been successfully developed for the synthesis of $SrBi_2Ta_2O_9$ (SBT) ceramics. Both methods avoid the use of toxic solvents such as 2-methoxyethanol by employing environmentally more friendly ethylene glycol and polyethylene glycol 200 (PEG) as solvents for the sol-gel process and the co-precipitation method, respectively. Ethylene glycol serves both as a solvent and a good complexing agent for the metal ions, keeping them from precipitating in solution. This allows the formation of a stable sol which can be further exploited for the deposition of SBT thin films in a future work. On the other hand, PEG is very effective in dissolving the starting reagents in the co-precipitation method at room temperature because of its metal binding affinity discussed in Sec. 6.1, allowing a homogeneous co-precipitation of the cations.

The ethylene glycol-based sol-gel method results in SBT ceramics with a denser and more homogeneous microstructure, and better dielectric and ferroelectric properties compared to the ceramics synthesized under the same processing conditions by the co-precipitation method. These soft chemical processes give rise to sintered SBT ceramics at a temperature of 1200 °C which is relatively lower than what is generally required in conventional solid state reactions.

A decrease in T_C is observed from 365 °C (for the sol-gel derived ceramics) and 385 °C (for ceramics synthesized by the co-precipitation method) to 330 °C upon increasing the sintering temperature and time. This is attributed to the loss of Bi_2O_3 at the

higher sintering temperatures which results in a change in the stoichiometry of the SBT ceramics. As a result, the ferroelectric phase is destabilized and hence, T_C decreases.

For the ceramics synthesized by the co-precipitation method, SEM shows a plate-like microstructure with preferential grain orientation along the (00$\underline{1}$0) plane, as confirmed by XRD. This preferred orientation leads to a lower ceramic density, and smaller dielectric constant (ε'_{max} = 850 at 1 kHz) and remnant polarization (P_r = 3.7 $\mu C/cm^2$) values, as opposed to an ε'_{max} of 950 and a P_r of 7.6 $\mu C/cm^2$ in the sol-gel derived ceramics. It is interesting to note that all these dielectric constant values are considerably higher than those (~500) reported so far in the ceramics synthesized by solid state reactions.

Therefore, the sol-gel method offers better grain control by minimizing the c-oriented grains, thereby leading to superior dielectric and ferroelectric properties in the material. The process can potentially be used to deposit thin films of SBT with controlled grain orientation and thereby improved remnant polarization, which is very useful for applications in non-volatile memory devices.

GENERAL BIBLIOGRAPHY

M. E. Lines, and A. M. Glass, *Principles and Applications of Ferroelectrics and Related Materials*, Clarendon Press, Oxford (1977).

A. R. West, 'Basic Solid State Chemistry', 2nd edition, John Wiley & Sons Ltd., (1996).

Y. Xu, *Ferroelectric Materials and Their Applications*, North Holland (1991).

G. Shirane, and S. Hoshino, *J. Phys. Soc. Jpn.*, **6**, 265 (1951).

L. E. Cross, *Ferroelectrics*, **151**, 305 (1994).

N. A. Spaldin, *Science*, **304**, 1606 (2004).

L. E. Cross, *Ferroelectrics*, **76**, 241 (1987).

Z.-G. Ye, *Ferroelectrics*, **184**, 193 (1996).

Z.-G. Ye, *Key Engineering Materials*, **155-156**, 81 (1998).

A. Bokov, and Z.-G. Ye, *J. Phys.: Condens. Matter*, **12**, L541 (2000).

A. Bokov, and Z.-G. Ye, *Phys. Rev. B.*, **65**, 144112 (2002).

A. Bokov, and Z.-G. Ye, *Phys. Rev. B.*, **66**, 064103 (2002).

G. A. Smolenskii, V. A. Isupov, A. I. Agranovskaya, and S. N. Popov, *Sov. Phys. Solid State*, **2** [11], 2584 (1961).

D. Viehland, S. J. Jang, and L. E. Cross, *J. Appl. Phys.*, **68**, 2916 (1990).

V. Westphal, W. Kleeman, and M. D. Glinchuk, *Phys. Rev. Lett.*, **68**, 847 (1992).

I. E. Myl'nikova, and V. A. Bokov, *Sov. Phys. Crystallography*, **Vol. 4**, 408 (1959).

V. A. Isupov, *Ferroelectrics*, **90**, 113 (1989).

G. A. Smolensky, and V. A. Isupov, *Soviet J. Techn. Phys.*, **24**, 1375 (1954).

V. A. Isupov, *Ferroelectrics*, **289**, 131 (2003).

Y. Yamashita, *Amer. Ceram. Soc. Bull.*, **73 (8)**, 74 (1994).

E. Husson, and A. Morell, *Key Engineering Materials*, **68**, 217 (1992).

L. E. Cross, S. J. Jang, R. E. Newnham, S. Nomura, and K. Uchino, *Ferrolectrics*, **23**, 187 (1980).

K. Uchino, *Ferroelectrics*, **151**, 321 (1994).

S. L. Swartz, and T. R. Shrout, *Mater. Res. Bull.*, **17**, 1245 (1982).

L. F. Francis, and D. A. Payne, *J. Am. Ceram. Soc.*, **74** [12], 3000 (1991).

A. S. Bhalla, R. Guo, and E. F. Alberta, *Materials Letters*, **54**, 264 (2002).

S. W. Choi, T. R. Shrout, S. J. Jang, and A. S. Bhalla, *Ferroelectrics*, **100**, 29 (1989).

O. Noblanc, P. Gaucher, and G. Calvarin, *J. Appl. Phys.*, **79**, 4291 (1996).

A. K. Singh, and D. Pandey, *J. Phys.: Condens. Matter*, **13**, L931 (2001).

Z.-G. Ye, B. Noheda, M. Dong, D. Cox, and G. Shirane, *Phys. Rev. B*, **64**, 184114-1 (2001).

B. Noheda, D. E. Cox, G. Shirane, J. Gao, and Z.-G. Ye, *Phys. Rev. B*, **66**, 054104 (2002).

B. Noheda, D. E. Cox, G. Shirane, J. A. Gonzalo, L. E. Cross, and S. E. Park, *Appl. Phys. Lett.*, **74**, 2059 (1999).

J. Kuwata, K. Uchino, and S. Nomura, *Jpn. J. Appl. Phys.*, **21**, 1298 (1982).

S. E. Park, and T. R. Shrout, *Mater. Res. Innovations*, **1**, 20 (1997).

S. E. Park, and T. R. Shrout, *J. Appl. Phys.*, **82** [4], 1804 (1997).

T. Shrout, Z. P. Zhang, N. Kim, and S. Markgraf, *Ferroelectr. Lett.*, **12**, 63 (1990).

S. E. Park, and, W. Hackenberger, *Curr. Opin. Solid State Mater. Sci.*, **6**, 11 (2002).

L. G. Tejuca, and J. L. G. Fierro, 'Properties and Applications of Perovskite-type Oxides', Marcel Dekker, Inc. (1993).

R. H. Mitchell, 'Perovskites – Modern and Ancient', Almaz Press Inc., Thunder Bay (2002).

B. Aurivillius, *Arki. Kemi*, **1**, 463 (1949).

D. A. Rae, J. G. Thompson, A. L. Withers, *Acta Crystallogr. B*, **47**, 870 (1991).

Ismundar, B. J. Kennedy, Gunawan, Marsongkohadi, *J. Solid State Chem.*, **126**, 135 (1996).

M. Kumar, A. Srinivas, G. S. Kumar, and S. V. Suryanarayana, *Solid State Chem.*, **104**, 741 (1997).

B. Aurivillius, and P. H. Fang, *Phys. Rev. A.*, **126**, 893 (1962).

G. A. Smolenskii, V. A. Isupov, and A. I. Agranoskya, *Sov. Phys. Solid State*, **3**, 651 (1961).

G. S. Murugan, and K. B. R. Varma, *J. Electroceram.*, **8**, 37 (2002).

A. Fouscova, and L. E. Cross, *J. Appl. Phys.*, **41**, 2834 (1970).

V. K. Seth, and W. A. Schulze, *IEEE Transactions on Ultrasonics, Ferroelectrics, and Frequency Control*, **36** (1), 41 (1989).

C. A. Paz de Araujo, J. D. Cuchlaro, M. C. Scott, L. D. Mcmillan, and J. F. Scott, *Nature*, **374**, 627 (1995).

S. B. Desu, and T. K. Li, *Mater. Sci. Eng. B*, **34**, L4 (1995).

P. C. Joshi, and S. B. Krupanidhi, *J. Appl. Phys.*, **72**, 5517 (1992).

B. H. Park, S. J. Hyun, S. D. Bu, T. W. Noh, J. Lee, H.-D. Kim, T. H. Kim, and W. Jo, *Appl. Phys. Lett.*, **74** (13), 1907 (1999).

Alain C. Pierre, 'Introduction to Sol-Gel Processing', Kluwer Academic Publishers, Boston/Dordrecht/London (1998).

D. A. Payne, *J. Sol-gel Sci. Techn.*, **2**, 311 (1994).

D. C. Bradley, *Chem. Rev.*, **89**, 1317 (1989).

R. E. Newhnam, Q. C. Xu, S. Kumar, and L. E. Cross, *Ferroelectrics*, **102**, 259 (1990).

S. L. Swartz, and T. R. Shrout, *Mat. Res. Bull.*, **17**, 1245 (1982).

M. Lejeune, and J. P. Boilot, *Ferroelectrics*, **54**, 191 (1984).

M. Lejeune, and J. P. Boilot, *Bull. Amer. Ceram. Soc.*, **64**, 679 (1985).

Z. Ye, P. Tissor, and H. Schmid, *Mat. Res. Bull.*, **25**, 739 (1990).

H.-C. Wang, and W. A. Schulze, *J. Am. Ceram. Soc.*, **73** [4], 825 (1990).

H. M. Jang, K.-M. Lee, and M.-H. Lee, *J. Mater. Res.*, **9** [10], 2634 (1994).

L. Zhang, 'Synthesis and Characterization of Relaxor-Based Piezo- and Ferroelectric (1-x)Pb(Zn1/3Nb2/3)O3–xPbTiO3 [PZN–PT] and (1-x)Pb(Mg1/3Nb2/3)O3–xPbTiO3 [PMN–PT]', Masters Thesis, Chemistry Department, Simon Fraser University, Burnaby, BC, Canada (2000).

J. F. Scott, and C. A. De Araujo Paz, *Science*, **246**, 1400 (1989).

C. A. Paz de Araujo, J. D. Cuchiaro, M. C. Scott, L. D. Mcmillan, and J. F. Scott, *Nature*, **374** (13), 627 (1995).

J. F. Scott, F. M. Ross, C. A. De Araujo Paz, M. C. Scott, and M. Huffman, *Mater. Res. Soc. Bull.*, **21** (1996).

J. J. Lee, C. L. Thio, and S. B. Desu, *J. Appl. Phys.*, **78** (8), 5073 (1995).

M. L. Calzada, R. Jimenez, A. Gonzalez, and J. Mendiola, *Chem. Mater.*, **13**, 3 (2001).

K. Kato, C. Zheng, J. M. Finder, S. K. Dey, and K. Torii, *J. Am. Ceram. Soc.*, **81** (7) 1869 (1998).

S. B. Desu, D. P. Vijay, X. Zhang, and B. P. He, *Appl. Phys. Lett.*, **69** (12) 1719 (1996).

M. L. Calzada, A. Gonzalez, R. Jimenez, C. Alemany, and J. Mendiola, *J. Eur. Ceram. Soc.*, **21**, 1517 (2001).

M. A. Zurbuchen, J. Lettieri, S. J. Fulk, Y. Jia, A. H. Carim, D. G. Schlom, and S. K. Streiffer, *Appl. Phys. Lett.*, **82** (26) 4711 (2003).

J. S. Yang, and X. M. Chen, *Mater. Lett.*, **29**, 73 (1996).

J.-K. Lee, B. Park, and K.-S. Hong, *J. Appl. Phys.*, **88** (5) 2825 (2000).

G. M. Anilkumar, and Y.-M. Sung, *J. Mater. Sci.*, **38**, 1391 (2003).

M. A. Gülgün, M. H. Nguyen, and W. M. Kriven, *J. Am. Ceram. Soc.*, **82** (3), 556 (1999).

N. Uekawa, T. Sukegawa, K. Kakegawa, and Y. Sasaki, *J. Am. Ceram. Soc.*, **85** (2), 329 (2002).

N. Sriprang, D. Kaewchinda, J. D. Kennedy, and S. J. Milne, *J. Am. Ceram. Soc.*, **83** (8), 1914 (2000).

M. E. Brown, 'Introduction to Thermal Analysis: Techniques and Applications', 2nd Edition, Dordrecht, Boston, Kluwer Academic Publishers (2001).

M. C. Morris, 'Joint Committee on Powder Diffraction Standards', 1st Edition, Swarthmore, Pa (1976).

V. K. Percharsky, and P. Y. Zavalij, 'Fundamentals of Powder Diffraction and Structural Characterization of Materials', Kluwer Academic Publishers, Boston (2003).

R. M. Silverstein, and F. X. Webster, 'Spectrometric Identification of Organic Compounds', 6th edition, Wiley, New York, (1998).

P. M. Fishbane, S. Gasiorowicz, S. T. Thornton, 'Physics for scientists and engineers', 2nd edition, Prentice Hall Upper Saddle River, New Jersey 07458 (1996).

D. A. Skoog, F. J. Holler, and T. A. Nieman, 'Principles of Instrumental Analysis', 5th edition, Harcourt Brace College Publishers (1998).

J. Ross Macdonald, 'Impedance Spectroscopy: Emphasizing solid materials and systems', J. Wiley & Sons, Inc. (1987).

J. T. S. Irvine, D. C. Sinclair, and A. R. West, *Advanced materials*, **2** [3], 132 (1990).

C. Elissalde, and J. Ravez, *J. Mater. Chem.*, **11**, 1957 (2001).

RT66A standard ferroelectric testing system manual.

S. J. Jang, K. Uchino, S. Nomura, and L. E. Cross, *Ferroelectrics*, **27**, 31 (1980).

Z.-G. Ye, and M. Dong, *J. Appl. Phys.*, **87** [5], 2312 (2000).

Z.-G. Ye, Y. Bing, J. Gao, and A. A. Bokov, *Phys. Rev. B.*, **67**, 104104-1 (2003).

S. L. Swartz, T. R. Shrout, W. A. Schulze, and L. E. Cross, *J. Am. Ceram. Soc.*, **67** [5], 311 (1984).

Ravindranathan, S. Komareni, A. S. Bhalla, and R. Roy, *J. Am. Ceram. Soc.*, **74** [12], 2996 (1991).

F. Chaput, J. P. Boilot, M. Lejeune, R. Papiernik, and L. G. Hubert Pfalzgraf, *J. Am. Ceram. Soc.*, **72** [8], 1355 (1989).

Y. Narendar and G. L. Messing, *J. Am. Ceram. Soc.*, **80** [4], 915 (1997).

M. P. Pechini, U.S. Pat. No. 3,330,697 (1967).

P. A. Lessing, *Am. Ceram. Soc. Bull.*, **68**, 1002 (1989).

L.-W. Tai, and P. A. Lessing, *J. Mater. Res.*, **7**, 502 (1992).

S. C. Zhang, G. L. Messing, W. Huebner, and M. M. Coleman, *J. Mater. Res.*, **5**, 1806 (1990).

K. Babooram, and Z.-G. Ye, *Chem. Mater.*, **16**, 5365 (2004).

L. E. Cross, *Ferroelectrics*, **76**, 241 (1987).

Z.-G. Ye, *Curr. Opin. Solid State Mater. Sci.*, **6** [1], 35 (2002).

J. H. Park, D. H. Kang, and K. H. Yoon, *J. Am. Ceram. Soc.*, **82** [8], 2116 (1999).

R. F. Service, *Science*, **275**, 1878 (1997).

B. Jaffe, W. R. Cook, and H. Jaffe, *Piezoelectric Ceramics*; Academic Press: London (1971).

A. Nijmeijer and H. Kruidhof, *J. Am. Ceram. Soc.*, **80** [10], 2717 (1997).

D. A. Payne, *J. Sol-Gel Sci. Technol.*, **2**, 311 (1994).

M. H. Nguyen, S-J. Lee, W. M. Kriven, *J. Mater. Res.*, **14** [8], 3417 (1999).

N. Uekawa, M. Endo, K. Kakegawa, and Y. Sasaki, *Phys. Chem. Chem. Phys.*, **2**, 5485 (2000).

Y. Shimizu, and T. Murata, *J. Am. Ceram. Soc.*, **80** [10], 2702 (1997).

K. R. Udayakumar, J. Chen, P. J. Schuele, L. E. Cross, V. Kumar, and S. B. Krupanidhi, *Appl. Phys. Lett.*, **60** [10], 1187 (1992).

Y. Lu, G.-H. Jin, M. Cronin-Golomb, S.- W. Liu, H. Jiang, F.-L. Wang, J. Zhao, S.-Q. Wang, and A. J. Drehman, *Appl. Phys. Lett.*, **72** [23], 2927 (1998).

R. Thomas, S. Mochizuki, T. Mihara, and T. Ishida, *J. Mater. Res.*, **17** [10], 2652 (2002).

D. L. Pavia, G. M. Lampman, and G. S. Kriz, *Introduction to Spectroscopy (2nd Ed.)*, Harcourt Brace College Publishers, Washington (1996).

S. Chattopadhyay, P. Ayyub, V. R. Palkar, and M. Multani, *Phys. Rev. B*, **52** [18], 13177 (1995).

J. F. Chang, and S. B. Desu, *J. Mater. Res.*, **9**, 955 (1994).

W. L. Warren, D. Dimos, B. A. Tuttle, R. D. Nasby, and G. E. Pike, *Appl. Phys. Lett.*, **65**, 1018 (1994).

S. B. Desu, and T. K. Li, *Mater. Sci. Eng. B*, **34**, L4 (1995).

B. Sih, J. Tang, M. Dong, and Z.-G. Ye, *J. Mater. Res.*, **16** (6), 1726 (2001).

J. S. Yang, and X. M. Chen, *Mater. Lett.*, **29**, 73 (1996).

Y. Shimakawa, Y. Kubo, Y. Nakagawa, T. Kamiyama, H. Asano, and F. Izumi, *Appl. Phys. Lett.*, **74** (13), 1904 (1999).

C. H. Luck, C. L. Mak, and K. H. Wong, *Thin Solid Films*, **298**, 57 (1997).

Y. Kim, H. K. Chae, K. S. Lee, and W. I. Lee, *J. Mater. Chem.*, **8**, 2317 (1998).

K. Babooram, H. Tailor, and Z.-G. Ye, *Ceramics International*, **30**, 1411 (2004).

S. D. Ramamurthi, Z. Xu, and D. A. Payne, *J. Am. Ceram. Soc.*, **73** [9], 2760 (1990).

G. H. Maher, C. E. Hutchins, and S. D. Ross, *Am. Ceram. Soc. Bull.*, **72** [5], 72 (1993).

C.-H. Lu, and S. K. Saha, *J. Am. Ceram. Soc.*, **83** [5], 1320 (2000).

N. Uekawa, M. Endo, K. Kakegawa, and Y. Sasaki, *Phys. Chem. Chem. Phys.*, **2**, 5485 (2000).

R. Ramesh, and D. G. Schlom, *Science*, **296**, 1975 (2002).

K. Sakata, T. Takenaka, and K. Shoji, *Ferroelectrics*, **22**, 825 (1978).

T. Takenaka, and K. Sakata, *Jpn. J. Appl. Phys.*, **19**, 31 (1980).

T. Takenaka, and K. Sakata, *Ferroelectrics*, **118**, 123 (1991).

B. Sih, A. Jung, and Z.-G. Ye, *J. Appl. Phys.*, **92** [7], 3928 (2002).

Y. Wu, M. J. Forbess, S. Seraji, S. J. Limmer, T. P. Chou, and G. Cao, *J. Appl. Phys.*, **89** (10), 5647 (2001).

J. S. Kim, C. Cheon, H. Shim, C.H. Lee, *J. Eur. Ceram. Soc.*, **21** [10-11], 1295 (2001).

H. Amorin, V. V. Shvartsman, A. L. Kholkin, and M. E. V. Costa, *Appl. Phys. Lett.*, **85** (23), 5667 (2004).

E. C. Subbarao, *J. Phys. Chem. Solids*, **23**, 665 (1962).

C. H. Lu, and B. K. Fang, *J. Mater. Res.*, **13**, 2262 (1998).

Kitamura, C. W. Lee, Y. Noguchi, and M. Miyayama, *Key Eng. Mater.*, **248**, 3 (2003).